Combining satellite altimetry and GPS-corrected tide gauge data for the reconstruction of sea level anomalies

Inauguraldissertation
zur Erlangung des Grades eines
Doktors der Naturwissenschaften
(Dr. rer. nat.)

am Fachbereich Geowissenschaften
der Freien Universität Berlin
vorgelegt

von
Dipl.-Phys. Nana Schön

Berlin 2012

Erstgutachter: Prof. Dr. Maik Thomas, FU Berlin
Zweitgutachter: PD Dr. Gregor C. Leckebusch, FU Berlin
Tage der Disputation: 20. Juli 2011

1 Zusammenfassung (German abstract)

Die vorliegende Arbeit behandelt die Rekonstruktion von Meeresspiegelanomalien mithilfe von Altimetriedaten und GPS-korrigierten Pegeldaten. Im ersten Teil der Arbeit wird der verwendete Algorithmus ("Optimal Interpolation" (OI(C)) genauer untersucht. Hierbei wird erstmals festgestellt, dass dieser bei Verwendung weniger Pegel einen hohen Grad an Stochastizität aufweist. Die Rekonstruktion ist stark von der relativen Lage der Pegel zu den im Algorithmus verwendeten Empirischen Orthogonalen Funktionen (EOFs) abhängig. Im zweiten Teil der Arbeit wird eine Rekonstruktion von globalen Meeresspiegelanomalien für den Zeitraum von 1970-2001 durchgeführt. Die hierfür verwendeten Pegelzeitreihen werden mithilfe von lineraren GPS-Trends um Landbewegungssignale korrigiert. Es wird darüber hinaus ein Glättungsalgorithmus vorgestellt, der Fehler, die durch Lücken in den verfügbaren Pegeldatensätzen entstehen, vermindert.

Selbständigkeitserklärung

Ich erkläre hiermit, dass ich die vorliegende Dissertation selbständig und ohne unerlaubte Hilfe angefertigt habe. Alle verwendeten Hilfsmittel und Quellen sind im Literaturverzeichnis vollständig aufgeführt und die aus den benutzten Quellen wörtlich oder inhaltlich entnommenen Stellen als solche kenntlich gemacht.

Berlin, 6. Dezember 2010

Die vorliegende Arbeit ist die inhaltlich geringfügig veränderte Fassung einer Dissertation, die im Juli 2011 dem Fachbereich Geowissenschaften der Freien Universität Berlin vorgelegt wurde.

Contents

2 Introduction

In the last few years, several attempts have been made to solve the problem of sparse historical in-situ data for the use in a reconstruction of sea level anomalies or sea surface temperatures. With the emergence of satellite measurements, a near-global coverage of sea level measurements was made possible, still, the short time series extracted from these missions cannot yet compete with the much longer, though sparsely distributed, in-situ tide gauge data set. Ocean and climate models depend on consistent historical data sets, whether for data assimilation, forcing or model verification purposes. The aim of this work is to create full global maps of historical sea level anomalies for the use in, e.g. ocean models that assimilate sea level anomalies. A special aim was to correct the existing tide gauge records for land movement using linear vertical trends derived from GPS observations. A large part of this work explains the difficulties arising from sparse or gappy tide gauge data. In Chapter 6, a smoothing routine is developed to overcome these difficulties.

Kaplan et al. ([18], [19]) developed the Optimal Interpolation (OI) technique, which estimates the covariance structure of observed sea surface temperature variability from satellite data, using it to interpolate the sparse but longer in-situ surface temperature data sets.

A similar method —the projection technique —was developed by Smith et al. [32] for sea surface temperatures and used by Chambers et al. [4] for a global mean sea level reconstruction.

Both OI and projection technique were used by Church et al. ([7], [6]) for their reconstruction of regional sea level change. These papers give good regional estimates of historical sea level change trend, but the reconstructions do not reproduce the seasonal cycle.

What the above methods have in common is that the global covariance structure is estimated from satellite measurements, in the form of empirical orthogonal functions (EOFs). Then, for each month, the corresponding amplitude time series are scaled to fit the available in-situ measurements (e.g., tide gauges) using either a simple (Smith et al. [32]) or more sophisticated (Kaplan et al. [18], [19]) least-squares fit.

In this study, it is shown that the OI and related algorithms show strong stochasticity related to the geographical distribution of the in-situ data. This problem has not, to the author's knowledge, been reported before. On the contrary, several authors (e.g. [7], [2]) have claimed that the algorithm is not sensitive to this. Chambers et al. [4], who first introduced the use of tide gauge data as in-situ data for the projection technique, also first remarked the influence of the regional distribution of tide gauges on the RMS difference for sparse tide gauge configurations. However, no explanation for this effect was mentioned in their study.

GPS corrections have been applied to tide gauge data by various authors (e.g., Wöppelmann et al. [41], Snay et al. [33], Teferle et al. [34]). In this paper, a rigorous combination of six different GPS solutions is used. The tide gauge records are examined individually to pinpoint the start of the land movement processes observed by the GPS.

This study is organized as follows: The concept of the reduced space approach and the calculation of EOFs is described in Chapter 3.1. Then, an overview on reconstruction algorithms is given in Chapter 3.2. In Chapter 3.3, the altimetry data used in this study is described. The influence of the geographical distribution of the tide gauge data and the problems associated with this are described in Chapter 6.1.1 using a regional simulated reconstruction example.

In Chapter 4, the tide gauge data used in the reconstructions is described, while in Chapter 5, the GPS land movement corrections are introduced in detail. In Chapter 6, a global reconstruction of sea level anomalies for the 1970-2001 period is presented, followed by a discussion and an outlook on future work in Chapter 7.

3 Reconstruction algorithms

3.1 Reduced space approach using EOFs

To reduce the dimensionality of a given data set, it makes sense to only retain the part of the data that contributes most to its variance[1], i.e., the part which explains most of its variability.

Principal component analysis is a technique to transform a data set to another coordinate system in which the largest variance by any projection of the data comes to lie on the first coordinate, the second largest on the second coordinate, and so forth. This coordinate system is built by decomposing the covariance matrix of the centered data set into i vectors, each chosen to be orthogonal to the first $i-1$ vectors, and to minimize the residual variance. The first few of these i basis vectors then span the new, reduced subspace, onto which the original data is subsequently projected. In this way, only the part of the data that carries its most predominant characteristics is preserved.

Intuitively speaking, one might say that, in the case of sea level anomalies, the main spatial patterns are extracted from the data; then, the original observations are expressed in terms of these patterns. This

[1] Unless otherwise noted, the terms covariance and variance are henceforth used interchangeably, following the notion that, for a vector-valued variable, the covariance matrix is a higher-dimensional generalization of the one-dimensional variance; viz, $\mathrm{var}(\mathbf{X}) = \mathrm{cov}(\mathbf{X}) = E((\mathbf{X} - E(\mathbf{X}))(\mathbf{X} - E(\mathbf{X}))^{\mathrm{T}})$.

has the advantage that, commonly, only very few EOFs (typically, less than 40) are needed to preserve large portions (i.e., 70-99 %) of the original variance (see, e.g. Church et al. [7]).

3.1.1 Calculation of EOFs

Mathematically, let $\mathbf{X}$ be a random vector-valued variable, (representing, in our case, monthly sea level anomalies), the distribution of which is unknown. To estimate the variance of $\mathbf{X}$, we consider our monthly measurements $\{\mathbf{x}_1, \mathbf{x}_2, ..., \mathbf{x}_n\}$ to be n different sample realizations of $\mathbf{X}$. From these, the sample covariance matrix $\tilde{\mathbf{C}}$ is calculated as an estimator for the unknown covariance matrix $\mathbf{C}$.

We then start looking for a first "pattern" e^1 with $\|e^1\| = 1$ which will cover the largest-most part of the variability contained in $\mathbf{X}$. That is, if we "reconstruct" $\mathbf{X}$ in a one-dimensional space spanned by the vector e^1, the reconstruction error will be minimal. This reconstruction in the e^1-subspace is of course done by simply projecting $\mathbf{X}$ onto e^1.

Then, the following holds:

Let

$$\tilde{\mathbf{C}} = \frac{1}{n} \sum_{j=1}^{n} (\mathbf{x}_j - \mu)(\mathbf{x}_j - \mu)^{\mathrm{T}} \tag{1}$$

(where $\mu = \frac{1}{n} \sum_{j=1}^{n} \mathbf{x}_j$) derived from a sample $\{\mathbf{x}_1, \mathbf{x}_2, ..., \mathbf{x}_n\}$ be the estimated covariance matrix of n realizations of $\mathbf{X}$. Note that $\tilde{\mathbf{C}}$ is positive-semidefinite with real, non-negative eigenvalues and orthonormal eigenvectors. Further, let $\lambda_1 \leq \lambda_2 \leq ...\lambda_n$ be the eigenvalues of $\tilde{\mathbf{C}}$ and let $\{e^1, e^2, ..., e^n\}$ be the corresponding eigenvectors. Then, the k eigenvectors corresponding to $\lambda_1, \lambda_2, ...\lambda_k$ minimize the reconstruction error

$$\epsilon_k = \sum_{j=1}^{n} \|\mathbf{x}_j - \sum_{i=1}^{k} < \mathbf{x}_j, e^i > e^i\|^2 \tag{2}$$

that results from approximating the full m-dimensional vector $\mathbf{X}$ in the subspace spanned by those k eigenvectors.

Minimizing the reconstruction error in each of the one-dimensional subspaces spanned by each e^i is equivalent to maximizing the variance of $\mathbf{X}$ that is contained in this very subspace.

The EOF coefficients

$$\boldsymbol{\alpha}_i =< \mathbf{X}, e^i >= e^{i\mathrm{T}}\mathbf{X} \tag{3}$$

are obtained by projecting the vector $\mathbf{X}$ on a single eigenvector or EOF e^i. In our case, where the EOFs represent spatial patterns of variance, the principal components or amplitude time series α represent the temporal evolution of the intensity of the corresponding EOFs.

EOF analysis can be seen as the empirical version of the Karhunen-Loève [21] decomposition. A calculation via Singular Value Decomposition (SVD) is also possible.

3.1.2 Switched calculation

For computational purposes, it is sometimes more convenient to work in the dual space when calculating the covariance matrix of $\mathbf{X}$. For example, covering a spatial 1°-grid would normally result in a huge covariance matrix with $(180 * 360)^2 = 4.199.040.000$ elements. To resolve this obstacle, one would chose to logically switch the time and space dimensions and hence to calculate the covariance matrix of the dual of $\mathbf{C}$, i.e. $\mathbf{C}^* = Cov(\mathbf{X}^{\mathrm{T}})$, which in this case is equivalent to the covariance of the transpose matrix. This way, the problem is solved in the time space, which greatly reduces dimensionality due to the fact that the number of measurements per spatial point is commonly much smaller than the number of spatial points. Preisendorfer suggests this Ansatz in [27]. The resulting eigenvectors, however, are no longer orthonormal, and must undergo normalization.

3.2 Missing data and gap-filling algorithms

3.2.1 Missing data mechanisms

When applying any gap-filling or imputation algorithms, it is important to give thought to the causes and, subsequently the independence of the mechanisms leading to data gaps.

As an example, in sea surface temperature measurements via satellite, there is a considerable 'fair weather bias' when measuring in the infrared, as no data can be collected when the sky is cloudy.

In the case of sea level data from tide gauges, these connections are mainly temporal, i.e., data is missing on consecutive days or weeks due to, e.g. the breakdown of instruments.

Obviously, there is also a strong spatial connection, given the fact that tide gauges are necessarily located at shore, and therefore, there are only very few tide gauges in the open ocean, the data quality of which, in turn, is often rather doubtful. Also, the proxy density is much larger on the Northern Hemisphere, especially when it comes to long time series.

However, since these constraints pose the motivation for our application of a gap-filling algorithm in the first place, it can be safely assumed that no hidden correlations have been overlooked as far as missing data mechanisms are concerned.

The coverage of the satellite altimetry data used for the extraction of EOFs is considered to be global and complete for the calibration period. The coverage of radar altimetry is, however, confined to the inclination of the satellite orbit ($\pm 67°$ in the case of the TOPEX/Poseidon mission used in this work), and the resolution along coastlines is rather poor, especially in areas with ragged coastlines.

3.2.2 Gap-filling algorithms

There is a large variety of gap-filling algorithms suitable for sea level reconstructions. In Kaplan et al. [20], the authors compare the advantages and drawbacks of the Kalman filter, Optimal smoother, both of which employ a linear model for the development in time, and Optimal Interpolation approach. The latter is a method similar to the "projection technique" developed by Smith et al. [32], but used a more sophisticated error estimate and enhanced stability against underdetermination. Church et al. [7] have

enhanced the OI algorithm by adding an artificial "EOF-0" to enable it to cover homogeneous sea level rise. Schneider [29] uses expectation maximization (EM) and ridge regression to iteratively estimate the mean and covariance matrix of the analyzed data set. At each iteration step, missing values are filled in by regularized regression with missing values on the variables with available values. Then the mean and covariance matrix are updated using all the data. However, the method works best for data sets with smaller gaps, and, therefore, not suitable for a tide gauge based sea level reconstruction where only a small fraction of data points is available. Kondrashov and Ghil's Multi-Channel Singular Spectrum Analysis (MSSA [23]) is an interesting generalization of Beckers and Rixen's ([1]) EOF-based gap-filling algorithm, which shares with Schneider [29] the advantage of an iteratively updated covariance matrix and employs temporal as well as spatial correlations. However, it is computationally far more expensive than the OI algorithm and not yet adapted to handle a tide gauge based sea level reconstruction, although the use of the tide gauge data as an additional channel is possible. In [5], Christiansen et al. compare Smith's projection technique with the OI algorithm (and the respective enhanced algorithms which include an additional EOF-0 to cover sea level rise) to a simple weighted mean from tide gauges as used in [11], which performs surprisingly well in comparison. However, since the initial aim of this project was to generate monthly sea level anomaly (SLA) fields for use in data-assimilated ocean models, the OI algorithm was used.

3.2.3 Optimal Interpolation (OI/OIC)

We follow the notation from Kaplan et al. [18] as presented in Christiansen et al. [5]. A detailed overview is also presented in [17].

The reconstruction comprises of a calibration step and a reconstruction step. In the calibration step, EOFs are calculated from the covariance matrix; then, in the reconstruction step, the principal components or amplitude time series are determined by fitting the truncated set of EOFs to the in-situ data in such a way that the cost function is minimized. In the validation period, the m temporal measurements of SLAs at n grid points are arranged in the data matrix $\mathbf{X}(n \times m)$. The (sparse) in-situ data from the tide gauges will be denoted as $\mathbf{G}(N \times M)$.

First, the covariance matrix is calculated from $\mathbf{X}$ as in (1). The resulting reduction of space is achieved by setting:

$$\mathbf{C} = \mathbf{E}\mathbf{\Lambda}\mathbf{E}^{\mathrm{T}} + \mathbf{E}'\mathbf{\Lambda}'\mathbf{E}'^{\mathrm{T}} \tag{4}$$

where $\mathbf{E}(n \times l)$ and $\mathbf{E}'(n \times l)$ comprise of the accepted l and the discarded $(n-l)$ eigenfunctions, and $\mathbf{\Lambda}(n \times l)$ and $\mathbf{\Lambda}'((n-l) \times (n-l))$ are diagonal matrices containing the accepted and discarded eigenvalues.

In the reconstruction step, coefficients (also called amplitude time series) $\boldsymbol{\alpha}(l \times M)$ are determined in a way that, for each point in time i (in our case, for each month i), $\mathbf{E}\boldsymbol{\alpha}_{|,i}$ is close to the in-situ measurement at locations where a tide gauge exists [2].

[2]The notation $\mathbf{M}_{|,i}$ denotes the i'th column vector of the matrix $\mathbf{M}$.

Now, let $\mathbf{H}$ be the sampling operator that selects the positions of the tide gauges, i.e., $\mathbf{H}_{j,k} = 1$ if the j'th tide gauge is positioned at the k'th grid point, and $\mathbf{H}_{j,k} = 0$, otherwise.

Then, $\boldsymbol{\alpha}$ is chosen such that the cost function

$$(\mathbf{HE}\boldsymbol{\alpha} - \mathbf{G})^{\mathrm{T}}\mathbf{R}^{-1}(\mathbf{HE}\boldsymbol{\alpha} - \mathbf{G}) + \boldsymbol{\alpha}^{\mathrm{T}}\boldsymbol{\Lambda}^{-1}\boldsymbol{\alpha} \tag{5}$$

is minimized. Here, $\mathbf{R}(N \times N)$ is the sum of the observational error covariance and a contribution of the truncation error:

$$\mathbf{R} = \mathbf{I} + \mathbf{HE}'\boldsymbol{\Lambda}'\mathbf{E}'^{\mathrm{T}}\mathbf{H}^{\mathrm{T}} \tag{6}$$

The solution that minimizes the cost function is thus

$$\boldsymbol{\alpha} = \mathbf{PE}^{\mathrm{T}}\mathbf{H}^{\mathrm{T}}\mathbf{R}^{-1}\mathbf{G} \tag{7}$$

with $P = (\mathbf{E}^{\mathrm{T}}\mathbf{H}^{\mathrm{T}}\mathbf{R}^{-1}\mathbf{HE} + \boldsymbol{\Lambda}^{-1})$. The solution is linear in the tide gauge matrix $\mathbf{G}$.

The last term in the cost function punishes low-energetic modes and encourages the algorithm to emphasize the high-energetic modes that explain the larger part of the variance in the validation period. The form is similar to a ridge (or Tikhonov) (see, e.g., in [37]) regression. The factor $\mathbf{R}^{-1}$ reduces the influence of tide gauges with a large observational error or those which are most influenced by the truncation. Without the second term, we arrive at the projection method presented by Smith et al. in [32]. It should be noted that the issue of regularization —which becomes important if the number of EOFs is larger or equal to the number of tide gauges, rendering $\mathbf{WW}^T$ singular or almost singular[3] —is dealt with through the second term of the cost function .

In the case that

- model and observational errors are white in time, and uncorrelated with each other,
- the estimated fields have zero mean and known spatial covariances, and
- the distributions of the observational errors are Gaussian,

the above solution becomes the maximum likelihood estimation [17]. In actual applications, this can hardly ever be guaranteed since the observational error covariance is not known.

Church et al. [7] have enhanced this algorithm be including an artificial, homogeneous EOF into the set derived from the data; and assigning to it an equally artificial eigenvalue of 1. This ensures that the constant rise in sea level can be reproduced when using the OI algorithm in global mean sea level (GMSL) reconstructions. This is because the "EOF-0" pattern is, loosely speaking, not "interesting" enough to receive a high eigenvalue in the covariance structure analysis, when the data on the validation period covers only a short time span.

[3] with $\mathbf{W} = \mathbf{HE}(N \times L)$

A similar "EOF-0" has been included in the reconstructions in this study to provide for a potential homogeneous rise in sea level anomalies. This version of the OI algorithm is termed "OIC" by Christiansen et al. [5].

3.2.4 Difficulties and drawbacks of the OI(C) algorithm

The difficulties and inconsistencies connected with the use of the OI algorithm have been discussed in detail by the author himself ([17]) and, recently, in a major study by Christiansen et al.[5].

We give a short overview and discussion of the known problems and indicate two further points that have not yet been discussed in detail.

Sampling error In the Proudman Oceanographic Lab's Permanent Service for Mean Sea Level (PSMSL) database [40], no error estimates for the respective stations are given. This reduces our possibility of consistently estimating the sampling error at tide gauges. It is unlikely that such estimates even exist, especially for the long records taken with tide gauge stations no longer in operation. Therefore, a homogeneous error of ± 0.5mm is assumed for all tide gauges. The OI(C) algorithm discards any modes that influence the reconstruction result below this threshold. Church et al. [7] use a considerably larger error of 4mm, however, we have found the resulting cut-off in higher-order variability too large for a reconstruction using unfiltered tide gauge data. Instead, it seems sensible to increase the error bars in the result instead, especially since the solution is linear in the tide gauges.

Covariance: stationarity assumption It has been noted by the author of the algorithm himself ([17]) that the assumption of stationarity does not hold rigorously. When computing covariance matrix estimates from different time windows in a given data set of SST temperatures, Kaplan remarks that the Frobenius norm (the sum of squares of all elements in the matrix difference) does not stay constant over time.

In Figure 1, a plot of Frobenius norms for sea level anomaly covariance matrices calculated from the TOPEX/Poseidon mission for different 3-year windows in the 1994-2001 validation period is given. Clearly, the norm does not stay constant. The 1997/98 ENSO event, which brought about a strong increase in positive sea level anomalies, produces a strong maximum for this period.

Covariance: resolution and coverage The resolution of the TOPEX/Poseidon mission altimetry data is well enough to enable a $1^\circ \times 1^\circ$ grid in the reconstruction. However, due to the inclination of the satellite orbit, areas beyond $\pm 67^\circ$ latitude are not covered and, therefore, are neglected in the reconstruction.

Insufficient length of the validation period One of the main points of critique mentioned in [5] is the inadequate length of the validation period. The authors show that, in a proxy-based simulation, a validation period of more than 500 years proves optimal for a sea level reconstruction, even when only few tide gauges are available. However, the lack of data in general —and the necessity to perform

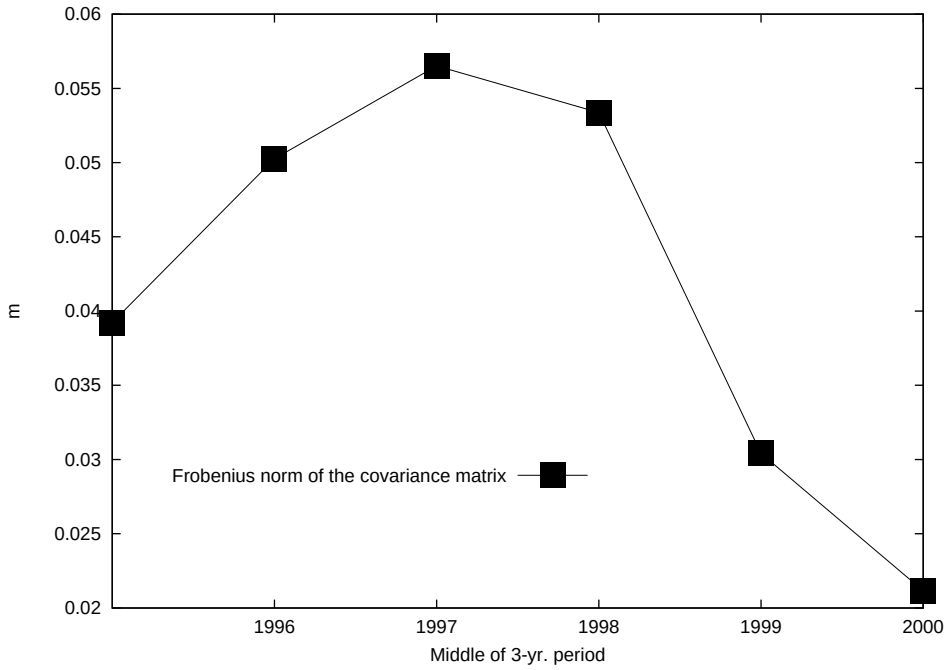

Figure 1: The development of the Frobenius norm of the covariance matrix of TOPEX SLAs estimated in different 3-year time windows.

analyses at a point when the data is not yet available —will remain the perpetual problem in geosciences. It is doubtful whether it can be resolved by the authors' proposition of using EOFs from long climate simulations alone, when these simulations depend strongly on data assimilation themselves.

Another way of improving the data basis for the validation period without altogether discarding observational data is the combination of different altimetry missions. This has been accomplished by Church et al. in [6], who uses combined data from TOPEX/Poseidon and Jason-1 from 1993-2004. The embedding of the Geosat altimetry mission could not yet be accomplished in a satisfactory way due to the bad orbit quality, although a first step has been made by the recalculation of orbits in a homogeneous and consistent way to ITRF2000.

However, a detailed look at the EOFs extracted from a 500-year validation period in [5] shows that the two leading EOFs (46% variance) show an almost homogeneous pattern, except for the larger intensity in the Arctic region. The latter is, of course, not covered by a reconstruction using observational data, since the orbits of the respective missions range from $\pm 67°$ latitude only. Aside from this, however, the homogeneous rise will be most probably covered by the 'EOF-0' artificially introduced by Church et al. in [7].

The third and fourth EOFs presented in Christiansen et al. (2009) are the well-known ENSO- and IOD (Indian Ocean Dipole, see [28]) related patterns. This explains very well the differing performance of the

OI (no homogeneous pattern) and OIC (homogeneous pattern) in relation to the length of the calibration period. When a short validation period is applied, the homogeneous patterns will explain only a minor fraction of the total variance, and, therefore, receive less weighting by the classical OI algorithm. As the validation period grows longer, the homogeneous pattern explains more and more of the total (500-year) variance. However, the modified OI(C) algorithm, which uses an artificial homogeneous pattern to begin with, profits significantly less from this expansion of the calibration period. In other words, it is impossible for the classical OI algorithm to reconstruct homogeneous sea level rise, since no *leading (i.e. highly energetic) homogeneous* EOFs are available for the short validation period.

A similar problem, however, arises from the fact that, in the TOPEX/Poseidon data set, the intensity of the ENSO- and IOD-related variability patterns is particularly enhanced due to the extreme 1997/98 ENSO event which dominates the variability pattern. In combination with the presence of only very few tide gauges, this may lead to an overestimation of related events, e.g., less intense El Niño events that have occurred in the past.

Summing up, instead of totally discarding modes extracted from observational data in favor of simulation data, it may be promising to incorporate further artificial modes with fixed and comparably high eigenvalues into the reconstruction. Carefully done, this might enable the rendering of patterns that are not present, or prominent, in the covariance structure extracted from the data, but which are expected to be necessary for a sound reconstruction.

Geographical distribution of in-situ data In 6.1.1, an excursus on the problem of the geographical distribution of tide gauges is presented. In contrast to what has been commonly acknowledged by various authors, e.g., ([2], [7]), it is shown that the OI(C) algorithm is indeed most sensitive to the geographical distribution of tide gauges when working with few stations. The examples given in this section also show that, in contrast to what Christiansen et al. [5] claim, the effects of an inclusion or refusal of single tide gauges may not be strictly local, i.e., the claim that regions with gauges are well reproduced, whereas regions without gauges are badly reproduced, does not hold in all rigor.

One must not forget that the OI algorithm was originally developed for the estimation of sea surface temperatures, not sea levels. Historical SSTs, sparse though they may be, tend to have the form of a continuous path (e.g., from ship routes) rather than the point-like scatter of tide gauge data. We suspect that this has an influence on the quality of the reconstruction.

3.3 Sea level anomalies from radar altimetry missions

For the extraction of the EOFs, fully corrected and harmonized monthly altimetric sea surface height anomaly data derived from the Altimeter Database and Processing System ADS (http://adsc.gfz-potsdam.de-/ads) are gridded into $1^\circ \times 1^\circ$ maps [30]. The validation period spans from 1994 to 2001, covering only times where the quality of the TOPEX/Poseidon mission data is excellent. An inverted barometer correction is applied to the SLA fields. The altimetric data is calculated in the same reference frame as the GPS data (ITRF 2005 , [31]). However, due to the lack of levelling information, the tide gauge

data cannot as of yet be transferred to any ITRF, which remains an important task for the future. The TOPEX/Poseidon mission spans an area of $\pm 67^\circ$ latitude; hence, only this area is reconstructed. Since the data quality on coastlines may vary, it is difficult to find an related grid point in areas with ragged coastlines.

4 Tide gauges

4.1 Introduction

The TIGA project [31] has collected a list of tide gauges with co-located GPS stations comprising 368 stations. Out of these, data from 254 stations is available from the PSMSL database [40], 215 of them have revised local reference (RLR) data quality. Only stations located within the area covered by TOPEX/Poseidon are used.

Again, from these, a set of tide gauges is chosen for which GPS trends are available in the combination solution provided by [31]. This leaves a preliminary set of 116 tide gauges.

4.2 Time series quality

4.2.1 Time series length and quality

The PSMSL [40] database provides monthly and annual mean sea level data from over 55.000 stations world-wide. A large part, though not all, are available in the so-called "Revised Local Reference" (RLR) format, which guarantees the year-to-year continuity of the reference measurement to which the sea level is measured. Because such consistency cannot be relied on with time series available only in "Metric" format data, their use is not recommended in reconstructions.

Jumps and gaps in a time series It is important to understand that the PSMSL collects all tide gauge data, i.e., also data from discontinued stations, and gappy time series. This means that, notwithstanding the impressive amount of data collected, the data continuity of the time series can differ tremendously, even in the RLR data set.

One typical example is Nain, Newfoundland (PSMSL 970/134). Nain has data from 1963-2007, but from the mid-1970 on, the time series has large gaps. The data is extremely sparse up to the 1990s; no data is available for 1988-2002; and the entire record is flagged for attention. The strong 2002-2007 downward trend of 8.0 mm/yr could probably to a large part explained by the uplift measured by the GPS trend (3.47 mm/yr) (Figure 2), as a matter of fact it may or may not have started earlier, possibly already in the 1980s. Faced with these difficulties, we have decided against including this tide gauge (and other stations showing similar gaps and jumps) in the reconstruction.

Since the OI(C) algorithm works with a month-wise reconstruction, it is possible to include also data from discontinued or gappy stations. We have shown in Chapter 6.1.1,however, that the OI(C) is under certain conditions not stable against the inclusion or exclusion of single tide gauges. This must

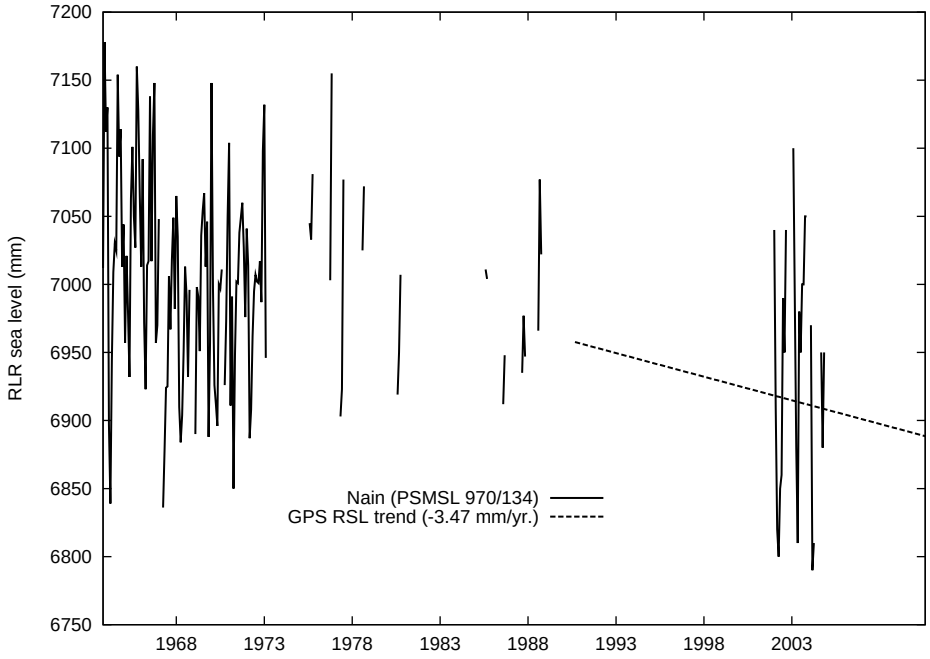

Figure 2: Even RLR quality tide gauges may be affected by jumps or gaps, rendering them largely useless for reconstruction purposes (Nain, Newfoundland (PSMSL 970/134))

be considered when changing the tide gauge configuration during the course of the reconstruction. In this study, we have decided to consider only stations whose quality measures up to a certain minimum standard that are explained in the following. [4]

4.2.2 Correlation with the open ocean

One important constraint in the selection of tide gauges was to include only data from station which show a medium to good correlation with the measurements at the next grid point. As will be shown in 6.1.1, this has proven to have a major influence on the quality of the reconstruction. This constraint of course limits the eligible tide gauges to those where data is available for the validation period (1994-2001), and a correlation coefficient (Pearson) could be determined.

Also, the geographical position of the tide gauges and their next altimetry grid points was checked carefully to make sure that the next grid point with the best correlation lies in the open ocean. One counter-example here is Tofino (PSMSL 822/116), where the grid point with the best correlation coefficient haphazardly lies just off Hernando Island, secluded within a bay 118km away from the tide gauge.

[4]Since the OI(C) solution is linear in the tide gauges, another possibility would have been to include into the reconstruction as many tide gauges as possible, whether there be GPS stations nearby or not, and only consider the difference in the resulting trends when comparing GIA and GPS corrections.

Generally, Douglas [12] and other authors have advised against the use of tide gauges located in bays and estuaries, because the behavior of such a tide gauge may not have a lot in common with the open ocean. Still, historically, a large number of tide gauges have been put up in estuaries and bays. In this study, we are confident that checking for homoscedasticity and correlation puts us on the safe side in this respect.

The sea level anomalies are extracted from the tide gauges by subtracting a long-term point-wise mean from the time series. To avoid a "hockeystick" effect [38], we take the mean over the same period that has been applied in the calculation of the radar altimetry sea level anomaly fields, i.e., the 1994-2001 period.

Coastal surge: variance of tide gauge data It has been mentioned before that the OI(C) algorithm was originally developed for the reconstruction of sea surface temperatures, not sea levels. An important aspect for the reconstruction of sea level is the fact that, since tide gauges are mainly located on the coastline, the observations taken here will always include coastal effects like, e.g., wave and wind surge, but also self-oscillation effects in near shore areas (e.g., [24]). Close inspection shows that, even though the correlation with the next grid point in the open ocean may be excellent, very few tide gauges show a similar variance amplitude. In critical areas, where gauges are located in bays, or archipelagos, the variance of the tide gauge is enhanced up to 300% compared to the RA time series. Given the OI(C) algorithm's tendency to overfitting, this would advise one to discard the stations most affected by this problem (see also [12]). Then again, this would result in the rejection of some of the longest records with excellent data quality, like San Francisco (with a record length of over 150 years, from 1854-2008) or Tofino (over 60 years of continuous data from 1940-2008), an idea which, given the scarcity of long records, is prohibitive.

Still, the problem persists, and we will show in Chapter 6.1.1 that the inclusion of a bad quality stations is likely to do more harm than good in the reconstruction, especially if the tide gauge and TOPEX/Poseidon measurements are strongly heteroscedastic.

The Levene test [25] is a modified T-Test to determine whether samples from two different populations have the same variance. In Table 1, test results for the stations used in the 1970-1990 reconstruction are given. A test result below 0.2 indicates that the variances from the TOPEX/Poseidon data set and the tide gauge data set are not equal.

One possible countermeasure for the problem of dissimilar variances would be to scale the records according to the variance measured by the TOPEX/Poseidon altimeter in cases where the Levene test for homoscedasticity fails. This results, of course, in the loss of data for the respective coastal areas in the reconstruction. In this study, this correction has not been applied so as not to blur the trend estimates from the GPS/GIA corrections. Tests have shown, however, that the correlation and the reproduction of the seasonal cycle will benefit from the scaling.

GPS Station	**Name**	**PSMSL ID**	**Levene test (p-value)**	**equal variances ?**
ABER	ABERDEEN	170/011	0.2041	yes
BRMU	BERMUDA	950/011	0.0130	no
BRST	BREST	190/091	0.2042	yes
CHA1	CHARLESTON, COOPER RIVER	960/041	0.0005	no
COCO	COCOS ISLAND	680/521	0.0008	no
CRO1	ST. CROIX	939/011	0.1229	yes
GALA	GALAPAGOS	845/031	0.4274	yes
GUAM	GUAM	701/001	0.2024	yes
HNLC	HONOLULU	760/031	0.0009	no
KIRI	KIRIBATI	730/008	0.2908	yes
MALD	MALDIVES	454/011	0.4438	yes
NPRI	NEWPORT	960/161	0.3470	yes
P101	OSHORO	641/042	0.0021	no
P110	KASHIWAZAKI	647/081	0.0127	no
P118	TAJIRI	647/047	0.0168	no
P123	AKUNE	645/045	0.2710	yes
P204	HAKODATE I	641/031	0.7867	yes
P205	OFUNATO	642/022	0.7733	yes
P207	TOYAMA	647/068	0.0073	no
P208	KUSHIMOTO	642/141	0.8177	yes
P209	HAMADA II	647/023	0.1079	yes
P211	ABURATSU	645/021	0.3347	yes
PALA	PALAU	711/021	0.0610	yes
PERT	PERTH	680/472	0.0000	no
PLUZ	PUERTO DE LA LUZ	370/041	0.0061	no
POHN	POHNPEI	710/031	0.3164	yes
SEAT	SEATTLE, PUGET SOUND	823/011	0.0009	no
SIO3	LA JOLLA	823/071	0.0143	no
THTI	TAHITI	780/011	0.4063	yes
TSEA	ACHORAGE	821/012	0.0001	no
TUVA	TUVALU	732/011	0.2536	yes

Table 1: The Levene test shows strongly dissimilar variances for a large part of the tide gauges used in the 1970-1990 reconstruction in Section 6.

5 GPS corrections for land movement processes

5.1 Introduction

Tide gauges are located at shore, and, therefore, affected by land movement. This constitutes a major drawback when measuring sea level with tide gauges. When trying to separate land movement from actual changes in sea level, the lack of quantitative data has restrained researchers to mere qualitative interpretation —to put it more severely, to informed guesswork —in this task. Tide gauge data evidently affected by land movement had to be ignored in reconstructions, constituting a painful loss of data given the already scarce availability of long time series.

Today, a growing network of GPS-stations located at or near tide gauges (e.g., the TIGA (GPS Tide Gauge Benchmark Monitoring - Pilot Project) network [31]) makes it possible to quantify land movement processes and incorporate this information into sea level change prognosis. Although land movement occurs in all directions, in this study, we limit ourselves to vertical land movement only.

A broad variety of scientific results based on individual TIGA solutions (e.g., [35], [36], [15], [30], [41], [42]) as well as other solutions ([34], for British tide gauges) have already been published. In their study on North American tide gauges, Snay et al. [33] apply a combination of different solutions obtained by taking a simple arithmetic mean. In this study, we use a rigorous combination of the six TIGA solutions.

The causes for land movement are manifold, as are the time scales on which they occur. Long-term geological processes include plate movement stemming from tectonic activity. Here, a special case is the post-glacial rebound or glacial isostatic adjustment (GIA), a term describing the viscous reaction of the Earth mantle following the melting of ice sheets after the last glacial period. This process affects mainly areas where northern Europe (especially Scotland, Fennoscandia and northern Denmark), Siberia, Canada, and the Great Lakes of Canada and the United States, whereas other areas are less affected. The effect of the GIA has been quantified in various models. In this study, we use the GIA data for tide gauges from Peltier's VM2 model [26] as provided by the PSMSL database.

Earth quakes or land slide events, which occur instantaneously and cause a sudden jump in the time series, can usually be quite easily identified from the data. However, their repercussions —like, e.g., changes in plate movement —are usually very hard to identify, much less quantify.

In the recent century, a major part of land movement processes stems from anthropogenic causes. These include mainly groundwater and hydrocarbon extraction, but also, e.g. harbor construction work.

5.2 Land movement caused by GIA

In the northern Canada region, GIA models and GPS corrections tend to match very well. One prominent example is the tide gauge at Churchill (PSMSL 970/141), where a massive uplift can be observed over the whole period covered by the PSMSL data (1940-2007). Here, Peltier's VM2 model [26] gives a trend of 11.81 mm/yr, only slightly stronger than the actual trend of the tide gauge at 9.71 mm/yr. The GPS observations arrive at a trend of 9.52 mm/yr.

It is clear from these figures that most of the observed sea level drop at Churchill is actually caused by

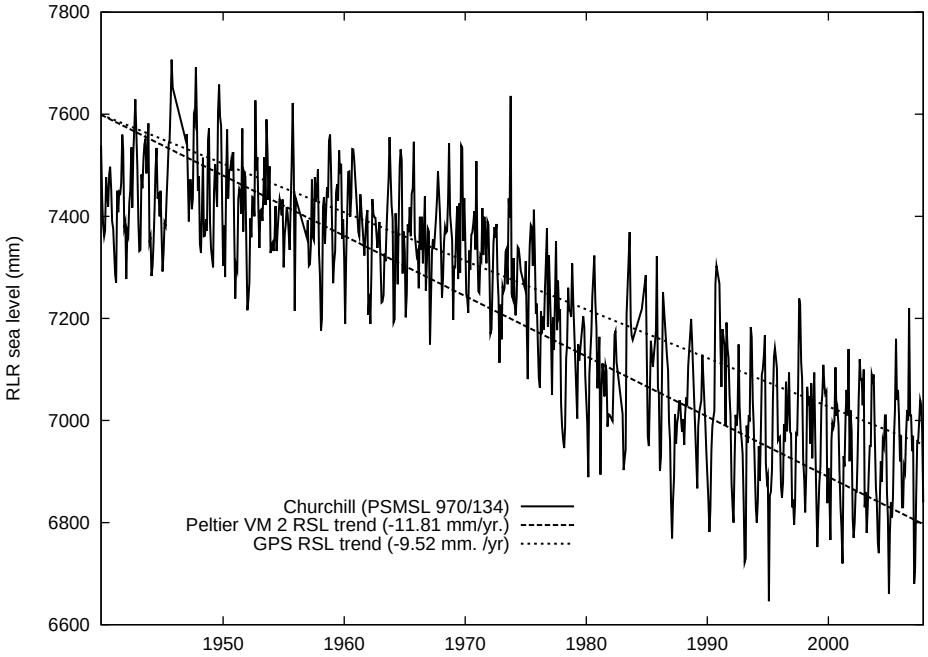

Figure 3: The tide gauge at Churchill (PSMSL 970/141) shows a good agreement between tide gauge trend, GIA model trend and GPS trend.

an uplifting tide gauge, and highly probable that, in large part, this uplift is due to post-glacial isostatic adjustment processes.

One of the main goals of this study is to correct trends in sea level which stem from land movement processes that are not covered by GIA models.

5.3 Land movement from anthropogenic causes

Charleston I (PSMSL 960/041) in South Carolina (USA) is one example where a strong sea level rise is observed (3.14 mm/yr from the tide gauge); however, only 0.83 mm/yr (in relative sea level rise) are caused by GIA ([26]). It has, however, long been suspected that the area is affected by subsidence caused by groundwater extraction ([10]). Here, the GPS trend reveals a strong subsidence signal of -4.61 mm/yr, suggesting that one may actually be faced with a decrease in sea level, which is completely covered up by the strongly subsiding gauge.

5.4 Diametrical observations in land movement processes

In quite a few cases, land movement signals cannot be viewed from the tide gauge time series as easily as the above examples suggest.

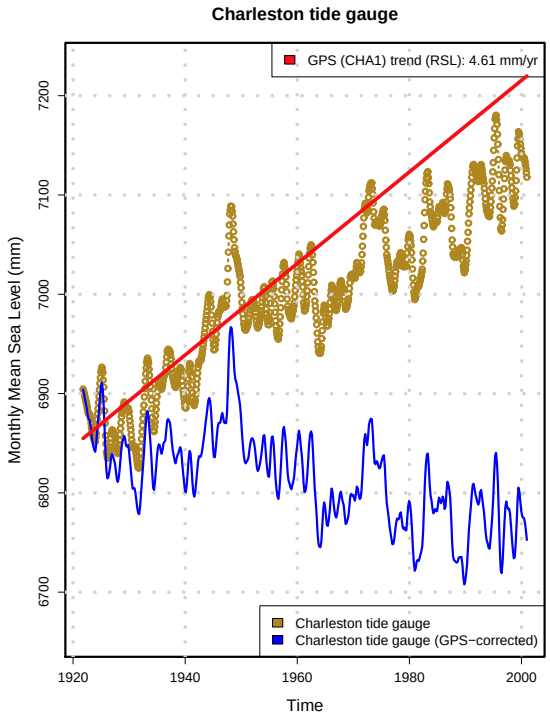

Figure 4: The rise in sea level at Charleston I tide gauge (PSMSL 960/041) is mostly caused by subsidence due to anthropogenic influences (Shown here are the deseasonalized original and the GPS-corrected time series).

Over the period of time covered by the tide gauge data, various processes may have occurred, and their retrospective separation may prove rather difficult.

Isoda et al. [16] have remarked that the Kushimoto tide gauge (PSMSL 642/141), although located on the (uplifting) Eurasia plate, shows a strong positive linear trend in sea level. Emery and Aubrey ([13]) suspect submergence caused by groundwater extraction. It is unclear what may have caused the sharp drop in sea level in the first half of the 1980s. From 1985 onwards, the trend is 7.05 mm/yr. Indeed, the GPS trend shows a massive subsidence signal of -7.29 mm/yr.

Here, is is evident from the tide gauge time series that the GPS trend, derived from a period of 4.7 years, is a fairly recent development, and should hence not be applied over the whole length of the 51-year tide gauge time series.

5.5 Co-location and distance

The distances between tide gauge and GPS stations used in this work range from zero (directly co-located stations) to 7400 m.

It is difficult to give an exact numerical limit for the distance between GPS station and tide gauge.

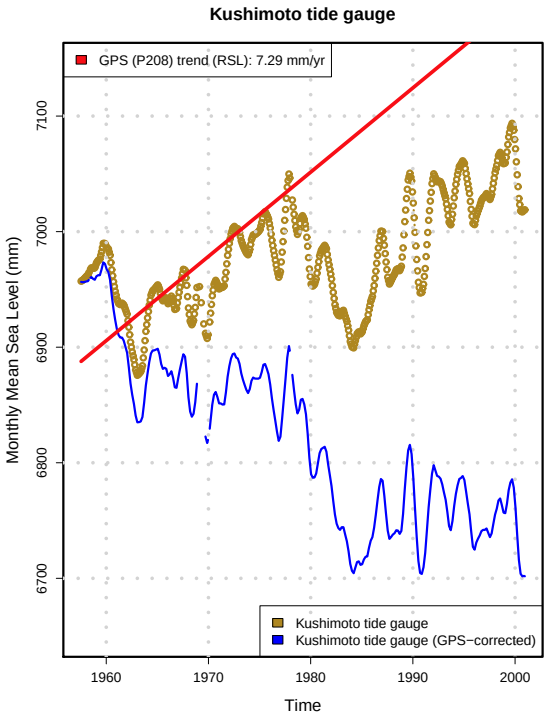

Figure 5: The observed sea level rise at Kushimoto tide gauge (PSMSL 642/141) is caused by strong subsidence starting around 1985, approximately. Events that have occurred before this date can obviously not be quantified by projecting the GPS trend further into the past.

Obviously, the ideal case is direct co-location, as even closely located stations may be subject to different land movement processes. This is especially true for regions where anthropogenic processes play a role, as the effects of these tend to be rather local. The specific conditions at the stations must be taken into account. A large distance between gauge and GPS station can work out perfectly fine, while the benefits of a small distance can be covered up if the station is subject to strongly local effects.

One prominent example is the tide gauge at Manila Harbour (Figure 6). Douglas ([12]) remarked that this station, with a record of over 100 years, shows a major rise in sea level from 1960 on. The moderate upwards trend of 2.12 mm/yr (1900-1959) jumps to an improbable 15.37 mm/yr (1960-2007), strongly suggesting subsidence by anthropogenic causes. Indeed, several authors mention harbor construction work as well as intensified groundwater extraction in the whole Manila Bay area. The PIMO GPS station at Manila Observatory, although located in the Manila metropolitan area at approximately 13 km distance, is apparently largely unaffected by this process, showing even a minor uplift trend of 0.49 mm/yr. One possible, alternative explanation is that the sea level rise is caused not by subsidence, but by sedimentation. This would also explain why it is not mirrored by the GPS station.

On the other hand, the process at tide gauge at Ratan (PSMSL 050/191) (Figure 7), which shows a

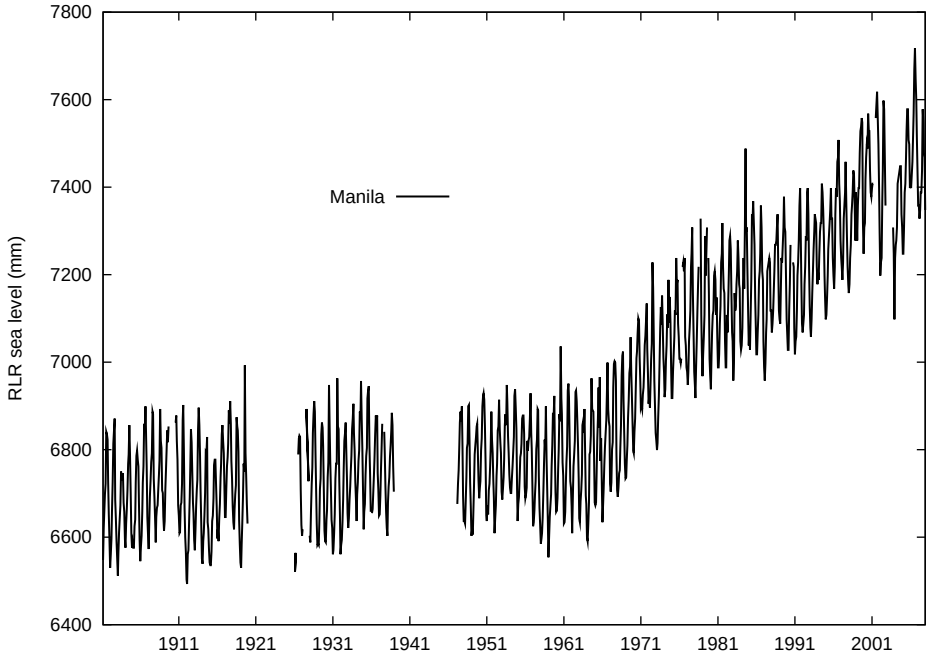

Figure 6: At Manila Harbor, the strong subsidence visible in the tide gauge time series is not detected by the GPS station at a 13 km distance.

major GIA-related uplift of 7.71 mm/yr (1892-2008), is covered very well by the MAR6 GPS station at Maartsbo (6.85 mm/yr), even though it is —like in the Manila case —located at approximately the same (11 km) distance.

For this reason, the TIGA project has refrained from putting up distance limits when including tide gauges with co-located GPS stations into their network, but has instead focused on levelling criteria [31].

5.6 GPS Time series quality

5.6.1 Time series length & consistency

The GPS corrections used in this study, provided by Daniela Thaller (University of Bern, personal communication), are obtained by a rigorous combination of six different weekly solutions from the following TIGA analysis centers (TACs):

ULR University La Rochelle (ULR), France (global network)

DGF Deutsches Geodätisches Forschungsinstitut (DGFI), Germany (regional network for the Atlantic region)

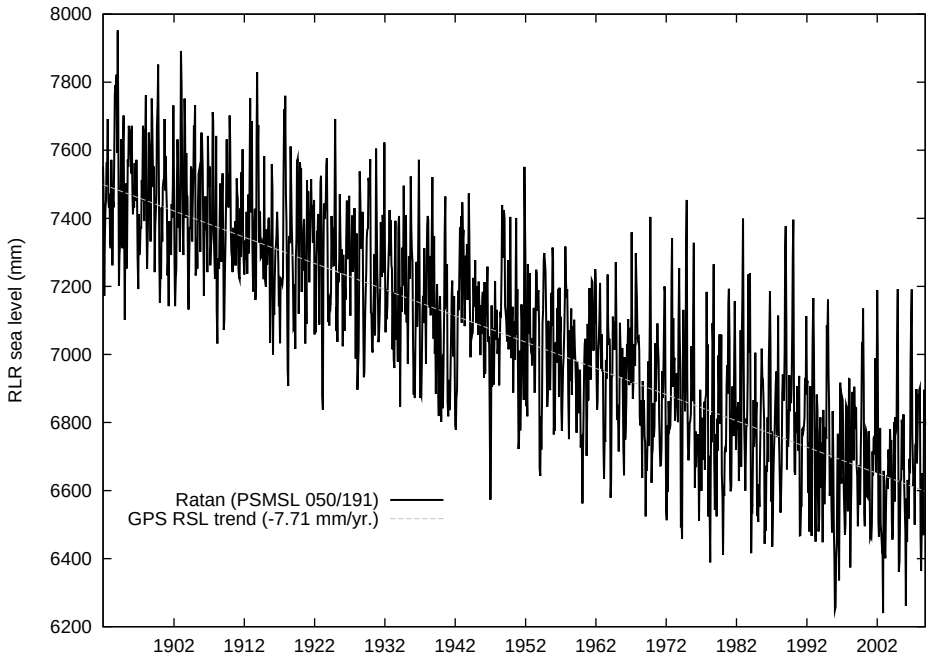

Figure 7: In the coastal area of the Gulf of Bothnia, a strong but comparably homogeneous, steady land movement rate of approximately 7 mm/yr is observed. As a result, at Ratan tide gauge, the land movement signal taken from the MAR6 station is reproduced nicely despite the very large distance between tide gauge and GPS station (> 380km).

ETG EUREF (combination of individual contributions by Bundesamt für Kartographie und Geodäsie (BKG), Frankfurt, Germany) (regional network for Europe)

GFT GeoForschungsZentrum Potsdam (GFZ), Germany (global network)

AUT GeoScience Australia, Geodetic Division, Australia (regional network with Antarctica, Australia, and Pacific region)

CTA University of Canberra, University of Tasmania, and Australian National University, Australia (regional network for Antarctica and Australia)

Details concerning the combination are contained in [31]. Following the recommendations by Blewitt and Lavallée [3], only trends from stations with time series longer than 2.5 years are used. In addition to this, we use only data from stations where the ratio of gaps to time series length is less than 20 percent. Several stations showing unexplained trend changes and jumps were discarded. One major source of error in GPS time series are (undocumented) antenna changes. Of course, also earthquakes result in major jumps in the time series. A rare example is North Shields (NSTG), where, apparently, for a few years' time, the GPS signal was disturbed by regular harbour crossings of a pilot boat carrying a radio receiver

(N. Teferle, personal communication). Other inconsistencies have in the past occurred in processing, especially due to ambiguous naming of stations.

All trends used in this study have been carefully examined for consistency. Wherever possible, the likely causes for trend changes are given in the comments for the individual stations.

5.7 Application of GPS corrections

When dealing with long-term land movement processes, it is hardly ever possible to pinpoint the exact date when the process started. This does not pose a problem if the land movement process occurs on time scales significantly larger than the reconstruction period or the length of the time series (e.g., for processes like GIA). Many anthropogenic land movement processes, however, have started, or increased, during the reconstruction period (1970-1990), parallel with the increasing technical possibilities for, e.g. large-scale hydrocarbon extraction, or similar human interference with the ecosystem. Therefore, a decision must be made regarding the point in time from which on the GPS trend correction should be applied to the tide gauge time series. Given the difficulty of separating different land movement processes, an individual assessment of the trends at different tide gauges seems the most sensible approach.

In Table 2, all stations used for the 1970-1990 reconstruction are given with their GPS and GIA land movement trends, length of the GPS time series and the weighted RMS values of the GPS vertical displacement.

In the following, the GPS corrections for all stations are specified in detail. A plot of the respective uncorrected and corrected time series is given for each station. For the examination of trend changes, the seasonal Mann-Kendall test ([22])was used. This test is a nonparametric rank test which assigns a value of 0 (no trend) to ± 1 (strong trend) to a time series when a trend is detected. The seasonal cycle has been removed in the plots using the STL algorithm [8], a Seasonal Trend Decomposition aglorithm based on Loess. The algorithm decomposes the time series into a seasonal component using multi-year monthly means, a nonlinear trend, and a remainder. The linear relative sea level trend is also depicted.

GPS ID	Name	PSMSL ID	GPS trend (mm/yr)	WRMS	TS length (yrs)	GIA trend (mm/yr)
ABER	ABERDEEN	170/011	1.13	4.47	9.26	0.89
BRMU	BERMUDA	950/011	0.02	4.91	9.77	-1.05
BRST	BREST	190/091	-1.03	5.34	9.16	-0.28
CHA1	CHARLESTON	960/041	-4.61	16.98	5.65	-0.83
COCO	COCOS ISLAND	680/521	-0.31	7.25	9.77	-0.09
CRO1	ST. CROIX	939/011	-1.57	5.81	7.12	-0.25
GALA	GALAPAGOS	845/031	-0.10	4.52	4.64	0.16
GUAM	GUAM	701/001	-1.08	5.73	7.66	0.24
HNLC	HONOLULU	760/031	-0.38	5.19	8.64	0.16
KIRI	KIRIBATI	730/008	-0.31	5.23	5.41	0.12
MALD	MALDIVES	454/011	-2.69	7.62	6	0.22
NPRI	NEWPORT	960/161	-0.10	4.14	8.14	-1.76
P101	OSHORO	641/042	-1.13	6.48	4.56	0.60
P110	KASHIWAZAKI	647/081	-1.08	4.3	4.04	0.73
P118	TAJIRI	647/047	-1.07	4.52	4.52	0.64
P123	AKUNE	645/045	-1.33	8.58	4.54	0.56
P204	HAKODATE I	641/031	0.00	4.73	4.69	0.61
P205	OFUNATO	642/022	-4.58	4.88	4.54	0.62
P207	TOYAMA	647/068	-1.38	5.21	4.56	0.71
P208	KUSHIMOTO	642/141	-7.29	4.91	4.73	0.60
P209	HAMADA II	647/023	-1.89	3.96	4.52	0.66
P211	ABURATSU	645/021	-1.72	4.85	4.58	0.53
PALA	PALAU	711/021	0.30	5.26	6.54	0.19
PERT	PERTH	680/472	-5.89	5.61	9.58	-0.01
PLUZ	Puerto de la Luz	370/041	-2.39	3.78	3.31	-0.15
POHN	POHNPEI	710/031	-0.43	5.23	4.64	0.15
SEAT	SEATTLE	823/011	-1.15	7.29	9.32	-1.31
SIO3	LA JOLLA	823/071	-0.36	5.44	7.98	-0.50
THTI	TAHITI	780/011	-2.50	6.39	8.43	0.22
TSEA	ACHORAGE	821/012	4.79	8.29	8.49	0.19
TUVA	TUVALU	732/011	0.31	4.83	6.08	0.06

Table 2: Stations used in the 1970-1990 reconstruction with GPS ID, station names and PSMSL ID. The vertical GPS trends and their respective WRMS values, the length of the GPS time series in years and the respective GIA corrections are given for comparison.

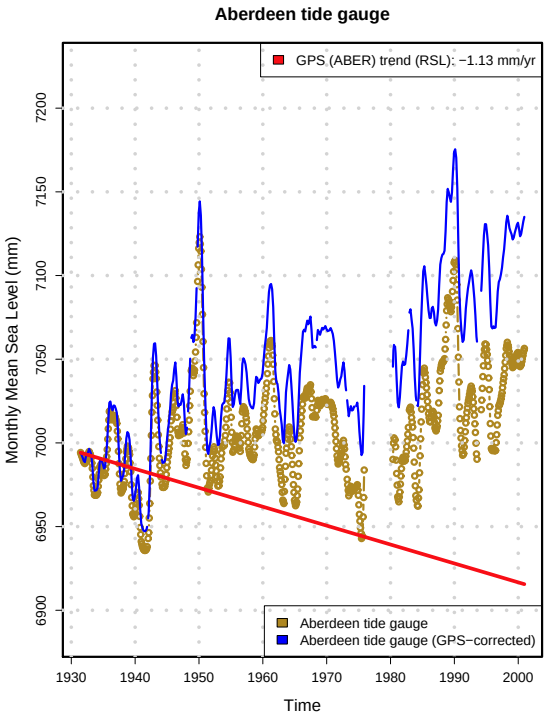

Figure 8: **Aberdeen (PSMSL 170/011)** While the tide gauge shows a steady sea level rise starting in 1980 (following a gap in the series), the GPS signal suggests a slight uplift (1.13 mm/yr). This is also in accordance with the 0.83 mm/yr uplift predicted by Peltier's VM2 GIA model as well as the result (1.0 ± 0.2mm/yr) from Teferle et al. in [34].

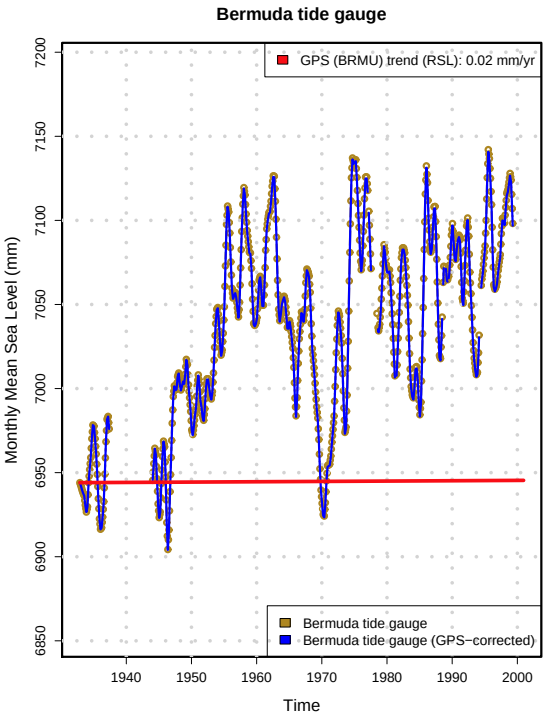

Figure 9: **Bermuda (PSMSL 950/011)** The station shows no clear trend changes, but a steady sea level rise. Events in 1970 and 1985 remain unexplained. It should be mentioned that the Bermuda earthquake of 1978 is not visible in the time series. It is suspected that the GPS trend (0.02 mm/yr) underestimates the true extent of the uplift at the tide gauge.

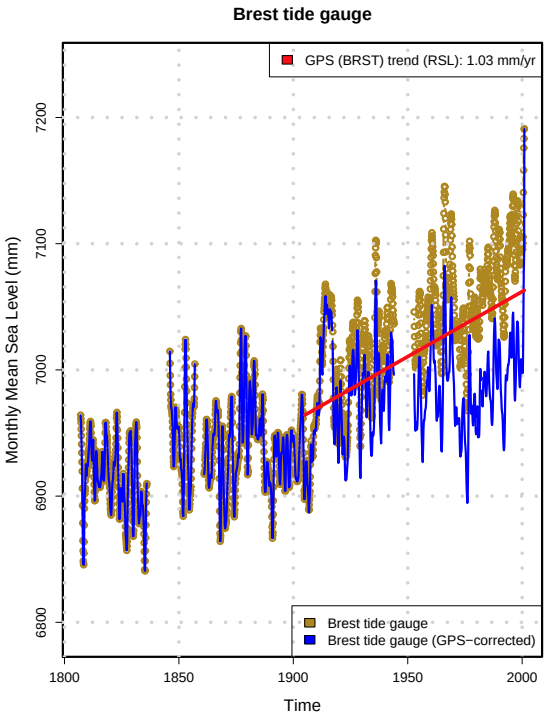

Figure 10: **Brest (PSMSL 190/091)** Subsidence at this exceptionally long record starts at 1905, with a τ value of 0.02 for the 1807-1904 series compared to $\tau = 0.421$ for the complete series. The GPS correction (-1.03 mm/yr) is applied from 1905 on.

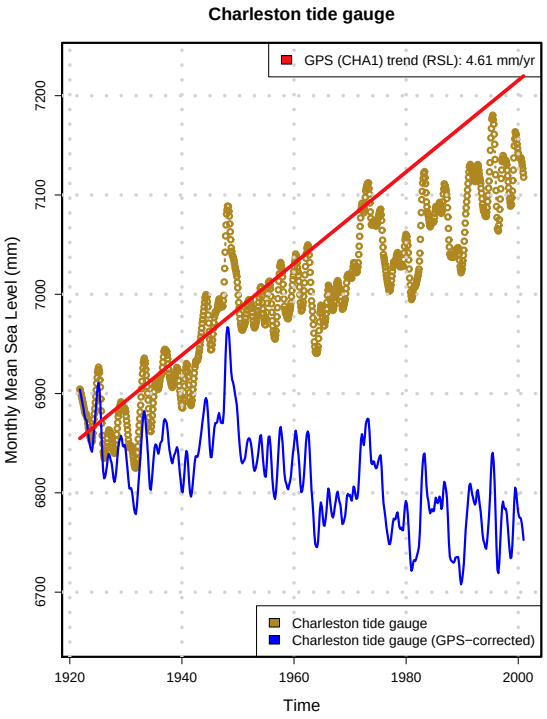

Figure 11: **Charleston (PSMSL 960/041)** The sea level rise at Charleston is to large extend caused by subsidence of the tide gauge. A comparison with the uncorrected time series shows that GPS trend of -4.61 mm/yr probably overestimates the trend. The comparably high WRMS value (see Table 2) is also an indication that trend results from single solutions may vary at this station. The tide gauge, however, does not show an increasing trend over the operation period of the GPS; rather, the opposite is the case. For now, we decide to apply the trend over the whole period covered by the time series, however expecting the GPS trend to decrease in a combination from a longer time series.

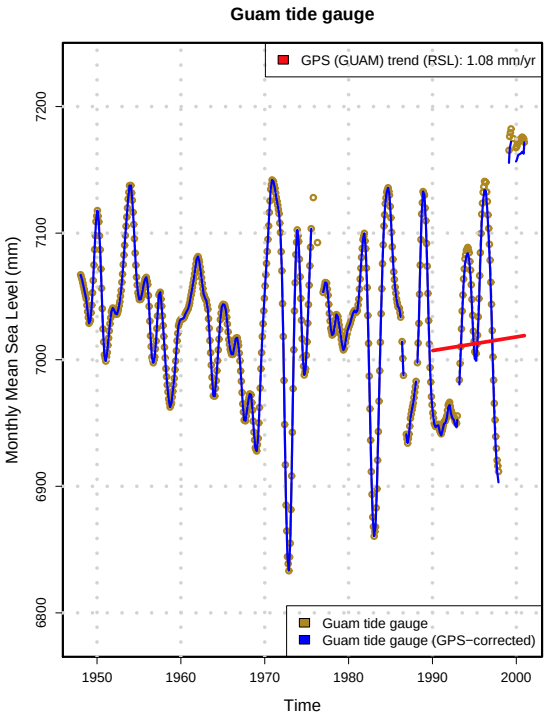

Figure 12: **Guam (PSMSL 701/001)** This station shows strong sea level rise from 1990 on. The seasonal Mann-Kendall test gives an in creased τ of 0.513 for the 1990s-time series, compared to 0.155 for the whole time series. The GPS trend is applied from 1990 on.

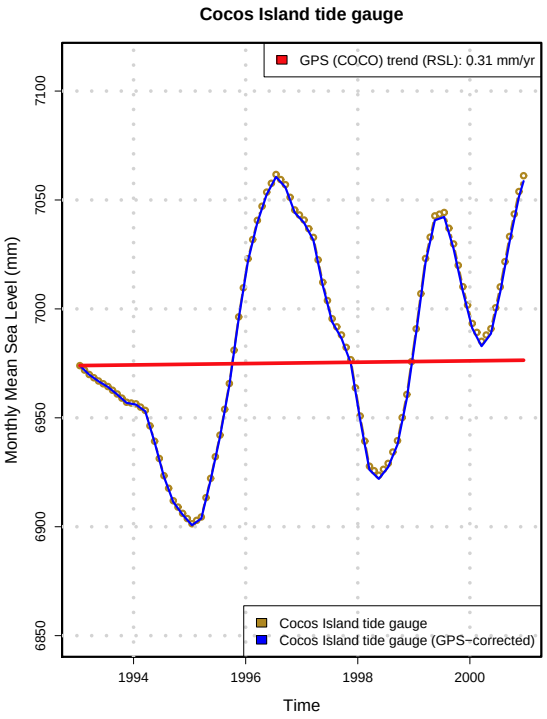

Figure 13: **Cocos Island (PSMSL 680/521)** This station shows strong IOD-related signals, but no distinct trend changes. A slight subsidence correction (-0.31 mm/yr) is applied from the beginning of the series on.

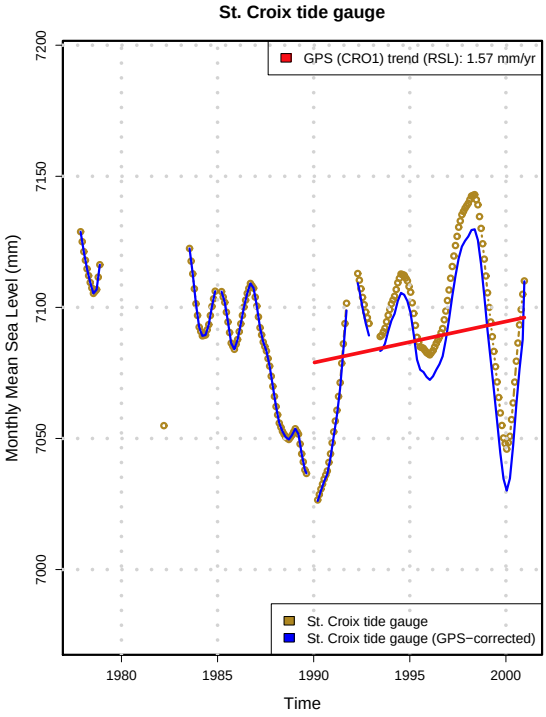

Figure 14: **St. Croix (PSMSL 939/011)** The deseasonalized tide gauge shows a slight subsidence signal starting approximately around 1990. The GPS correction (-1.57 mm/yr) is applied from this time on.

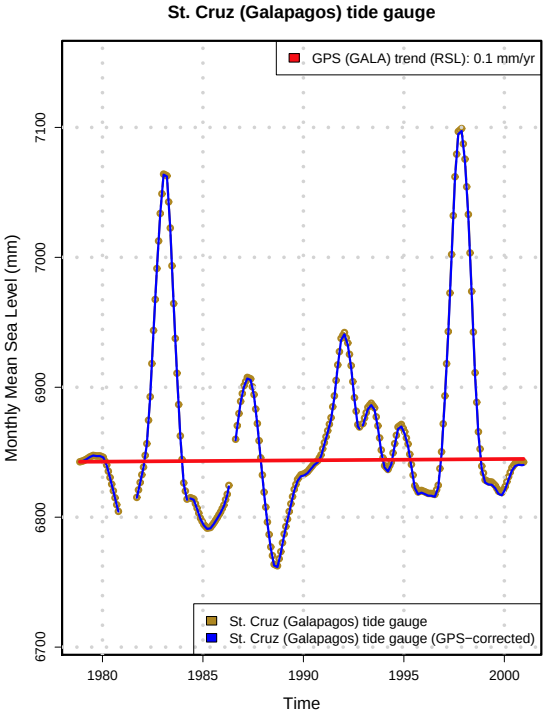

Figure 15: **Santa Cruz (845/031)** As expected, the station located on the Galapagos Islands shows strong El Niño-related signals. No trend changes are observed. A slight subsidence correction (-0.10 mm/yr) is applied from the beginning of the series on.

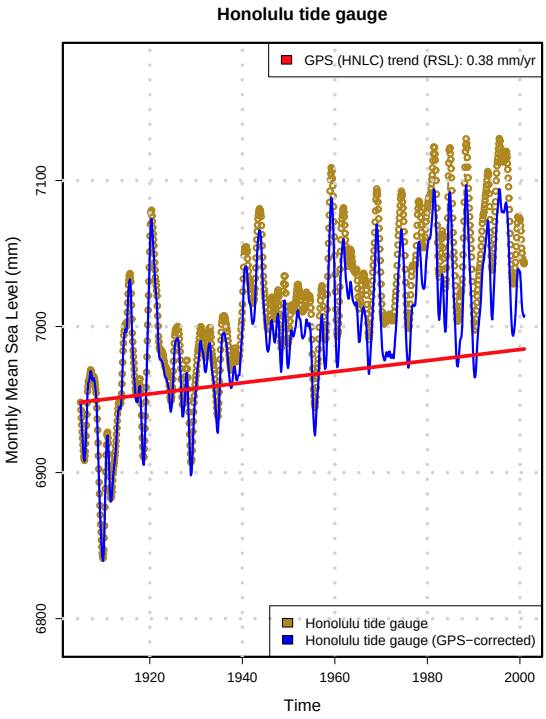

Figure 16: **Honolulu (PSMSL 760/031)** A long record showing a moderate but steady sea level rise that can, in part, be explained by slight subsidence (-0.38 mm/yr). The correction is applied from the beginning of the series on. Data from the adjacent Hawaiian island Kaua'i (KOKB, Kokee Park) is not used, since the GPS and tide gauge stations are located on opposite sides of the island, and the GPS trend is not visible in the tide gauge time series.

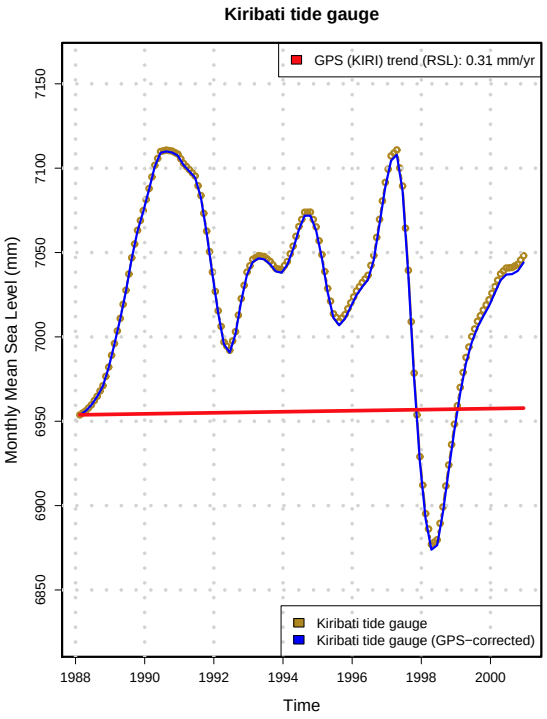

Figure 17: **Tarawa / Kiribati (PSMSL 730/008)** This tide gauge time series shows strong El Niño / IOD-related signals, but no distinct trend changes. A slight subsidence correction (-0.31 mm/yr) is applied from the beginning of the series on.

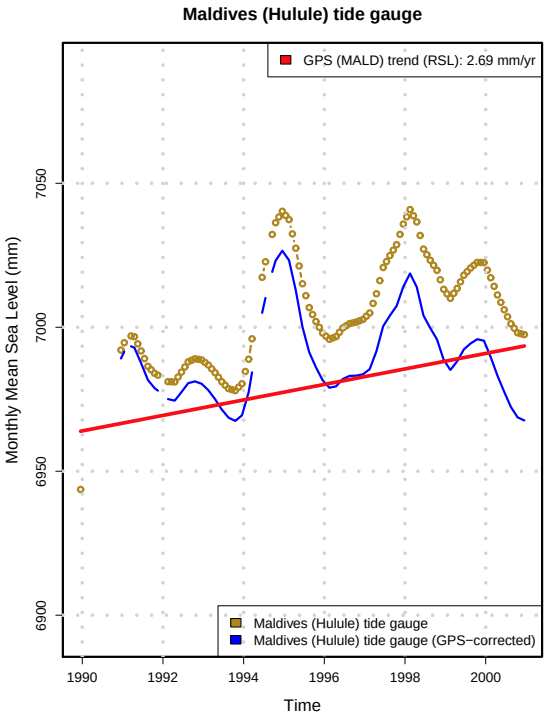

Figure 18: **Male-B (Maldives) (PSMSL 454/011)** No indication of a trend change. The GPS correction is applied over the whole time series. A closer look at the GFT solution for MALD suggests that the GPS trend of -2.69 mm/yr taken from the combination may be slightly too high.

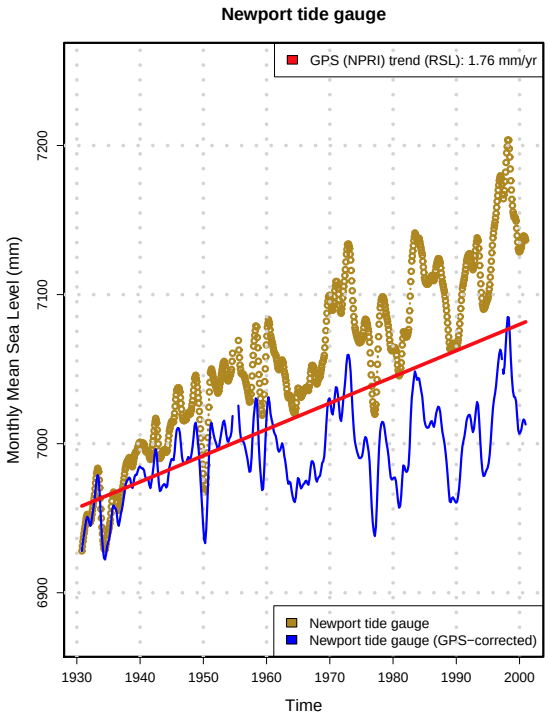

Figure 19: **Newport Rhode Island (PSMSL 960/161)** The strength of the well-documented ([9]) subsidence process at this station has decreased significantly over the last 10 years ($\tau = 0.615$ from 1930-2008, compared to $\tau = 0.222$ from 1999-2008). The GPS trend shows only moderate subsidence (-0.1 mm/yr). The GIA correction is applied for the 1930-1999 period, afterwards, the GPS correction is applied.

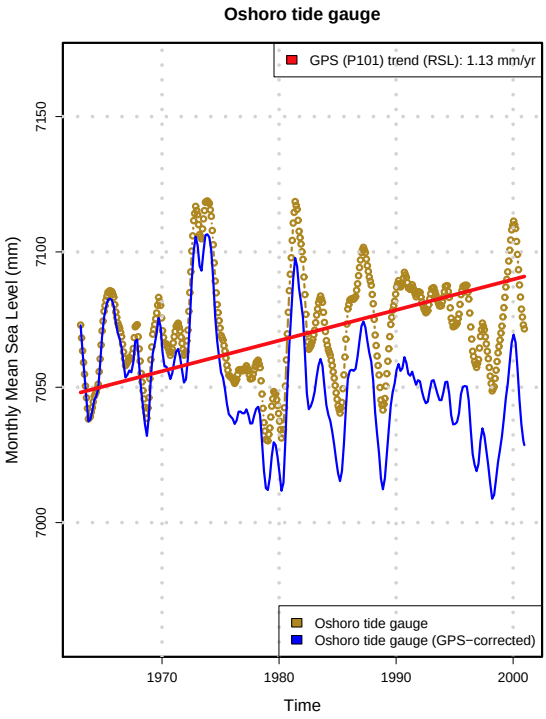

Figure 20: **Oshoro P101 (PSMSL 641/042)** A station with strong interdecadal signals but no distinct trend changes. The GPS correction (-1.13 mm/yr) is applied from the beginning of the time series.

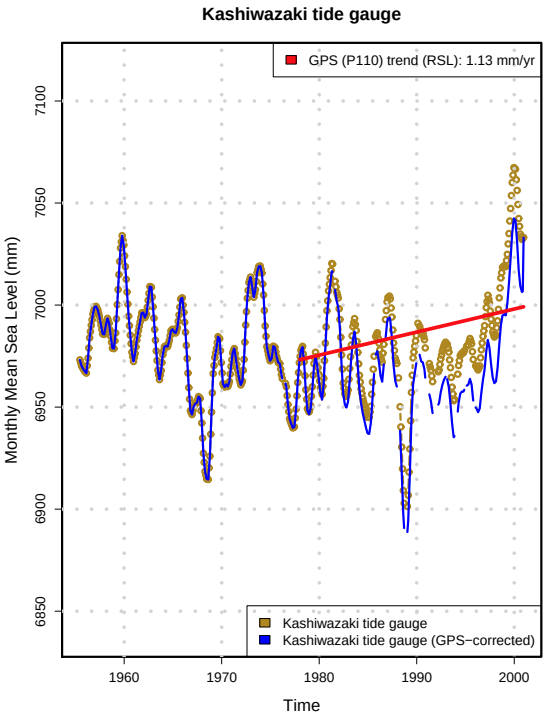

Figure 21: **Kashiwazaki P110 (PSMSL 647/081)** A station which shows moderate sea level rise from 1978 on. The seasonal Mann-Kendall test gives an in creased τ of 0.303 for the 1978s-time series, compared to 0.155 for the whole time series. The GPS trend (-1.08 mm/yr) is applied from 1978 on.

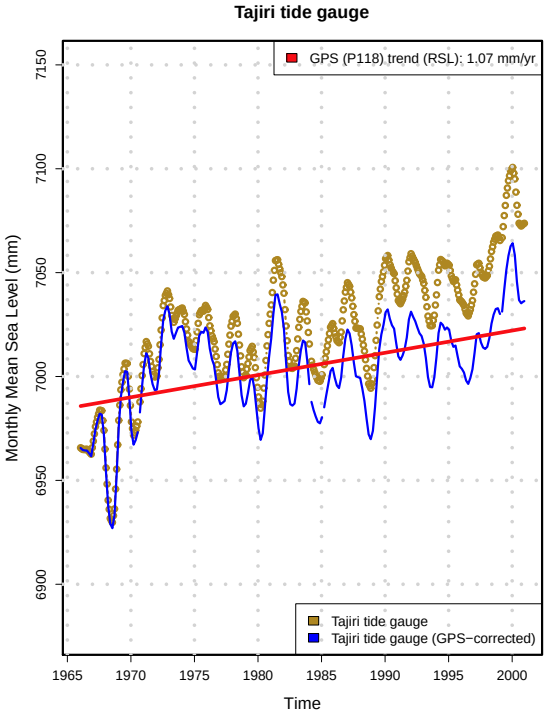

Figure 22: **Tajiri P118 (PSMSL 647/047)** The station shows a strong oscillatory pattern with an approximately 10 yr. frequency, overlayed by a slight subsidence signal. The GPS correction (-1.07 mm/yr) is applied from the beginning of the time series.

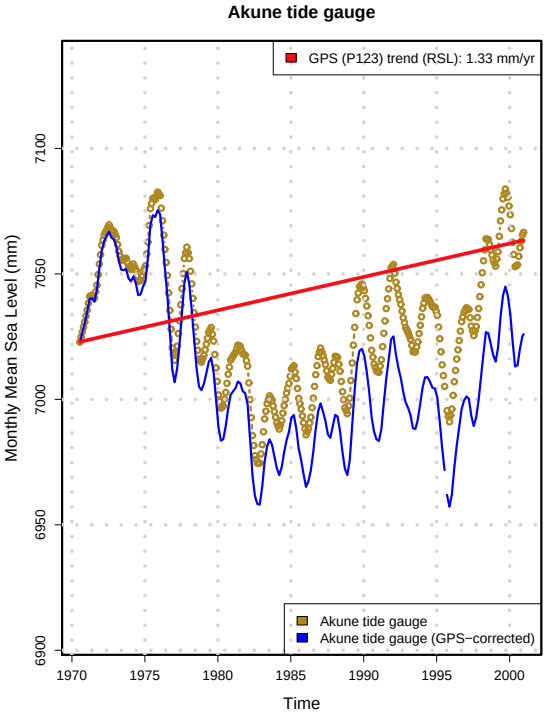

Figure 23: **Akune P123 (PSMSL 645/045)** The GPS correction (-1.33 mm/yr) is applied from 1983 on, where a distinct trend change is visible in the deseasonalized series.

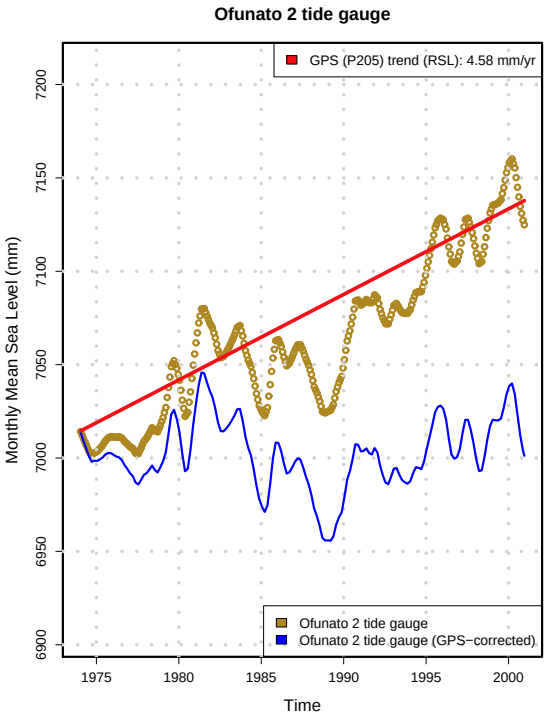

Figure 24: **Ofunato P205 (PSMSL 642/022)** The sea level rise is very well explained by the strong subsidence at Ofunato tide gauge (-4.58 mm/yr). The trend shows unexplained events around 1986 and 1989, but apparently, none of them is land movement related.

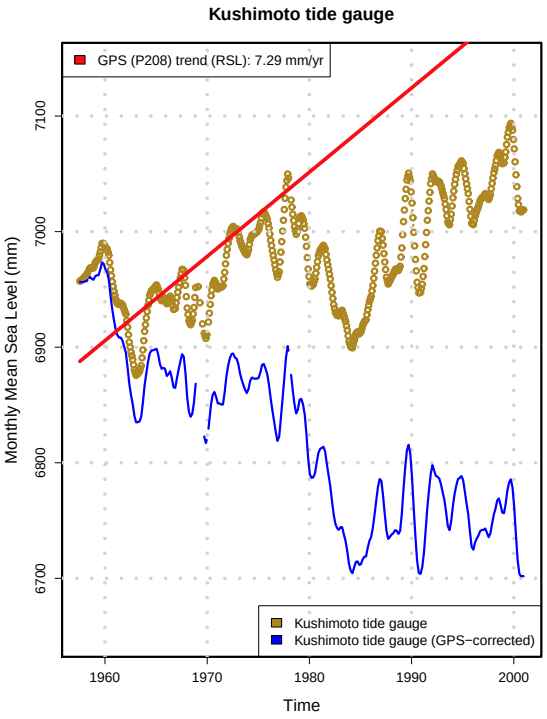

Figure 25: **Kushimoto P208 (PSMSL 642/141)** As discussed in Section 5.4. Kendall's τ increases from 0.383 to 0.454 when the time series is taken from 1985 on only. Hence, the correction is applied from 1985 on.

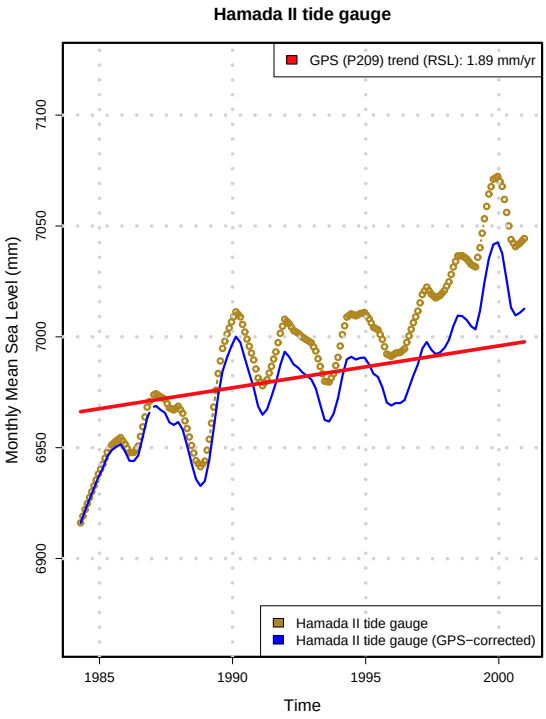

Figure 26: **Hamada II P209 (PSMSL 647/023)** The GPS trend of -1.89 mm/yr probably underestimates the trend of the tide gauge. A clear subsidence signal is visible throughout the whole series.

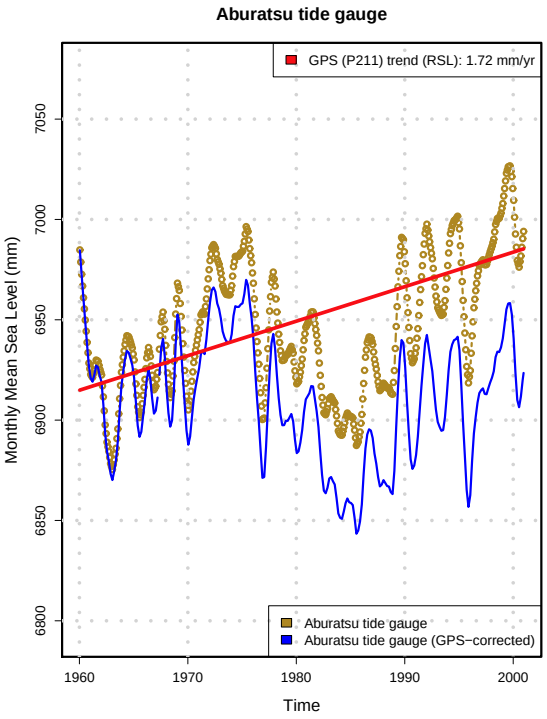

Figure 27: **Aburatsu P211 (PSMSL 645/021)** The station shows a strong oscillatory pattern with an approximately 25 yr. frequency, overlayed by a slight subsidence signal. The GPS correction (-1.72 mm/yr) is applied form the beginning of the time series.

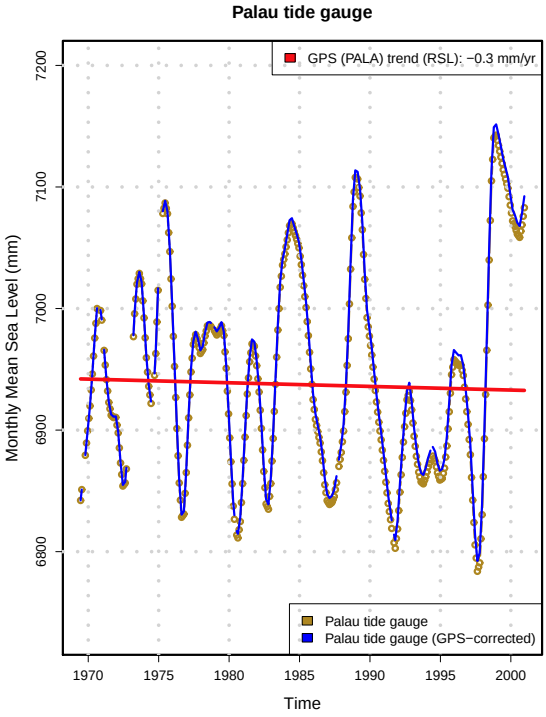

Figure 28: **Palau (PSMSL 711/021)** Like Cocos Island, the station shows strong IOD-related signals, but no distinct trend changes. A slight uplift correction (0.30 mm/yr) is applied from the beginning of the series on.

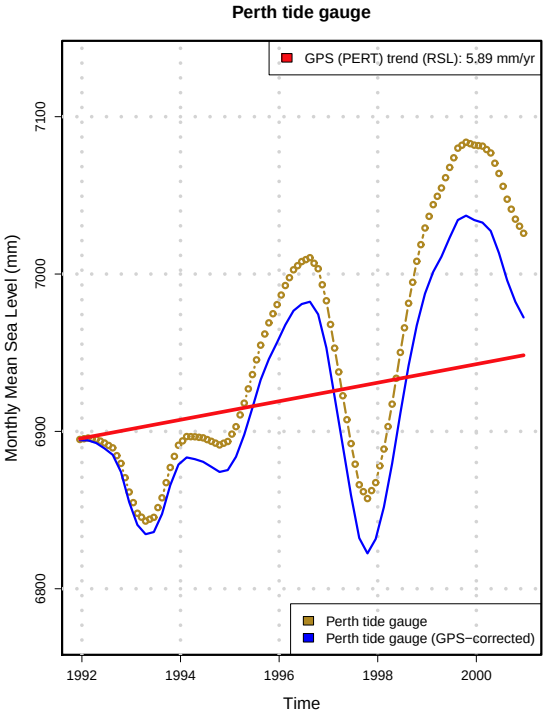

Figure 29: **Perth (Hillarys) (PSMSL 680/472)** The tide gauge shows strong El Niño signals in 1997/98 and 2002/2003, but no apparent jumps. A clear upwards trend is visible, only a part of which can be explained by subsidence. The comparison with TOPEX SLA data gives good agreement with no indicators of trend changes. Continuous subsidence from the beginning of the time series on (1992) is assumed.

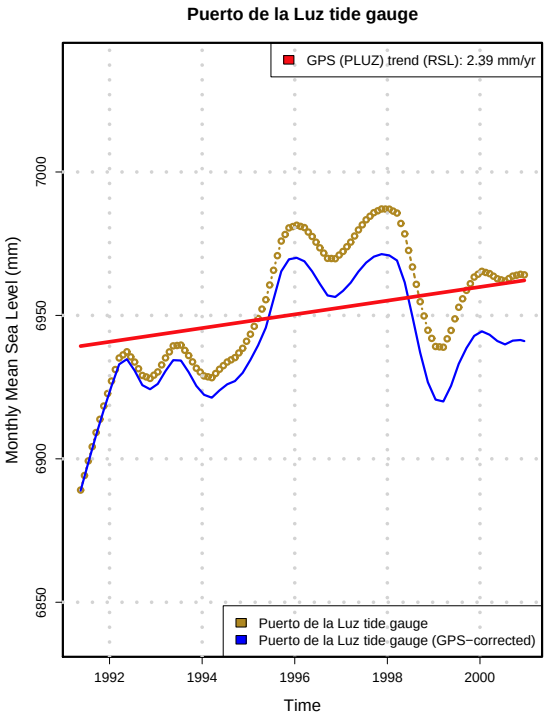

Figure 30: **Puerto de la Luz (PSMSL 370/041)** Here, the deseasonalized tide gauge time series (Figure 30) shows a steady upward trend from 1995 on, which agrees well with the subsidence signal from the GPS correction. The GPS correction (-2.39 mm/yr) is applied from 1995 on.

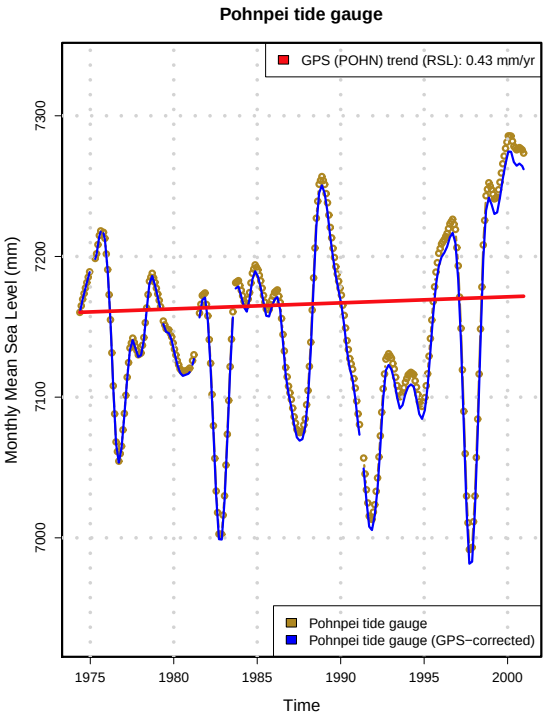

Figure 31: **Pohnpei (PSMSL 710/031)** A station with strong El Niño/IOD-related signals and a light sea level rise, but without any distinct trend changes. The GPS correction (-0.47 mm/yr) is applied from the beginning of the time series.

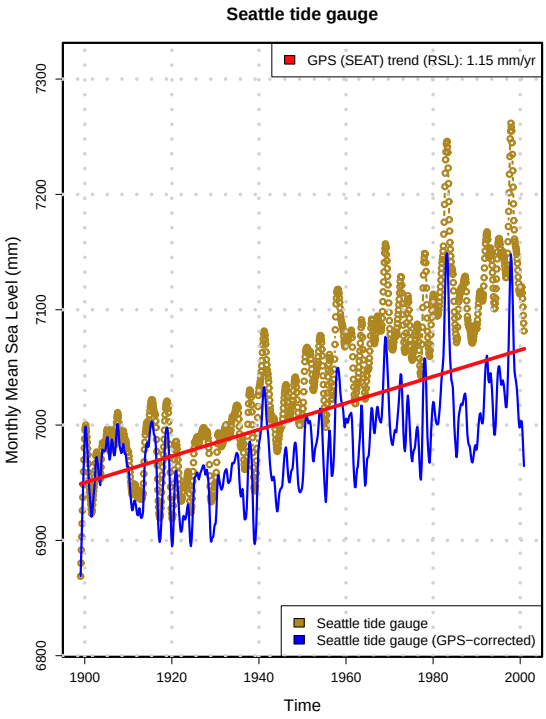

Figure 32: **Seattle (PSMSL 823/011)** The tide gauge shows a steady sea level rise that can be explained in part by steady subsidence of the station (-1.15 mm/yr). The correction is applied from the beginning of the time series.

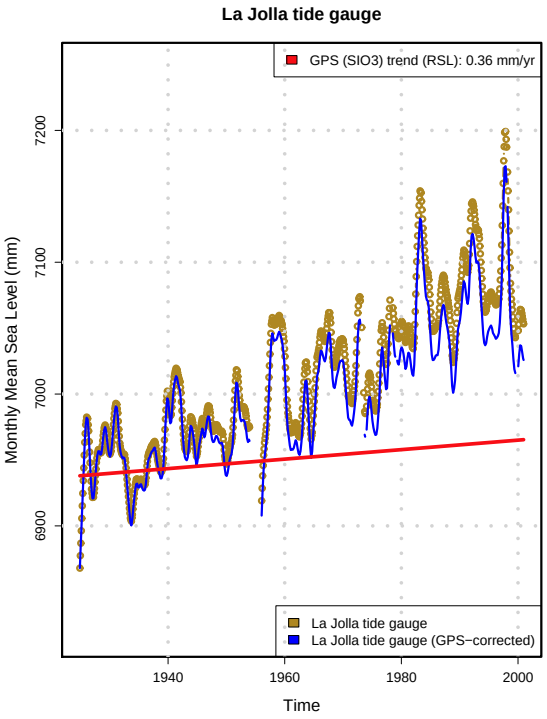

Figure 33: **La Jolla (PSMSL 823/071)** Very much like Honolulu; a long record showing a moderate but steady sea level rise that can, in part, be explained by slight subsidence (-0.36 mm/yr). The correction is applied from the beginning of the series on.

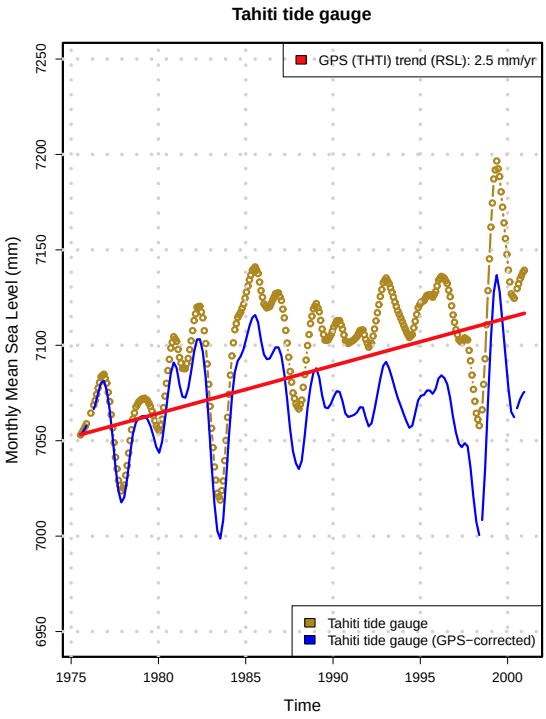

Figure 34: **Tahiti / Papeetee (PSMSL 780/011)** The tide gauge time series shows a constant rise over the whole period, with strong Niño signals in 1997/8 and (probably) 1983, but no apparent jumps or trend changes. The correction (-2.5 mm/yr) is applied from the beginning of the time series, completely eliminating the tide gauge's trend. The sea level rise at Papeetee can be explained by subsidence only.

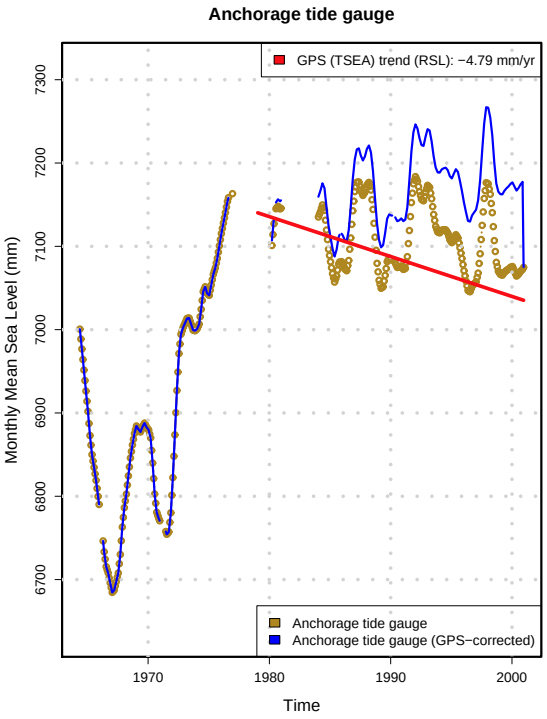

Figure 35: **Anchorage (PSMSL 821/012)** One of the main signals in the Anchorage tide gauge is tectonic activity caused by earthquakes in the region. Strong uplift dominates the signal from 1964 (Great Alaskan Earthquake) to 1965 (Rat Islands Earthquake); with equally strong subsidence following up to 1979 (St. Elias Earthquake), where the trend is stopped and replaced by a moderate uplift signal (see also [14]). The seasonal Mann-Kendall test gives $\tau = -0.429$ for the series starting in 1979 compared to $\tau = 0.278$ from the complete time series. Hence, the GPS correction (4.79 mm/yr) is applied from 1979 on.

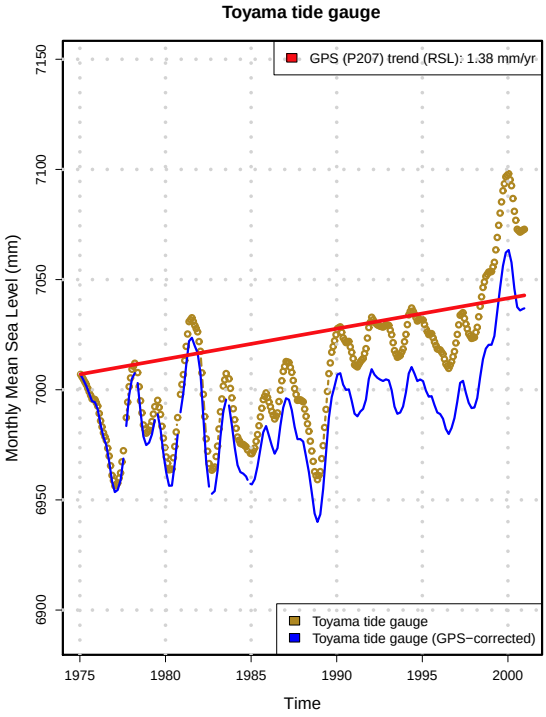

Figure 36: **Toyama P207 (PSMSL 647/068)** The station shows a clear uplift signal starting at 1990. The trend is applied from that time on.

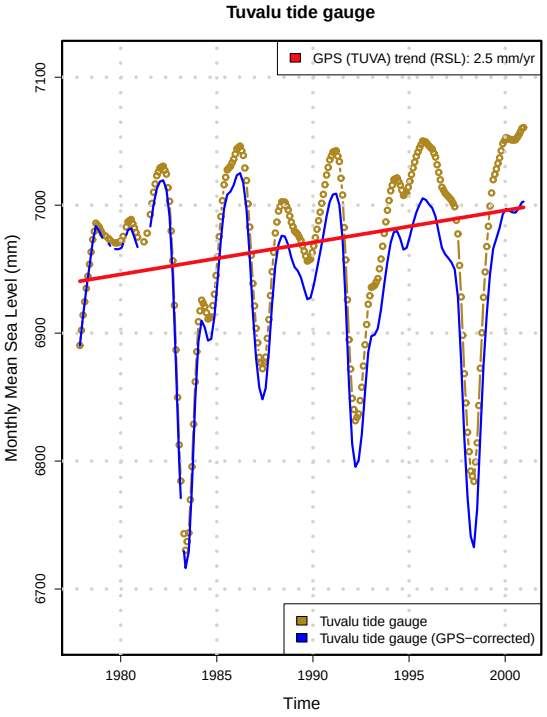

Figure 37: **Tuvalu (PSMSL 732/011)** A station strongly dominated by El Niño signals, but without any distinct trend changes. It should be mentioned that the station shows slight uplift and that the sea level rise is moderate. The GPS correction (0.31 mm/yr) is applied from the beginning of the time series.

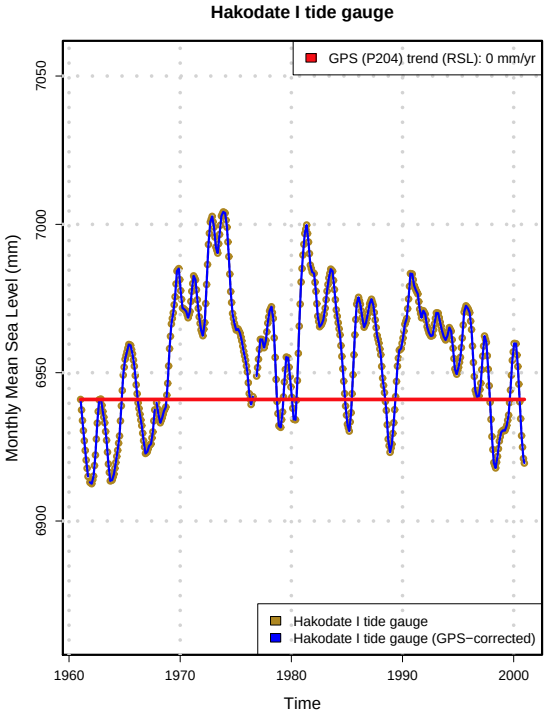

Figure 38: **Hakodate I P204 (PSMSL 641/031)** The tide gauge shows constant uplift from 1972 to 1999, when the process is apparently halted or slowed down ($\tau = -0.23$ from 1972-2008, compared to $\tau = -0.065$ from 1999-2008). The GPS shows no trend (0.00 mm/yr).

6 Reconstruction results

During the course of this work, doubts have arisen concerning the stability of the OI algorithm. For this reason, a sensitivity analysis was performed to analyse the sensitivity of the algorithm against possible sources of error. The following issues were addressed:

- geographical distribution of the tide gauges
- preparational filtering
- influence of missing tide gauges
- correlation and trend differences between tide gauge and TOPEX grid point data
- land movement correction

The first four issues were tested using a simulated reconstruction that uses TOPEX altimetry data at the position of the tide gauges. The last issue was tested using a 1970-2001 reconstruction of with tide gauge data, and a trend estimate using the method introduced by Douglas [11] and applied by Woeppelmann et al. [41].

Possible sources for error in an OI reconstruction include differences in correlation, differing trends at tide gauges and TOPEX grid points, and an unfavorable positioning of the tide gauges. As a matter of fact, the mere density of tide gauges at one coast will not necessarily improve the stability of the reconstruction.

The ideal case is based on the following assumptions: The variability described by the EOFs is the same that has been ruling sea level anomalies over the past. Therefore, it is assumed that comparable states of variability will lead to the activation of the correct variability patterns. I.e., the principal components ruling the respective EOFs (e.g., roughly speaking, EOF 1 for El Nino events, or EOF3 for Kuroshio variability etc. - always keeping in mind that the EOFs cannot be directly linked to physical phenomena) should be activated if and only if these phenomena actually take place. The PCs should therefore (more or less) follow the course of those obtained from a simulated reconstruction. As far as the principal component ruling the "trend" EOF (or "EOF0") is concerned, a different course is expected, since this EOF was added artificially to allow for a homogeneous trend component not present (or separately available) in the altimetry data.

However, since the tide gauge time series necessarily differ from the altimetry data, this ideal case is not usually met in reality. This leads to inconsistencies in the reconstruction which will be described in the following.

If a tide gauge is positioned within a maximum (or minimum) of variability, i.e., inside the maximum or minimum of a lower-order EOF, the possibility increases that, during the course of the reconstruction, a strong anomaly at this tide gauge will be explained by an under- or overestimation of the respective EOF. This effect becomes stronger when less tide gauges are used for the reconstruction. The lack of gauges in an area ruled by strong variability phenomena, i.e. in a maximum of variability, can lead to an

underestimation of events governing not only the immediate vicinity of the gauge, but the global ocean. The latter effect becomes increasingly important when dealing with a time-varying tide gauge array. The inclusion of tide gauges in areas of high variability can lead to unphysical jumps in the reconstruction. In the example given below, it is shown that a jump of 20-30 mm in global sea level is not uncommon. In such a case, adding more information ironically leads to a major deterioration of the reconstruction result. It cannot be stressed enough that a time-varying tide gauge array is the major source of error for the OI algorithm.

On the other hand, tide gauges positioned at "neutral" locations, i.e., locations where variability is generally low, will usually have a stabilizing effect on the reconstruction. A strong anomaly at a "neutral" location, however, will cause the algorithm to randomly activate EOFs when trying to account for this anomaly. This can lead to a massive under- or overestimation of global sea level anomalies. It is important to stress that these effects are not merely local. Even when many tide gauges are available, the percentage of open-water gauges is necessarily low, so that large parts of the world ocean remains unconstrained against the erroneous activation of variability patterns.

In the following, some examples for this behaviour and an error estimate will be given. The analysis starts out with a schematic example showing the effect of the geographical distribution of tide gauges, then moves on to analyse different filtering methods, the effect of correlation and different variances, the effect of a time-changing tide gauge array and gaps in the time series, and finally, the effect of land movement corrections.

6.1 Influence of the geographical distribution of tide gauges

6.1.1 Introduction

The sensitivity of the Optimal Interpolation (OI) and related reconstruction algorithms to the geographical distribution of the in-situ data is examined in this section. It can be shown that the reconstruction of sea level anomalies (SLA) differs significantly depending on whether or not the tide gauge stations used for the reconstruction lie within an extremum of the spatial pattern defined by the leading empirical orthogonal functions (EOFs). This vulnerability suggests that more care must be examined when choosing appropriate tide gauges to avoid a significant underestimation of SLAs in the reconstruction.

Typically, the availability of reliable tide gauge data decreases as one goes back in time. This is especially true for long records and for stations in the southern hemisphere. In this case, the OI and related reconstruction algorithms are influenced by the fact that regional gaps in data availability are not evenly distributed with respect to the spatial EOF patterns. Examples for this claim will be given in the following.

6.1.2 Simulation methodology

For the reconstruction of sea level anomalies (SLA) in this excursus, the Optimal Interpolation (OI) algorithm ([18]) is applied. The OI algorithm as developed by Kaplan et al. ([18], [19]) as described in [7] is used. Tests have shown that the projection technique developed by Smith et al. ([32]) and used, e.g., in Berge-Nguyen et al. ([2]) suffers from the same flaw.

Monthly altimetric sea surface height anomaly data are gridded into $1^\circ \times 1^\circ$ maps and are used to estimate the global covariance structure as expressed in empirical orthogonal functions (EOFs). Thereafter, the amplitude of these EOFs is estimated using tide gauge records. In this way, the main spatial patterns of sea level anomalies are extracted from the satellite data, while their amplitude time series are reconstructed using the tide gauge data.

This excursus aims to only examine the influence of the geographical distribution of these tide gauges, not the tide gauge data. For this reason, the geographical coordinates of tide gauges available at the PSMSL database are used. To assure their eligibility, the length and integrity of these tide gauge records is examined; and the correlation coefficient with the TOPEX altimetry measurements at the nearest grid point is determined.

However, the real tide gauge measurements are *not* used in this simulated reconstruction. Rather, an 'artificial "proxy" in-situ measurement' is created for every tide gauge and each month of the reconstruction by using the respective TOPEX altimetry measurement from the nearest grid point.

In this way, the same radar altimetry data set is used both for the extraction of the EOFs and as a replacement for the in-situ data. Thus, a faithful reproduction of the altimetry data set should be achieved, provided that the reconstruction algorithm works perfectly.

In the following, different sets of tide gauges are used for the reconstruction of different 'time periods'. For example, we select all tide gauges from our initial set that have time series longer than 80 years.

Afterwards, a simulated reconstruction for the period 1994-2001 is performed using this subset of tide gauges; i.e. using the locations of the tide gauges which have been measuring since the 1920s.

Of course, in this case, using the original tide gauge data from the 1920s would not lead to any verifiable results. When using the 'proxy in-situ data' extracted from the 1994-2001 TOPEX altimetry maps, however, the reconstruction result should be largely the same —viz, the original TOPEX altimetry SLA map for the respective month —regardless of the subset of tide gauges used for the reconstruction.

Throughout this excursus, the first 25 EOFs for the OI reconstruction are used since a larger number of EOFs was found to only increase the computational effort without introducing any significant improvements ([7]). When less than 25 tide gauges are used, the number of EOFs accordingly is adjusted to six to avoid solving an underdetermined problem. (The comparison, is, of course, carried out using only six EOFs as well). The effect, however, is the same for both constellations, and the variability covered by the first six EOFs is enough to carry out a satisfactory reconstruction (compare also [6]).

6.1.3 Sensitivity analysis

In the following example, sea level anomaly data on the American West coast is examined. Altimetry data from the TOPEX mission covering the period from 1994-2001 is used. Note that the variability in this period is strongly dominated by the 1997/98 ENSO event. Figure 39 shows the first EOF, making up for about 38 % of the variance in this region and period. The typical positive sea level anomaly (equatorial 'tongue pattern') is clearly visible.

A selection of PSMSL tide gauges (Table 3) is chosen for which RLR (revised local reference, Woodworth and Player 2003, [40]) data with a time series of more than 40 years is available. This is to ensure the quality and consistency of the tide gauge data. Next, we further limit the selection by imposing the following prerequisites necessary for a sensible reconstruction:

1. existence of altimetry measurements at the nearest $1^\circ \times 1^\circ$ grid point,
2. the tide gauge time series shows strong correlation (> 0.6) with the altimetry measurements for the given period (1994-2001).

In areas with a high density of tide gauge stations, some tide gauges share a common nearest grid point. As no real tide gauge sea level data is used in this simulated reconstruction, this ambiguity must not necessarily be resolved —in a real reconstruction, of course, one would have to decide which station to pick. In our selection presented below, the station with the longest tide gauge record and, as a second criterion, the one with the best correlation coefficient is used.

In some cases, the correlation coefficient could not be determined as no tide gauge data was available for the TOPEX period used (1994-2001). None of these tide gauges could be used for the reconstruction. The resulting set encompasses 25 tide gauges with RLR time series lengths ranging from 41 to 151 years.

Figure 39 shows the distribution of the 25 tide gauges with respect to the first (dominant) EOF in this region. Note that, in this example, the Ecuadoran tide gauge 'La Libertad II' (PSMSL 845/012, $2^\circ 12' $ S, $80^\circ 55' $ W) lies in the maximum of the EOF pattern (Figure 39).

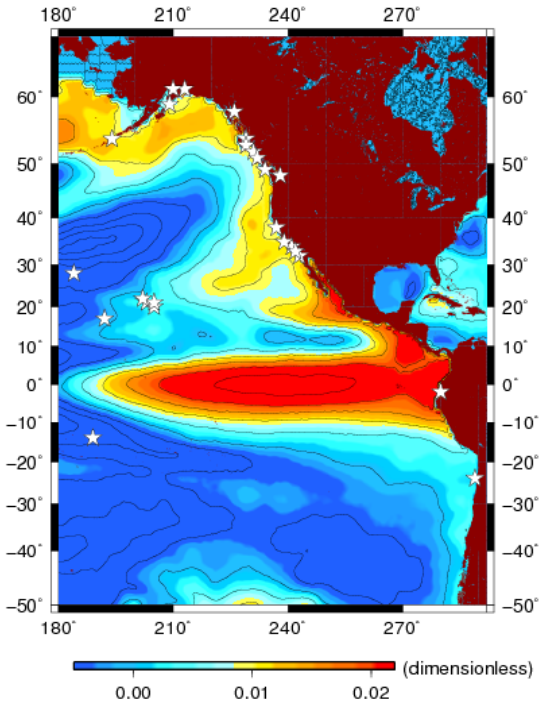

Figure 39: The first (dominant) EOF extracted from TOPEX SLA measurements (1994-2001) in the examined region. Tide gauges are depicted by stars. Note that only one tide gauge, "La Libertad II" (PSMSL 845/012) lies within the maximum of the first EOF. (The scale is dimensionless intensity, with contour lines at 0.005).

Figure 40 shows the TOPEX SLA pattern for May 1997. The onset of the 1997/98 El Niño phenomenon can be observed here, with a rather thin pin-like tongue pattern emerging in the tropics. The reconstruction using all 25 available tide gauges (Figure 41) is good with an RMS difference of 2.18 cm compared to the original altimetry data.

Going back in time, the number of available tide gauges typically becomes smaller. As an example, the tide gauge set is reduced to TGs with time series longer than 80 years. This corresponds (more or less) to the configuration of available tide gauges in the 1920s[5].

Now the same month as before (May 1997) is reconstructed, using only those tide gauges that were already available 80 years ago. This limits the size of the data set to only 8 stations. In this way, the

[5]Note that a subset including all tide gauges with an 80-year minimum time series length need not necessarily cover all tide gauges that have been available 80 years ago. In this example, however, the configurations are largely the same. For this example, tide gauges that have —at some point —been available over the course of the last 80 years, but are no longer in operation today, are ignored. In a real reconstruction, the inclusion of these tide gauges may improve the quality of the reconstruction if their values are well correlated with the surrounding ocean. The detrimental effect of a time-changing tide gauge array will be discussed later in this chapter.

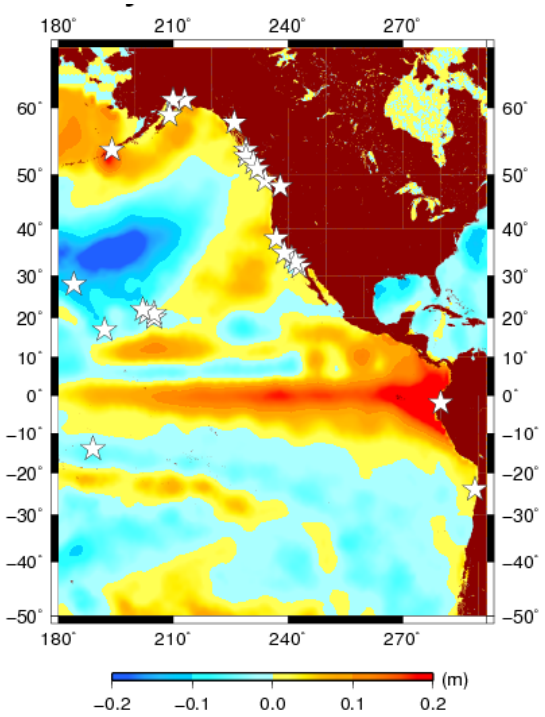

Figure 40: TOPEX altimetry SLA data for May 1997. The onset of the 1997/1998 El Niño with its characteristic "tongue pattern" is clearly visible. Tide gauges are depicted by stars.

reconstruction can be compared to the original altimetry data as well as to the reconstruction using all 25 tide gauges.

The result of the reconstruction in this case is quite unsatisfactory (Figure 42). Not only is the tongue-like anomaly not reproduced, but the overall amplitude of the SLAs is severely underestimated throughout the observed region. The RMS difference is more than twice as high at 5.12 cm.

For test purposes, 'La Libertad II' (with a time series length of 55 years) is now added to the set of tide gauges. The tide gauge was previously deselected to meet the 80-year time series length criterion. In Figure 43 it is shown that, only by adding one single station, almost the full variability is regained. The reconstruction of the original data is quite as good as the one achieved using all 25 tide gauges. The characteristic tongue pattern reappears, and although the negative anomaly north of the Hawaiian Islands is not sufficiently reproduced, the RMS difference of 3.21 cm is quite satisfactory.

Clearly, this result disproves the assumption that the reconstruction result does not depend on the geographical distribution of the in-situ data used.

We give another example to make it clear that it is indeed its position with respect to the leading

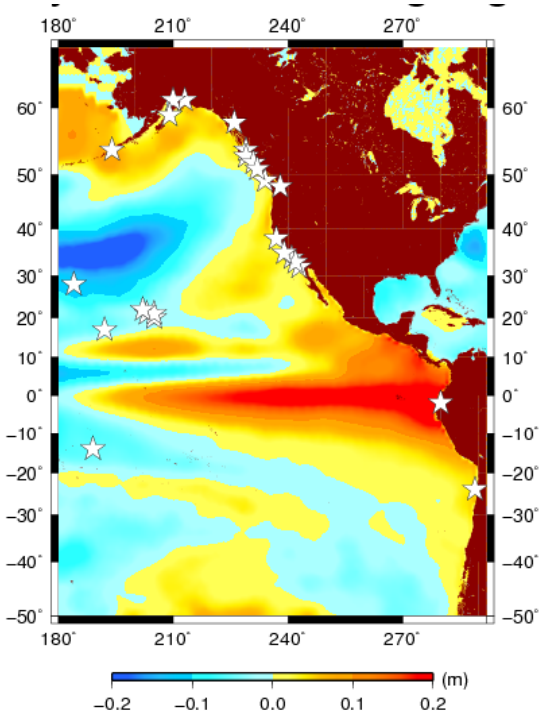

Figure 41: An SLA reconstruction for May 1997 using the full set of 25 PSMSL tide gauges. The result is quite good (RMS 2.18 cm); all characteristic patterns are reproduced. The tide gauges used in the reconstruction are depicted by white stars.

EOF, and not its absolute position, that makes a tide gauge influential.

The Panamanian tide gauge 'Balboa' (PSMSL 840/011)[6] lies well within the positive SLA (tongue pattern) we are trying to reproduce (see Figure 39). However, it lies just outside the maximum of the leading EOF pattern. Hence, it is expect that, if added to the reduced set of tide gauges, it will not improve the quality of the reconstruction significantly.

Figure 44 shows the result of the reconstruction (using 'Balboa' instead of 'La Libertad II', as in Figure 43). Indeed, there is no improvement compared to Figure 42, and the RMS value is even higher at 5.15 cm.

It becomes clear from the examples given that, with a decreasing number of available tide gauges, the influence of a single station can become crucial. Reconstructions for the near past, where a sufficient number of tide gauges were available, are typically less influenced by this problem.

[6]Note that the 'Balboa' tide gauge was not included in the original reconstruction as it did not meet the selection criteria. Since RLR data for this tide gauge is only available up to 1996, the correlation for the full TOPEX altimetry period could not be determined.

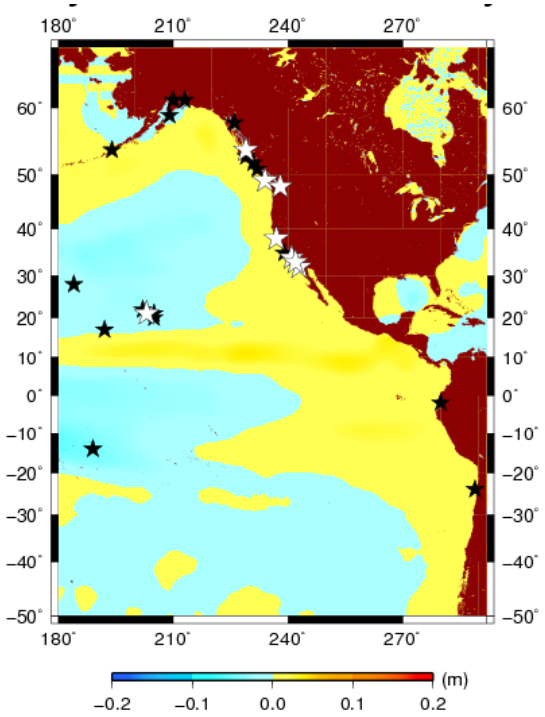

Figure 42: An SLA reconstruction for May 1997 using a set of only 8 tide gauges with time series longer than 80 years. The reconstruction fails to reflect the characteristic SLA patterns and underestimates the overall amplitude. The tide gauges used in the reconstruction gauges are depicted by white stars (not used: black stars).

6.1.4 Effect of heteroscedasticity and correlation

We would like to close the example with a note on the effect of dissimilar variance (heteroscedasticity) between tide gauge and radar altimetry measurements. It is quite common that the variance of a tide gauge measurement is enhanced when compared to altimetry measurements, as coastal effects such as wind surge or resonance may intensify the signal at the gauge. For test purposes, such a situation is simulated by reducing the artificial tide gauge measurement for 'La Libertad II' to only 10% of its original value for the said month.

Clearly, Figure 45 shows that the result is just as unsatisfactory as if one had not included 'La Libertad II' in the first place. The intensity of the SLA patterns is no longer reproduced, and with an RMS value of 5.00 cm, the quality of the reconstruction is almost as bad as in Figure 42.

The same result can be expected when the correlation between tide gauge and altimetric data is low, i.e., when the tide gauge data does not mirror the processes in the open ocean.

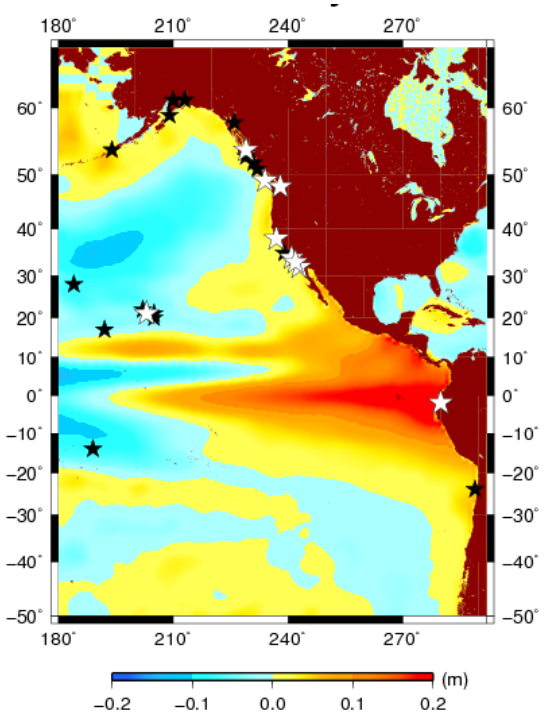

Figure 43: SLA reconstruction as in Figure 42, but with "La Libertad II" (PSMSL 845/012) added to the set of tide gauges. Note that the reconstruction is greatly improved by adding only a single tide gauge. The tide gauges used in the reconstruction gauges are depicted by white stars (not used: black stars).

6.1.5 Effect on the sea level change trend

When looking at the sea level trend for the observed region and time period (1994-2001), only a minor difference between the reconstructed trends and the original trend is noted. The radar altimetry data gives a positive linear trend (0.5 mm/yr), while the reconstruction using the full set of tide gauges results in a slight negative trend (-0.2 mm/yr). The reconstructed trend when using the subset of tide gauges with times series longer than 80 years is roughly the same (-0.1 mm/yr).

Having also tested the global constellation ([31]), we quite agree with Berge-Nguyen et al. [2], in the point that the influence of the location of the tide gauges on a long-term regional linear trend —as in this case —as well as on a long-term global linear trend is minor.

Still, the influence will be stronger when considering a shorter trend, or a regional trend only. For comparison, we choose the 'critical' period from 1994-1997 (Figure 46). Here, the original data —naturally —gives a very strong positive trend of 5.1 mm/yr, mirroring the regional rise in sea level due to the strong ENSO event of 1997/1998. The full set reconstruction gives a satisfactory, if distinctly lower result of 2.8

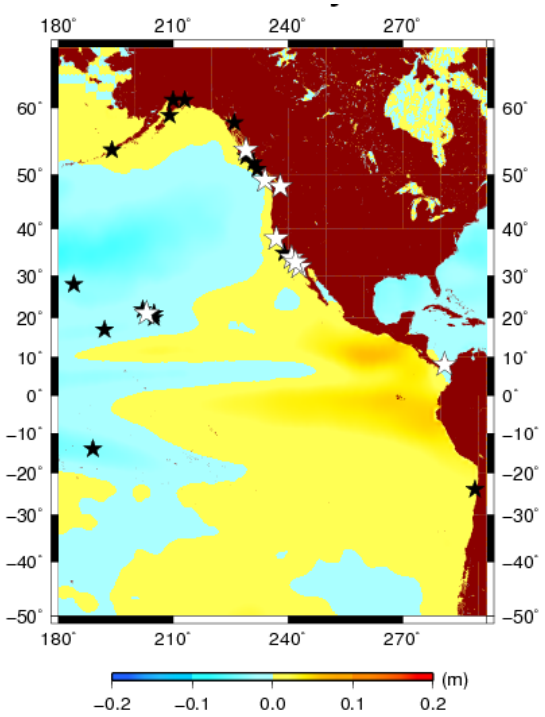

Figure 44: SLA reconstruction as in Figure 42, but with "Balboa" (PSMSL 840/011) added to the set of tide gauges instead of "La Libertad II". Note that there is hardly any improvement in the reconstruction when compared to Figure 42. The tide gauges used in the reconstruction gauges are depicted by white stars (not used: black stars).

mm/yr. The 80-year subset reconstruction, however, completely fails to reproduce the effect of the ENSO event and thus arrives at a trend of only 0.4 mm/yr. When including 'La Libertad II' in the tide gauge subset, the trend jumps up to 2.5 mm/yr (not shown). Summing up, the reconstructed linear trend for the 1994-1997 period will differ tremendously (ranging from 8% to 55 % of the original trend) depending solely on the geographical distribution of the tide gauges used.

Figure 47 shows the influence of missing tide gauges, in prospect of the EOF1 intensity at their position, on the trend difference and RMS. The "EOF intensity" is absolute value of the deviation of the EOF 1 from its mean at the tide gauge position. The scatter plot shows a strong correlation on the trend estimate (0.42 for 25 tide gauges, 0.40 for 8 tide gauges). When considering the shorter trend (1994-1997) - not shown here - the effect is even more pronounced (correlation 0.49 and 0.64, respectively). The effect on the RMS difference is much stronger at correlation 0.58 (25 tide gauges) and 0.92 (8 tide gauges).

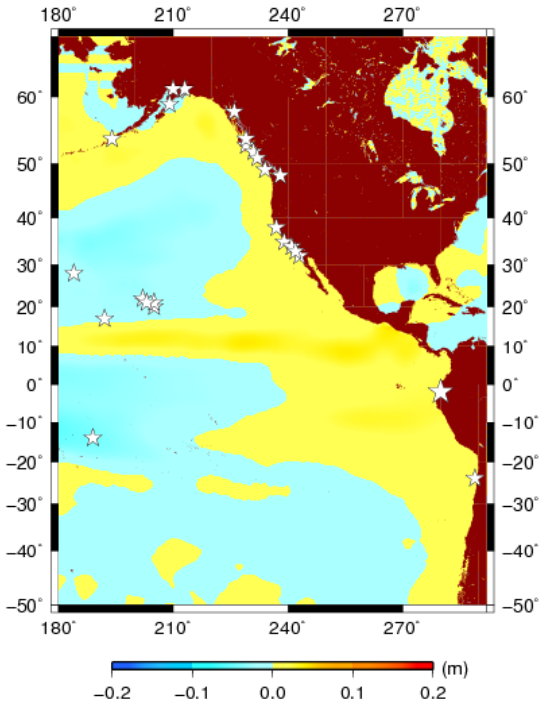

Figure 45: As in Figure 43, but with the proxy tide gauge measurement for "La Libertad 2" for May 1997 reduced to 10% of its original value. The tide gauges used in the reconstruction gauges are depicted by white stars, "La Libertad 2" is depicted by a slightly bigger white star.

6.1.6 Discussion and corrective approaches

The geographical distribution of the in-situ data has a major influence on the reconstruction result, especially when only few tide gauges are used. This situation will normally arise when reconstructing long time periods, but also when the full set of tide gauges is constricted to include, e.g., only tide gauges operated by a certain agency, or only open water tide gauges.

To illustrate and summarize the effect described above, we give a short schematic example (Figure 48).

The problem described in this example typically arises when one tries to fit a fixed wave form or graph to an incomplete set of data points. If the maximum values in the data set are missing, the maximum of the wave form or graph will be fitted to one of the lower values in the data set.

Consider an arbitrary data set of 10 points, representing the sea level data. Here, a simple fourth grade polynomial (representing the fixed spatial pattern of the leading EOF) is used to fit this data set (dotted line). If the maximum values are now taken out to simulate a gappy data situation (few

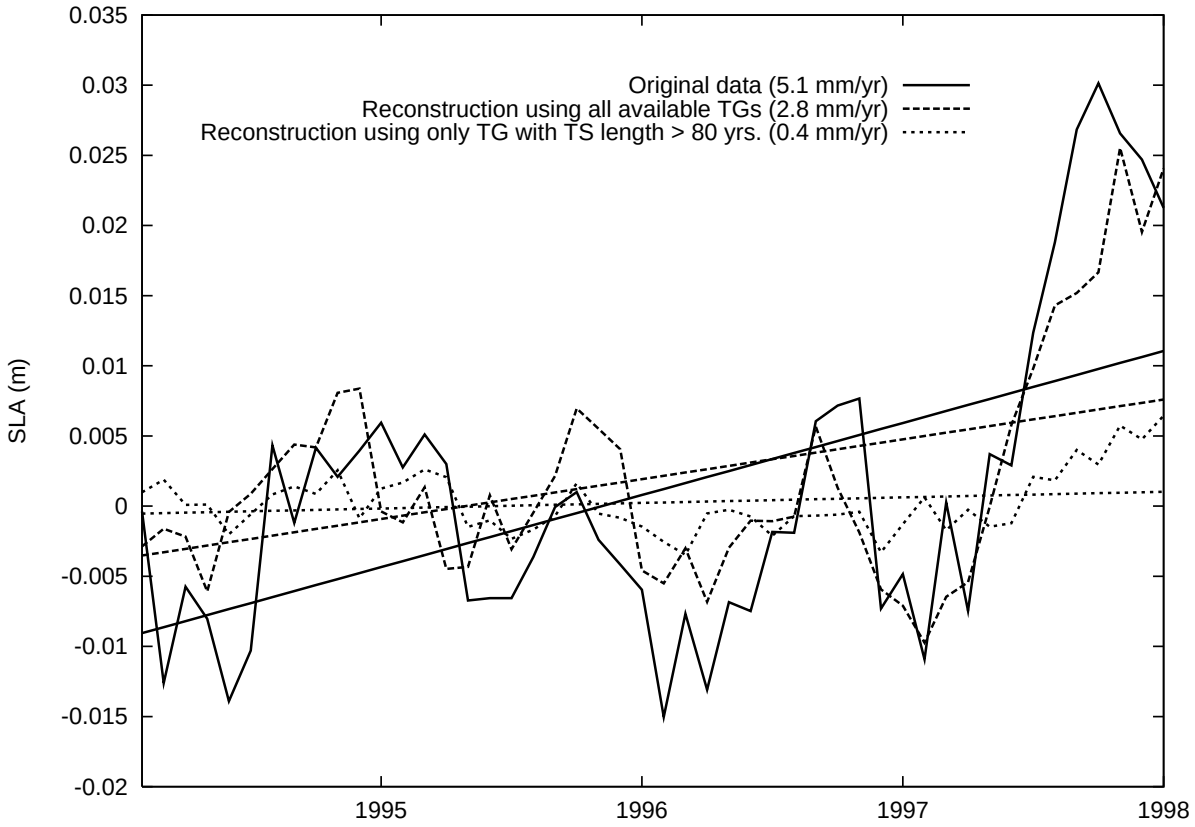

Figure 46: Regional SLA Trends for the 1994-1997 period resulting from different reconstructions. The reconstruction using only long time series fails to reproduce the El Niño event in the area and arrives at an erroneously low trend of 0.4 mm/yr.

tide gauges), the same graph fits the data better when it is shifted by -1 in the y-direction (black line), representing a 'lower intensity' of the said EOF.

The same effect occurs in the examples given in this study. If the values lying in the maximum of the curve are taken out, the fit is shifted, resulting in an erroneously low reconstruction of the SLA pattern. Of course, the problem will not occur if the missing data is evenly distributed over the whole EOF pattern. In a real reconstruction, however, this can not be guaranteed.

It should be noted that an similar, but opposite effect will also occur when using badly correlated data. If a strong anomaly is forced on a tide gauge at which there is normally very little variability, the respective EOF will be strongly overemphasized by the OI(C) algorithm unless other tide gauges constrain this process. This can lead to an artifactual overestimation of variability patterns. This effect will be discussed in detail in the following section.

The influence of the geographical distribution is most conspicuous in areas that show the largest SLA

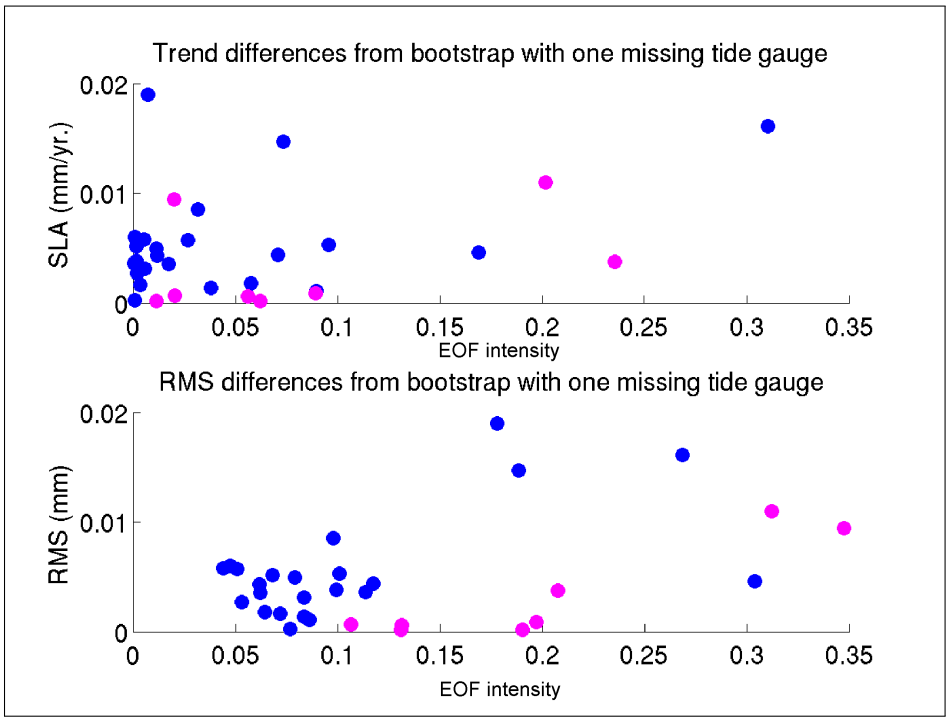

Figure 47: Effects of missing tide gauges for a Bootstrap using 25 (blue) and 8 (pink) tide gauges. One tide gauge per run is deleted. Both panels show a linear increase of trend deviation versus EOF intensity, which is the (dimensionless) squared value of the EOFs at the tide gauge position.

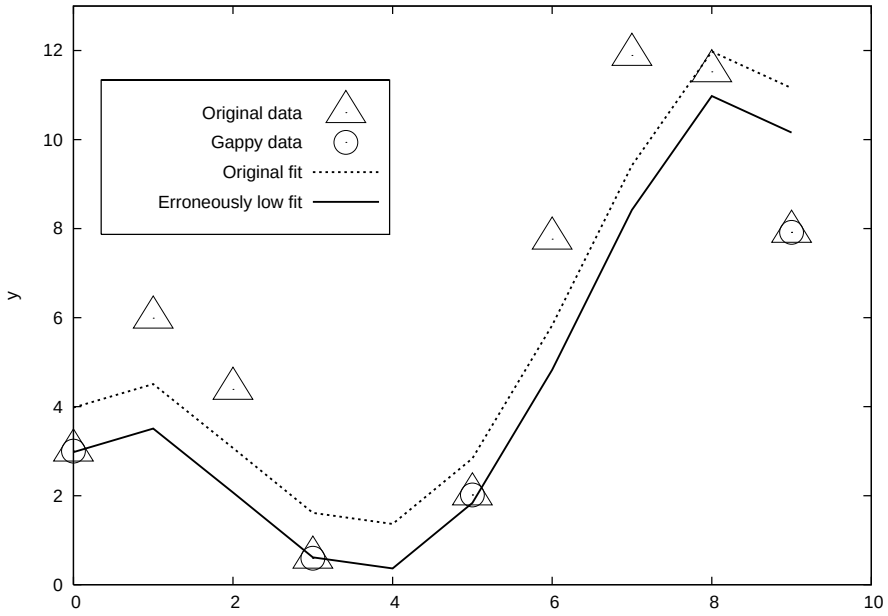

Figure 48: A schematic example showing the effect of gappy data on a reconstruction. If the maximal points are missing in the data set, the fit applied by the algorithm is too low. Units are arbitrary dimensionless quantities.

variability (especially the equatorial Pacific region and the Indian Ocean). The leading EOFs in the said region represent the El Niño and IOD events, respectively. At their peak, both events lead to a strong positive anomaly covering large areas. Here, the reconstruction will typically hold, because in such extreme conditions, even the values lying further away from the extrema of the EOF pattern will be enhanced.

At the onset of an El Niño event, however, the resulting anomaly is strong but rather localized. In the latter case, a reconstruction error is quite likely if the in-situ data is scarce.

Summing up, it can be said that, when reconstructing a month in which the influence of the leading EOF is strong but localized

- leaving out tide gauges that lie *within* the maximum of the leading EOF pattern results in an underestimation of the leading EOF and subsequently, to erroneously low SLAs.
- including tide gauges that lie within the maximum of the leading EOF pattern, but which show *little* or *no correlation* with the altimetry data (at the adjacent grid point), leads to an underestimation of the leading EOF.
- including tide gauges that lie within the maximum of the leading EOF pattern, but which show *a strongly dissimilar variance* compared to the altimetry data (at the adjacent grid point), leads to an under- or overestimation of the leading EOF, respectively.

Also, the findings indicate that

- including more tide gauges does not necessarily lead to a better reconstruction, rather, the position of the tide gauge with respect to the leading EOF patterns is important.
- adding more tide gauges in a certain region does not necessarily improve the reconstruction in the said region. Rather, due to the dependence of their position within the EOF patterns, it is possible that the influence of tide gauges in a remote region is unexpectedly large.

Currently, it seems that there is no easy way to avoid this problem. The only way to avoid such underestimations is to perform a simulated test with every eligible tide gauge data set and to check the results visually as well as statistically. In any case, for reconstruction studies using the OI(C) and related algorithms, only tide gauges which show strong correlation with the radar altimetry data the adjacent grid points should be used. The inclusion of uncorrelated in-situ data has been shown to do more harm than good in a reconstruction.

It is not yet clear whether the methods using an iteratively updated covariance matrix for the extraction of EOFs (as developed by Schneider [29], Beckers and Rixen [1] as well as Kondrashov and Ghil [23]) are also affected by this problem. It is possible that the problem described above has less influence on such methods, as the spatial EOF patterns used here are not stationary. Instead, the EOFs are recalculated in every time step, viz, the position of their maxima will change slightly during the course of the reconstruction. Still, it is unclear whether this shift is sufficient to avoid the problem.

In a recent paper, Berge-Nguyen et al. [2] mentioned some discrepancies between the trend map taken from their own reconstruction and the one performed by Church et al. [7] . The strongest discrepancies are localized in the equatorial Pacific and the Indian Ocean, the areas that —with the 1997/98 El Niño and the 1998 IOD event —show the strongest variability in the TOPEX mission period. It is suggested that these discrepancies may well be due to the use of different sets of tide gauges.

Name	PSMSL	TS (yrs)	correlation	lat	lon	used
Anchorage	821012	41	0.61	61	210	yes
Antofagasta	850011	58	0.51	-24	289	yes
Bella Bella	822016	44	0.69	52	231	yes
Cordova	821020	41	0.76	61	213	yes
Hilo, Hawaii Island	760061	59	0.69	20	205	yes
Honolulu	760031	100	0.69	21	203	yes
Johnston Island	760011	53	0.66	17	192	yes
Juneau	821044	69	0.61	58	226	yes
Kahului Harbor	760051	58	0.73	21	205	yes
Ketchikan	821051	86	0.82	54	229	yes
La Jolla (Scripps Pier)	823071	81	0.64	33	242	yes
La Libertad II	845012	55	0.90	-2	279	yes
Los Angeles	823051	82	0.66	34	241	yes
Midway Island	760001	58	0.57	28	184	yes
Nawiliwili Bay	760021	50	0.68	22	202	yes
Pago Pago	745001	58	0.92	-14	189	yes
Port Hardy	822020	41	0.63	51	232	yes
Port San Luis	823042	60	0.68	35	239	yes
Queen Charlotte City	822008	48	0.73	53	229	yes
San Diego	823081	99	0.71	32	243	yes
San Francisco	823031	151	0.55	38	237	yes
Seldovia	821015	41	0.73	59	209	yes
Tofino	822116	96	0.74	49	234	yes
Unalaska	820021	50	0.61	54	194	yes
Victoria	822101	96	0.80	48	238	yes
Alameda	823032	66	0.58	38	237	(San Francisco)
Friday Harbor	823006	71	0.87	49	237	(Victoria)
Point Atkinson	822051	91	0.72	49	237	(Victoria)
Prince Rupert	822001	96	0.83	54	229	(Ketchikan)
Santa Monica	823049	72	0.66	34	241	(Los Angeles)
Seward	821017	41	0.72	60	212	(Cordova)
Sitka	821031	67	0.51	57	226	(Juneau)
Vancouver	822071	95	0.79	49	237	(Victoria)

Table 3: The set of tide gauges used in the working example in 6.1.1. Of all available tide gauges (TGs) in the area with time series length (TS) longer than 40 years, only those showing strong correlation > 0.6 to the TOPEX altimetry data at the adjacent grid point were used. In the case where multiple tide gauges share the same next grid point, the TG used in the reconstruction is given in brackets.

TOPEX trend	3.29 ± 0.00 mm/yr
Unfiltered reconstruction	3.43 ± 0.02 mm/yr
Deseasonalized reconstruction	3.31 ± 0.01 mm/yr
Trend reconstruction	3.28 ± 0.00 mm/yr

Table 4: Effect of preparational filtering.

6.2 Preparational filtering

The sensitivity analysis starts out with a comparison of different filtering methods for the tide gauge time series. A bootstrapped reconstruction is performed for the 1994-2001 period using TOPEX "proxy" data at tide gauge positions like in the preceding chapter. Three different filtering methods are tested - unfiltered, deseasonalized, and retaining only the nonlinear trend. Church et al. [7] use data where the seasonal component is removed. While the trend remains comparatively stable, retaining the seasonal component leads to a far more volatile reconstruction result, as is shown in Figure 49. The "raw" (unfiltered) reconstruction results in a rather noisy time series with a trend of 3.45 mm/yr, while the deseasonalized version has lower amplitude and a trend of 3.3 mm/yr. To improve the stability of the reconstruction, a pure trend reconstruction, where all signals except for the nonlinear trend has been removed from the original time series using the STL (Loess [8]) algorithm. The stability of this version is comparable with that of the Church et al. [7] annual reconstruction while keeping in mind the original goal of obtaining monthly anomaly fields from the reconstruction. Figure 50 shows the stability of the three different reconstructions against missing tide gauges. Here, a bootstrap reconstruction using TOPEX data was performed where one tide gauge per run was deleted. The resulting trend and RMS difference are shown in Figure 52 and Figure 53. It is quite apparent that the stability of the "trend" reconstruction is very high, with trend and RMS differences an order of magnitude below the accuracy of 0.1 mm/yr. The trend estimate with standard deviations are given in Table 6.2.

The pure trend reconstruction performs best, with the result closest to the TOPEX trend (which should be reproduced) and the smallest sensitivity against missing gauges. Generally, the error levels in this simulation are quite low. This is due to the fact that the reconstructed variability is exactly the same as the one the EOFs were extracted from. The resulting trend differences stem from differences in the PC-0, i.e., the principal component ruling the EOF-0, only. It will be shown in the following that this level of accuracy is obtained only in a "simulated" reconstruction using the same data that the EOFs were extracted from. In the following, all reconstructions are performed with trend-only filtered data.

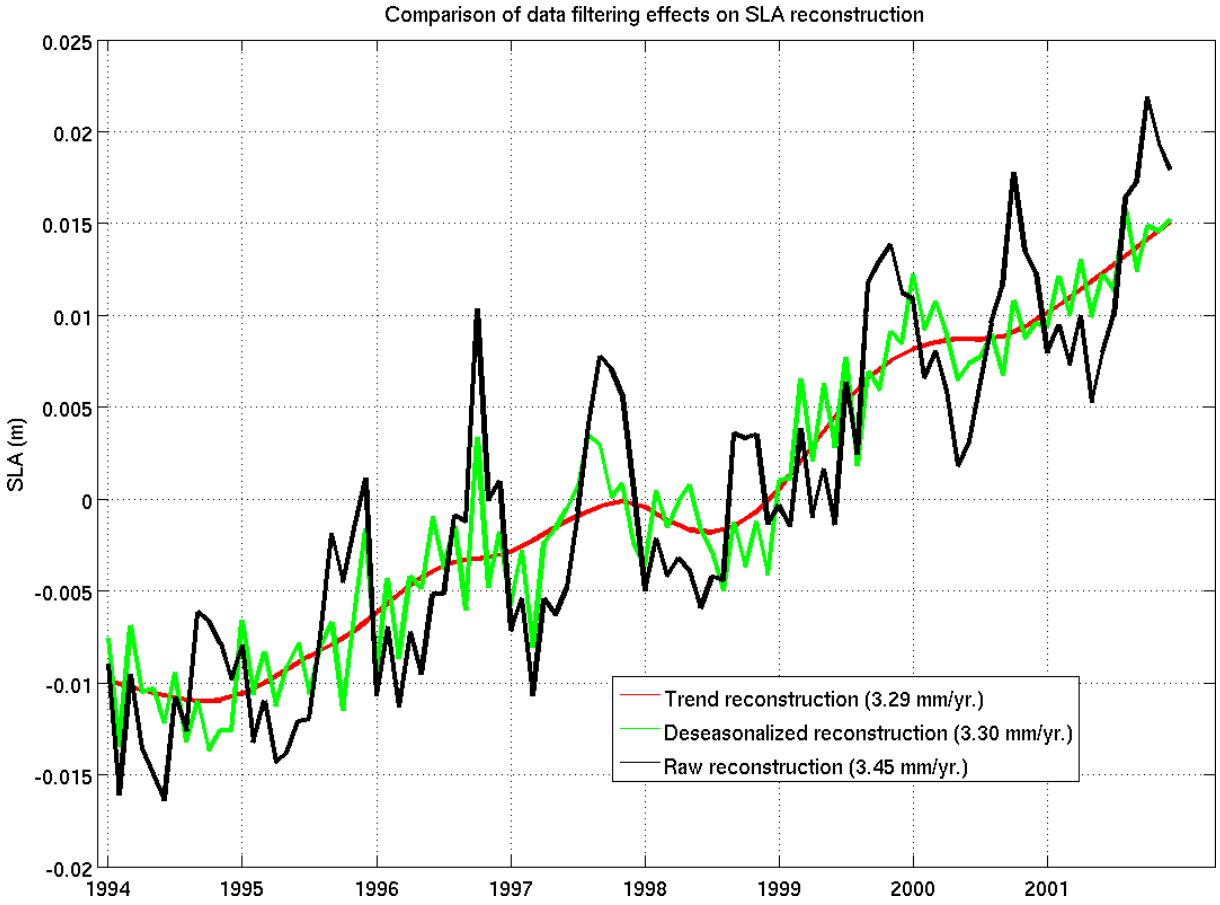

Figure 49: SLA Trends from differently filtered data.

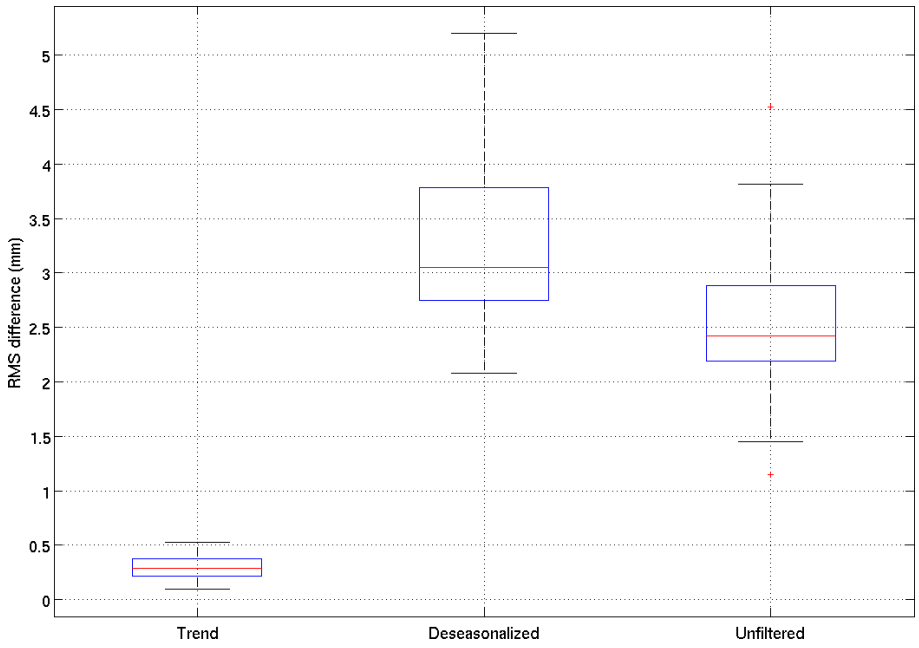

Figure 50: RMS difference from a bootstrap run of reconstructions where one tide gauge is deleted from the initial set. The data used is TOPEX altimetry data at tide gauge positions. The resulting RMS comparison with the full reconstruction gives an error estimate of the reconstruction's sensitivity against leaving out single tide gauges. The three boxes represent the "trend" (left) reconstruction, the "deseasonalized" (middle) and the unfiltered (right) reconstruction. The outliers are Auckland (PSMSL 690/002, high RMS) and Nawiliwili Bay, Kauai Island (low RMS, PSMSL 760/021), for the unfiltered reconstruction. The other two reconstructions show no outliers. On each box, the central mark is the median, the edges of the box are the 25th and 75th percentiles, the whiskers extend to the most extreme data points not considered outliers, and outliers are plotted individually.

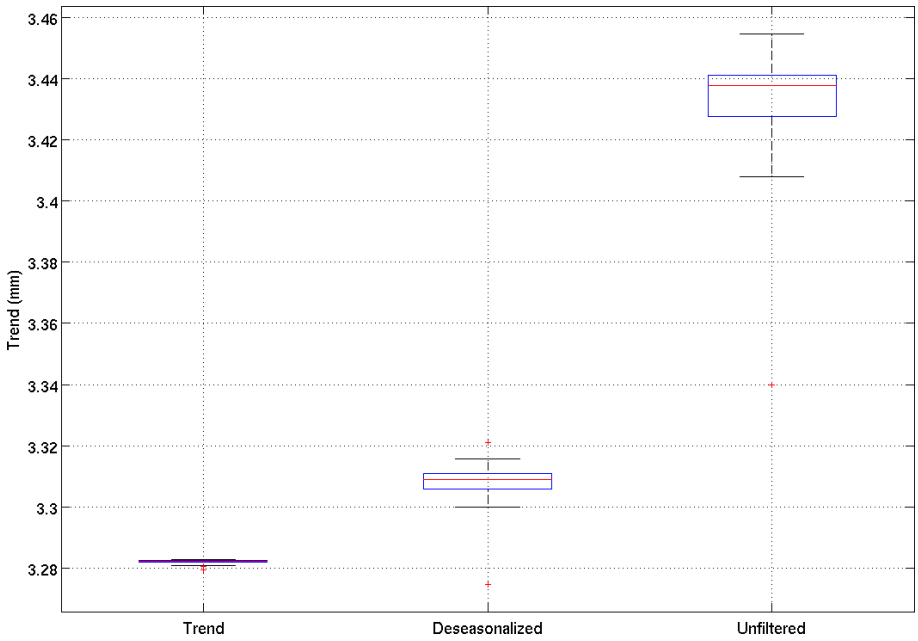

Figure 51: Trends from a bootstrap run of reconstructions where one tide gauge is deleted from the initial set. The data used is TOPEX altimetry data at tide gauge positions. The comparison of the resulting trend with the one obtained from the full reconstruction gives an error estimate of the reconstruction's sensitivity against leaving out single tide gauges. The three boxes represent the "trend" (left) reconstruction, the "deseasonalized" (middle) and the unfiltered (right) reconstruction. The outliers are Oshoro (PSMSL 641/042), Toyama (PSMSL 647/068), Hakodate I (PSMSL 641/031), and Cocos Island (PSMSL 680/521) for the trend reconstruction, (barely visible here), Hakodate I (PSMSL 641/031) and Charleston (PSMSL 960/041) for the deseasonalized reconstruction, and Auckland (PSMSL 690/002) for the unfiltered reconstruction.

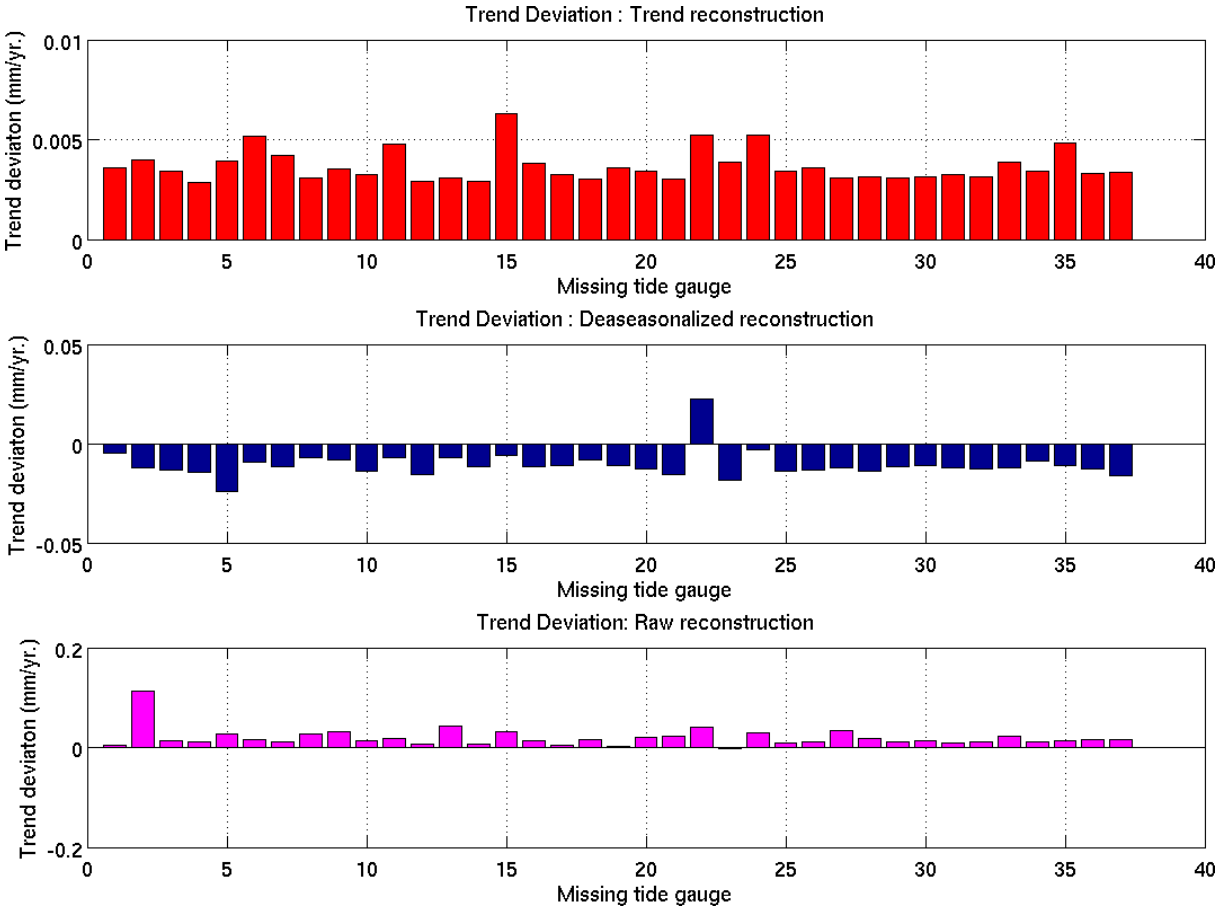

Figure 52: Trends from a bootstrap run of reconstructions where one tide gauge is deleted from the initial set. The data used is TOPEX altimetry data at tide gauge positions. The comparison of the resulting trend with the one obtained from the full reconstruction gives an error estimate of the reconstruction's sensitivity against leaving out single tide gauges. Shown here are the effects of leaving out tide gauges (numbered 1-37) from the "trend" reconstruction (upper), the "deseasonalized" (middle) and the unfiltered (lower) reconstruction. The outliers are Oshoro (PSMSL 641/042), Toyama (PSMSL 647/068), Hakodate I (PSMSL 641/031), and Cocos Island (PSMSL 680/521) for the trend reconstruction, (barely visible here), Hakodate I (PSMSL 641/031) and Charleston (PSMSL 960/041) for the deseasonalized reconstruction, and Auckland (PSMSL 690/002) for the unfiltered reconstruction.

Internal	**GPS ID**	**Name**	**PSMSL ID**	**GPS trend [mm/yr]**	**WRMS [mm]**	**TS length [yrs]**	**GIA trend [mm/yr]**
1	ABER	ABERDEEN	170/011	1.13	4.47	9.26	0.89
2	AUCK	AUCKLAND	690/002	-1.75	6.2	9.76	0.29
3	BRMU	BERMUDA	950/011	0.02	4.91	9.77	-1.05
4	BRST	BREST	190/091	-1.03	5.34	9.16	-0.28
5	CHA1	CHARLESTON	960/041	-4.61	16.98	5.65	-0.83
6	COCO	COCOS ISLAND	680/521	-0.31	7.25	9.77	-0.09
7	CRO1	ST. CROIX	939/011	-1.57	5.81	7.12	-0.25
8	GALA	GALAPAGOS	845/031	-0.10	4.52	4.64	0.16
9	GUAM	GUAM	701/001	-1.08	5.73	7.66	0.24
10	HNLC	HONOLULU	760/031	-0.38	5.19	8.64	0.16
11	KIRI	KIRIBATI	730/008	-0.31	5.23	5.41	0.12
12	KOKB	Nawiliwili Bay	760/021	0.72	7.04	9.77	0.15
13	MALD	MALDIVES	454/011	-2.69	7.62	6.00	0.22
14	NPRI	NEWPORT	960/161	-0.10	4.14	8.14	-1.76
15	P101	OSHORO	641/042	-1.13	6.48	4.56	0.60
16	P103	ASAMUSHI	647/121	1.24	4.42	4.73	0.61
17	P104	OGA	647/096	3.18	3.99	4.56	0.60
18	P110	KASHIWAZAKI	647/081	-1.08	4.3	4.04	0.73
19	P117	KAINAN	643/013	3.89	3.55	4.54	0.66
20	P118	TAJIRI	647/047	-1.07	4.52	4.52	0.64
21	P123	AKUNE	645/045	-1.33	8.58	4.54	0.56
22	P204	HAKODATE I	641/031	0.00	4.73	4.69	0.61
23	P205	OFUNATO	642/022	-4.58	4.88	4.54	0.62
24	P207	TOYAMA	647/068	-1.38	5.21	4.56	0.71
25	P208	KUSHIMOTO	642/141	-7.29	4.91	4.73	0.60
26	P209	HAMADA II	647/023	-1.89	3.96	4.52	0.66
27	P211	ABURATSU	645/021	-1.72	4.85	4.58	0.53
28	PALA	PALAU	711/021	0.30	5.26	6.54	0.19
29	PERT	PERTH	680/472	-5.89	5.61	9.58	-0.01
30	PLUZ	Puerto de la Luz	370/041	-2.39	3.78	3.31	-0.15
31	POHN	POHNPEI	710/031	-0.43	5.23	4.64	0.15
32	SEAT	SEATTLE	823/011	-1.15	7.29	9.32	-1.31
33	SELD	SELDOVIA	821/015	10.8	$\pm$1.5	7.50	0.19
34	SIO3	LA JOLLA	823/071	-0.36	5.44	7.98	-0.50
35	THTI	TAHITI	780/011	-2.50	6.39	8.43	0.22
36	TSEA	ACHORAGE	821/012	4.79	8.29	8.49	0.19
37	TUVA	TUVALU	732/011	0.31	4.83	6.08	0.06

Table 5: Stations used in the 1970-1990 reconstruction with GPS ID, station names and PSMSL ID. The vertical GPS trends and their respective WRMS values, the length of the GPS time series in years and the respective GIA corrections are given for comparison. For Seldovia (33), the trend was obtained from personal communication with Dr. Freymuller (University of Alaska); therefore, only a confidence interval is given instead of a WRMS value.

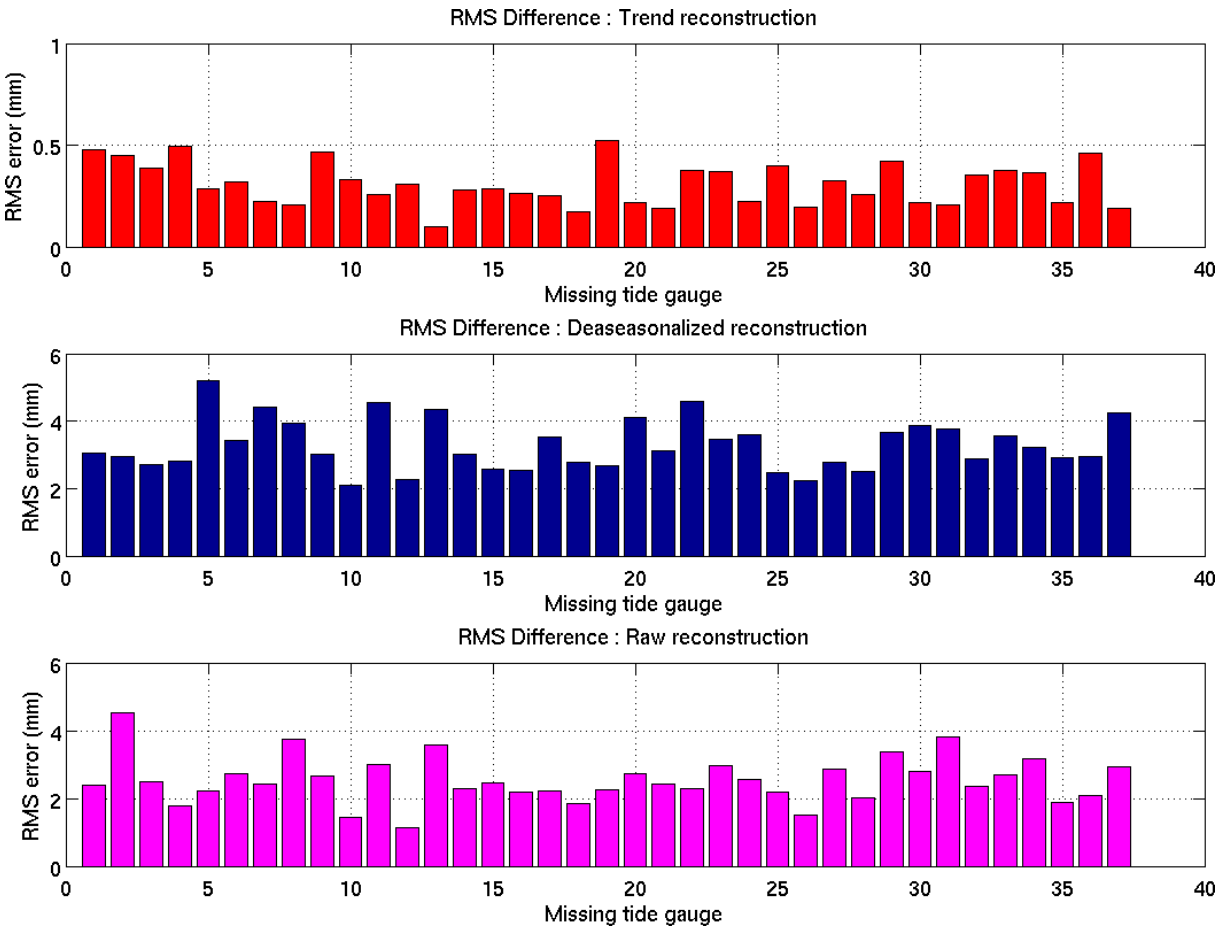

Figure 53: RMS differences from a bootstrap run of reconstructions where one tide gauge is deleted from the initial set. The data used is TOPEX altimetry data at tide gauge positions. The comparison of the resulting RMS difference with the full reconstruction gives an error estimate of the reconstruction's sensitivity against leaving out single tide gauges. Shown here are the effects of leaving out tide gauges (numbered 1-37) from the "trend" reconstruction (upper), the "deseasonalized" (middle) and the unfiltered (lower) reconstruction.

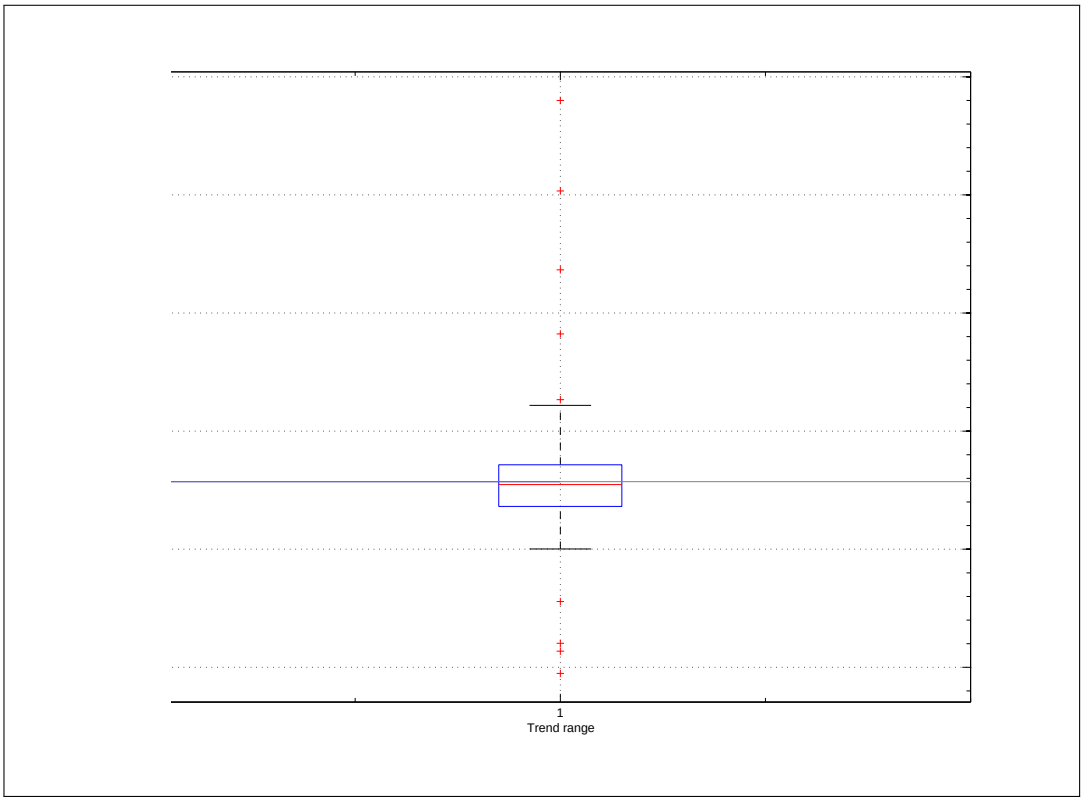

Figure 54: Trend range from the bootstrapped reconstruction using 36 TOPEX time series (1994-2001) and one tide gauge time series, respectively.

6.3 Influence of badly correlated tide gauge data

To test the effect of badly correlated data, a simulated bootstrap for the TOPEX period (1994-2001) was performed in which TOPEX data was used for all but one gauge positions in every run, i.e., only one time series of "real" observational tide gauge data was used per run. To exclude the influence of gappy data, gaps in the tide gauge time series were patched using a very simple patching algorithm.[7] It should be noted that the effect of unequal variance between tide gauge and TOPEX grid point mentioned in Section 4 persists and has been shown to lead to similar effects. In this section, this effect is integrated in the examination of RMS differences between tide gauges and TOPEX time series.

The resulting trend differences are shown in Figure 54. The median lies slightly below the full TOPEX reconstruction result of 3.29 mm/yr, with a wide spread of outliers ranging from 2.47 mm/yr to 4.90 mm/yr.

Overall, the simulation arrives at an estimate of 3.3 ± 0.5mm/yr with extrema ranging from 2.4

[7]For every gap, the missing data was replaced by TOPEX data fitted to the last observation in the tide gauge time series.

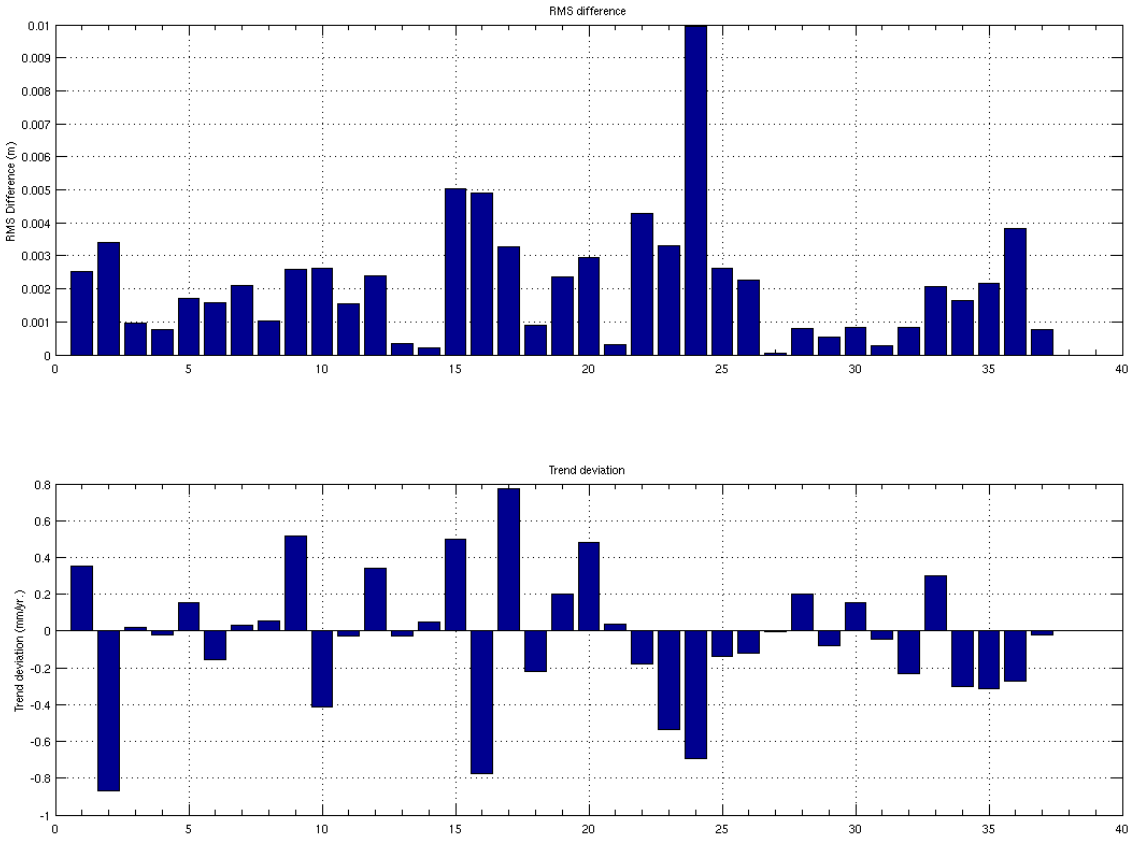

Figure 55: Trend and RMS differences from the bootstrapped reconstruction using 36 TOPEX time series (1994-2001) and one tide gauge time series, respectively.

to 4.9mm/yr. This broad range in a reconstruction where only one time series at a time stems from observational data is conspicuous and shows the strong effect of less-than perfect correlation on the trend estimate. The reason for this is that, unlike the full simulation, other lower-order EOFs (except for the EOF-0) are erroneously activated. The same effect, with respect to the the trend and RMS differences, can be seen in Figure 55.

6.3.1 Largest RMS deviations

The inclusion of the following tide gauges leads to the largest RMS deviations: 15, 16, 17, 22, 24 ('OSHORO II', 'ASAMUSHI', 'OGA', 'HAKODATE I', 'TOYAMA'). The difference is most notable for the period ranging from March 1995 to June 1996 (see Figure 56). While for all tide gauges, the observational values in this period lie below the TOPEX values, the effect of their inclusion in the reconstruction is

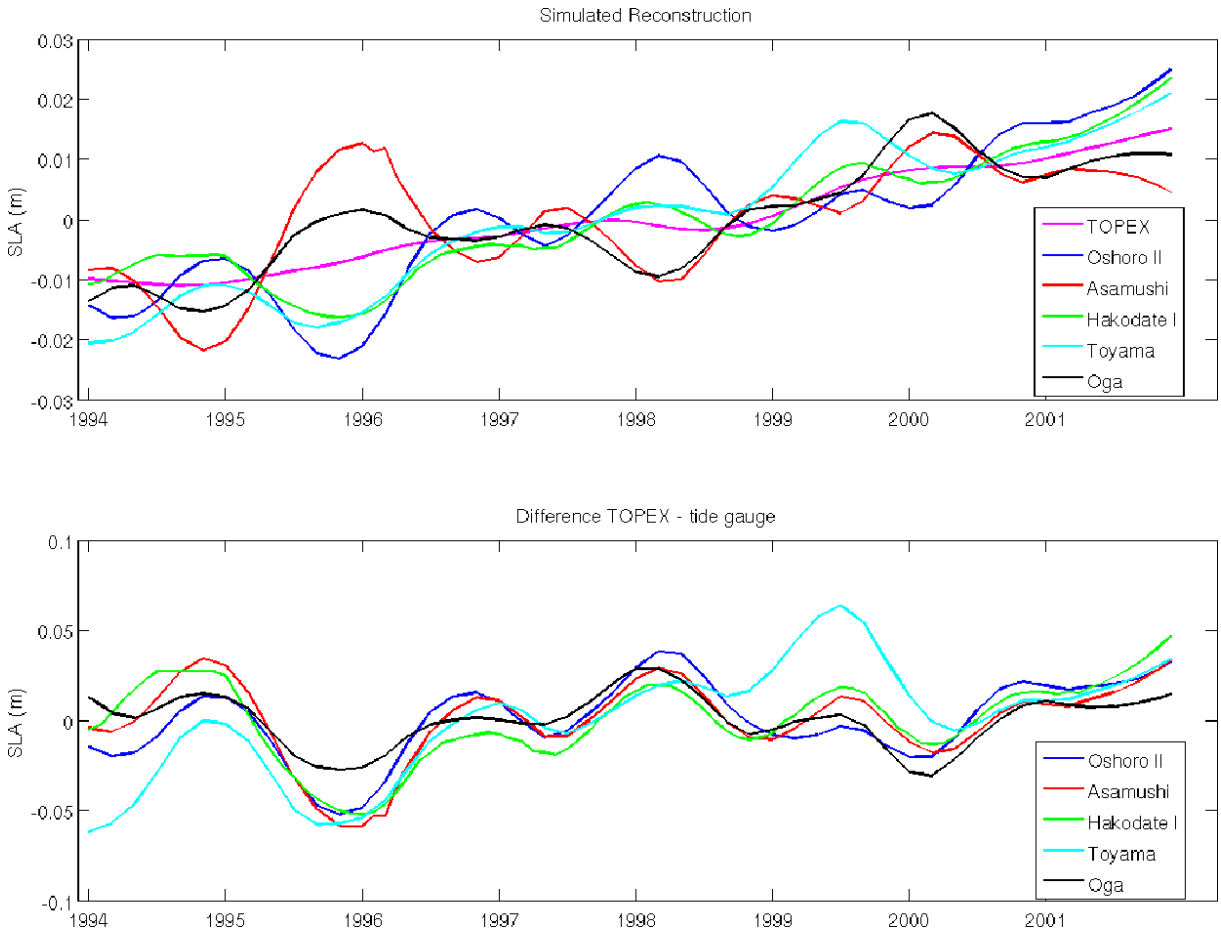

Figure 56: SLA Trends from the bootstrapped reconstruction using 36 TOPEX time series (1994-2001) and one tide gauge time series, respectively.

different. Including Oshoro II, Hakodate I, and Oga leads to an erroneous underestimation of the global SLA, while the inclusion of Asamushi and Toyama lead to an overestimation (see Figure 56).

The possible causes for the RMS deviations are listed below in Table 6 with their respective correlations on RMS deviance. The correlation between tide gauge and TOPEX grid point is given for the full 1994-2001 period as well as for a critical period from March 1995 to June 1996, where many (especially Japanese) tide gauges show the largest differences to the TOPEX time series. As expected, insufficient correlation between tide gauge and TOPEX time series has the largest influence on RMS difference, followed by the EOF intensity at the tide gauge, which is the strength of the variability at the tide gauge position calculated by the sum of the EOF values, weighted by their respective eigenvalues, at the tide gauge position. The inclusion badly correlated tide gauges at "neutral" positions lead to the largest RMS differences. This result supports the theory that large anomalies at neutral positions lead to an increased

Correlation Tide gauge / TOPEX (full period)	-0.47
Correlation Tide gauge / TOPEX (critical period)	-0.61
EOF intensity	-0.43
RMS Tide gauge/TOPEX	0.22 mm
Trend difference Tide gauge/TOPEX	0.34 mm/yr

Table 6: Correlation table: Influence of different factors on RMS differences.

Correlation Tide gauge / TOPEX (full period)	−0.44
Correlation Tide gauge / TOPEX (critical period)	−0.20
EOF intensity	−0.33
RMS Tide gauge/TOPEX	0.21
Trend difference Tide gauge/TOPEX	0.64

Table 7: Correlation table: Influence of different factors on trend deviations.

random activation of lower-order EOFs.

6.3.2 Largest trend deviations

The causes for trend and RMS deviations in a reconstruction differ. In general, it is observed that the trends are more stable, so that including "real" data a certain tide gauge can cause large RMS deviations but may still reproduce the trend very well (e.g. "Toyama", scoring fourth in RMS deviations while the trend deviations are below the accuracy). A large overall RMS deviation may cancel out in the trend and hence do less harm than one that ranges only over a smaller part of the reconstruction period.

The correlation Table 7 given below shows that, unsurprisingly, the main influence (correlation coefficient 0.64) on trend deviations in the simulated bootstrap lies in trend differences between the tide gauge and its nearest TOPEX gridpoint. This is an expected and plausible result. The correlation between gauge and grid point plays a minor role (-0.44), followed by the EOF intensity with a correlation coefficient of -0.33. The influence of EOF intensity on trend deviations and RMS differences is shown again in Figure 57.

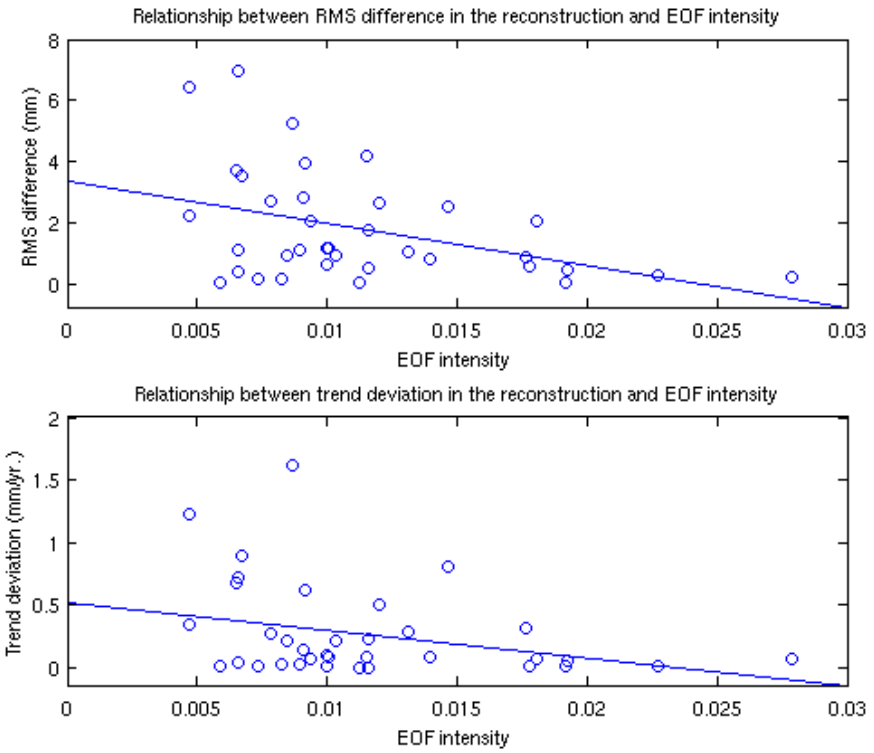

Figure 57: Relation between trend deviation in the reconstruction, trend deviation between tide gauge and TOPEX grid point, and EOF intensity.

6.4 Influence of a time-changing tide gauge array

In this section, the effects of a time-changing tide gauge array are examined. The observational tide gauge data from the full set of tide gauges given in Table 5 is used, the reconstruction period is from 1970-2001. The correlations and trend differences for these tide gauges are shown in Figure 58.

It must be stated that the influence of the EOF intensity at the position of a tide gauge is two-fold. For once, tide gauges at positions with low EOF intensity tend to stabilize the reconstruction. It was shown in the preceding chapter that including badly correlated data from these positions will lead to large RMS deviations, which can also result in trend deviations. Generally, the more areas remain unconstrained by tide gauge data, the worse the reconstruction for the respective month. However, the largest jumps in the trend result from adding or deleting tide gauges during the course of the reconstruction. This effect is shown in an exemplaric manner in Figure 59. Here, the presence or absence of two tide gauges with high EOF intensity is given by shaded areas in the plot. It is apparent that major jumps appear when tide gauges are added or deleted.

Again, a bootstrap with one missing tide gauge per run is performed to obtain an error interval. It results in an estimate of 0.8 ± 1.0mm/yr for the whole 1970-2001 period, where, in the beginning, 45 percent of the gauges are missing. For a shorter period with better data availability (1980-2001), the trend estimate is 1.16 ± 0.5mm/yr.

The problem of a gappy tide gauge array can of course be rectified by using conventional gap-filling or smoothing algorithms on the tide gauge time series, e.g., Wenzel [39]. However, the fact that also the addition of tide gauges can and will lead to jumps, results in the problem that no tide gauges can be added during the course of the reconstruction without risking inconsistencies. Therefore, a smoothing algorithm is introduced in the following Chapter 6.6.

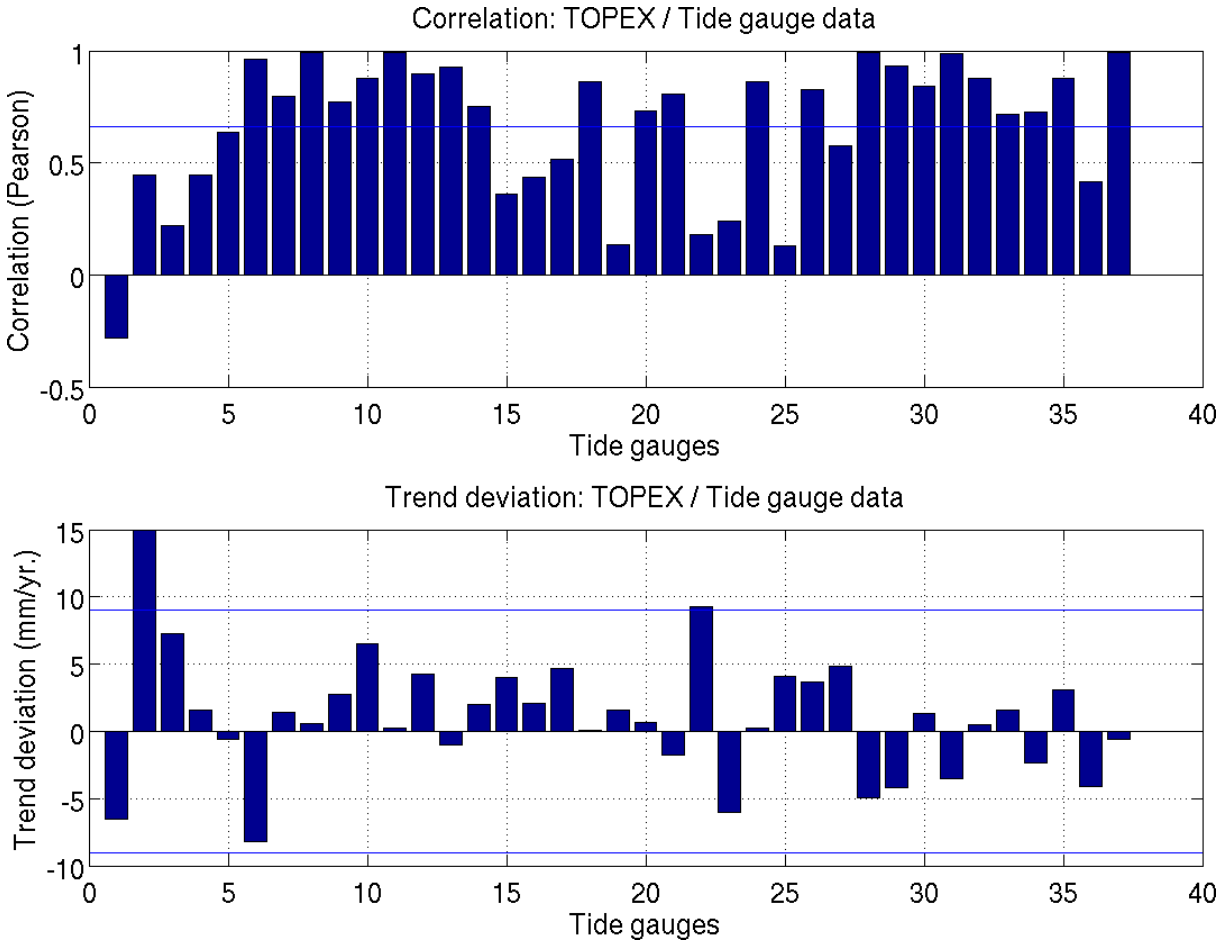

Figure 58: Correlations and trend deviations between tide gauge and TOPEX grid point time series for the trend filtered data set. The horizontal line in the upper plot indicates the mean, in the lower plot, it marks two times the standard deviation of the trend differences.

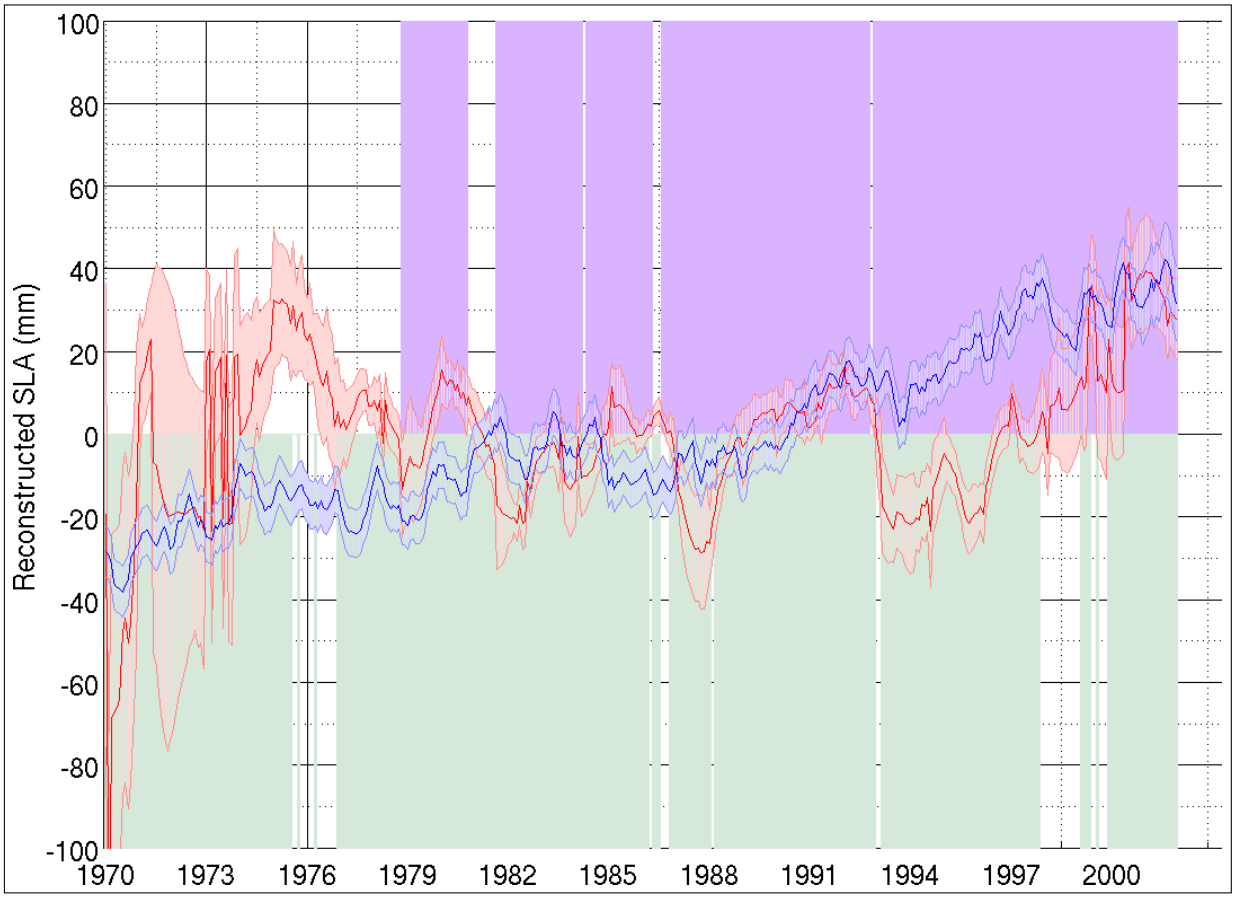

Figure 59: Effect of a time-changing tide gauge array. Reconstruction for 1970-2001 using 37 tide gauges (red). The Church et al. [7] reconstruction is shown in blue for comparison. It can be seen that the largest jumps (here: 1982 and 1992/93) appear when tide gauges at locations with high variance are added. The shaded areas mark the presence of tide gauges "Santa Cruz (Galapagos)" (in violet) and "Guam"(green), both of which have high values (rank 3 and 4) of EOF intensity.

Period	**1970-2001**
without LM corrections (mm/yr)	0.8 ± 1.0
GIA LM corrections (mm/yr)	0.0 ± 1.0
GPS LM corrections (mm/yr)	1.31 ± 1.3

Table 8: Effect of spurious jumps in the trend for different land movement corrections.

6.5 Influence of land movement corrections

Two reconstructions were performed to compare the influence of GIA vs. GPS land movement corrections at tide gauges.

Figure 61 shows the reconstruction for 1970-2001 with GIA and GPS land movement corrections, respectively. The Church et al. [7] reconstruction is shown in the same plot for comparison. It is clear that the latter, using more tide gauges, results in a more stable trend.

Again, it can be seen that, when using only few tide gauges, both deleting as well as including tide gauges may result in spurious jumps in the trend. The largest jumps appear when tide gauges at positions with high variability are added or deleted.

In the following, the resulting trends are given. It is immediately apparent that the reconstruction gives unrealistically low trends due to the fact that too many tide gauges areas missing, especially over the first 10 years, which leads to spurious jumps in the trend.

Apart from the unrealistically low trends, the GPS-corrected version results in a higher trend than the GIA-corrected one. This is an unexpected result, since the greater part of GPS land movement corrections applied are corrections for subsidence, not uplift. Therefore, the resulting trend should be smaller than the one obtained from the GIA corrected reconstruction. A comparison using the method used by [12] and [41], is performed by taking an area-weighted mean of the regional trends.

Area	**GIA correction (mm/yr)**	**GPS correction (mm/yr)**	**GPS correction minus GIA correction (mm/yr)**
Atlantic & North Sea	2.9	2.66	-0.24
English Channel	3.04	2.29	-0.75
North American East Coast (N)	0.58	0.58	0
North American East Coast (S)	2.1	-1.68	-3.78
Central America	0.55	0.29	-0.26
North American West Coast	2.1	2.24	0.14
North East Pacific	-0.99	3.18	4.17
Japan	1.9	0.57	-1.34
West Pacific	1.47	0.99	-0.49
Mean	**1.52**	**1.24**	**0.28**

Table 9: Results of the weighted-mean approach (as in Douglas [12]) to sea level anomaly trend estimation.

Using this method, GPS correction lowers the trend by -0.28 mm/yr compared against the GIA-corrected version. This decrease agrees well with the results obtained by Wöppelmann et al. [41], which to date is the only substantial resource for GPS-corrected sea level assessment. It should be noted that the set of tide gauges does not allow a direct comparison with [41], since our gauges are differently distributed, and the period covered is much shorter. In the set used here, no Northern Europe or Meditarrenean gauges areas are used, instead, there is a large emphasis on the Western Pacific and Japan, for which Douglas and Wöppelmann use only "Honolulu" (PSMSL 760/031). Hence, these results should not be taken as valid estimates for global sea level but rather as a check on the dubious results obtained from the OI reconstruction. Estimates for the Indian Ocean are left out, as the tide gauge time series here start only in the mid-1990s.

The comparison with the Douglas/Wöppelmann trend estimates shows that the OI reconstruction algorithm is not suitable for comparing GIA vs. GPS corrections at tide gauges. The different land movement corrections result in the activation of different variability patterns when they should mainly affect the trend.

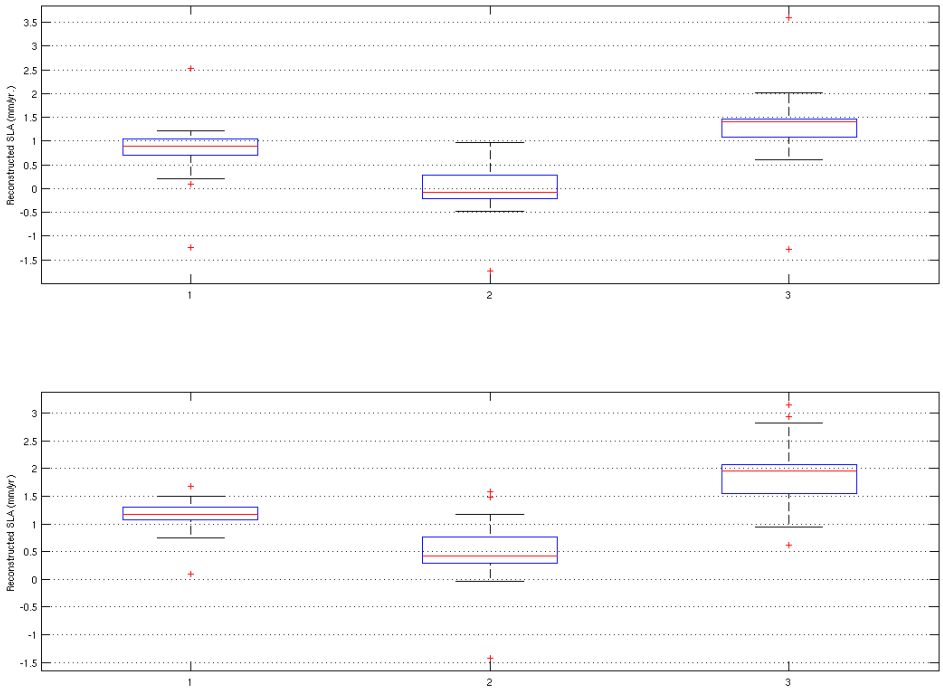

Figure 60: Effect of land movement corrections on the reconstructed SLA trend for 1970-2001 (upper panel) and 1980-2001 (lower panel). Left (1): No land movement corrections, Middle (2): GIA land movement corrections, Right (3): GPS land movement corrections. The higher percentage of missing tide gauges in the 1970-1980 period leads to unrealistic global SLA trends, especially for the GIA-corrected version. In the GPS-corrected version, the higher land movement correction rates hide the effect.

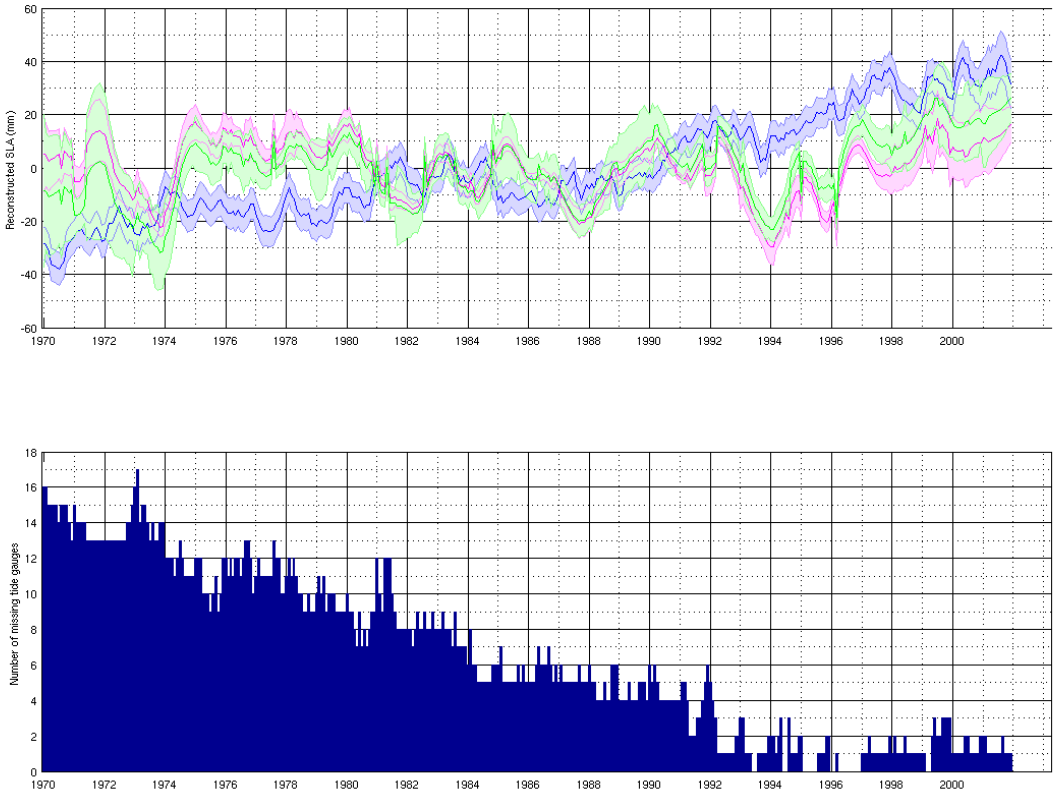

Figure 61: Reconstructed SLA for 1970-2001 with GIA corrections (pink) and GPS corrections (green) applied. The Church et al. [7] reconstruction (blue) is shown for comparison. In the lower panel, the number of missing tide gauges is given.

6.6 Correcting the errors caused by missing tide gauges

As the preceding chapters show, one major cause of error are gaps in the tide gauge time series, as well as the addition or exclusion of tide gauges during the course of the reconstruction. While gaps in the time series can always be closed using conventional gap-filling algorithms, the addition or exclusion of tide gauges is crucial to the usability of the OI algorithm. Therefore, a new smoothing routine is proposed here to decrease the error caused by a time-changing tide gauge array.

The main assumption of the OI algorithm is that the variability patterns of the sea level derived from the altimetry data remain constant. A second assumption is now introduced: to avoid spurious activation of variability patterns, it is assumed that, in the amplitude time series derived from the algorithm, the difference between two consecutive months will remain inside a certain limit. That is, unphysical jumps in the amplitude time series will be corrected. As a threshold, the standard deviation of the difference between the amplitude time series time steps derived from a simulated run of the OI(C) algorithm is used. After performing a reconstruction run using altimetry proxy data, for each amplitude time series, the difference between adjacent time series is calculated. The standard deviation is computed from the resulting time series. A multiple of this value is taken as a threshold for "allowed jumps" in the principal components (PCs) derived from the real reconstruction run. The spurious jump is removed and replaced by a smaller jump (equal to one standard deviation) in the same direction. Finally, the sea level anomaly fields are computed from the smoothed PCs.

In this way, unphysical jumps caused by tide gauge array changes and land movement corrections are avoided.

Since the OI(C) algorithm has no time dependency, and every time step is computed by and of itself, it is unnecessary to build in the constraint into the cost function directly. An alternative procedure would be to enhance the cost function in such a way that unphysical jumps at every spatial point are avoided. However, this would result in an unwarranted increase in computational effort.

Therefore, to retain the original efficiency of the algorithm, only the PCs themselves are smoothed after performing the optimization. The smoothing can be imagined as a piecewise concatenation of the time steps derived by optimization. Obviously, the smoothed PCs lose their optimality qualities due to the smoothing. However, it seems more reasonable to apply this additional, statistical constraint on the PCs to improve the reliability of the reconstruction. Figure 62 shows the effect of the smoothing at three different tide gauges. It can be observed here that, in the period before tide gauge data is available, the reconstructed variance at the tide gauge location is highly heteroscedastic. The resulting SLA variations must be considered unphysical without any doubt. This is the reason why the smoothing should not only be applied whenever changes in the tide gauge array occur, but throughout the reconstruction.

A similar but less pronounced effect arises when tide gauge data is present, but tide gauges are added or deleted from the dataset.

Two remaining questions are treated in the following. Firstly, a reasonable multiple of the standard deviation must be determined. Since the PCs represent variability, it is assumed that the time series of the differences between adjacent time steps is normally distributed and white in time. Anything else

would contradict the assumption that the main variability in sea level remains constant. This, of course, is not true for the artificially added "EOF-0" amplitude time series. For this PC, and only for this, an underlying trend in the difference time series is expected and must be allowed by the smoothing routine. Therefore, the smoothing of the "EOF-0" amplitude time series is performed if and only if a change in the tide gauge array has occurred.

In outlier detection, it is common to use three times the standard deviation as a threshold. However, especially with the strong trends introduced via the GPS land movement corrections, it is possible that a spurious mode will be activated not in a jump-like, but a slower trend-like manner. The maximum values for jumps between adjacent time steps in the TOPEX proxy run range from 1.9 to 2.9 times the standard deviation. In the following, a maximum threshold of 3.6 times the standard deviation is used. In Figure 63, the error intervals obtained from smoothing thresholds between 2.0 and 4.0 times the standard deviation are shown.

Examination of the regional trends shows that, although the global mean sea level change trend is comparable to the results found by Church et al. [7], the regional trends are stronger in this reconstruction. Comparison with the uncorrected version, however, shows that this effect is unrelated to the smoothing applied to the reconstructed fields. Instead, it is more likely that the increased strength of the trends is due to the shorter reconstruction period (1974-1993 (20 yrs.) in contrast to Church's 1950-2001 (51 yrs.)).

For the TOPEX period (1994-2001), regional maps of correlation and local RMS are given: Figures 65 and 66 show the correlation of the smoothed reconstruction fields with the original TOPEX altimetry data.

The smoothing improves the mean regional correlation values by 59 % (from 0.31 to 0.53) for the GPS-corrected version and by 56 % (from 0.32 to 0.56) for the GIA-corrected version. The mean regional RMS values are improved by 57 % for the GPS version and by 26% for the GIA version.

Figure 66 shows that the correlation with TOPEX is very good (> 0.6) for both reconstructions, with few patches of lower values. Some areas, especially in the South Atlantic, show negative values, which is due to the scarcity of tide gauges in the area. The comparison of the two reconstructions shows that, generally, correlation is improved at tide gauge locations. At the gauges where correlation is reduced, this is most probably caused by an overestimation of the land movement trends. This is, e.g., the case for Ofunato (-4.58 mm/yr), Charleston (-4.61 mm/yr), Anchorage (4.79 mm/yr) and Seldovia (10.8 mm/yr).

In Figure 67, areas with high RMS can be identified. The distribution of these areas is ruled by the variability patterns that are activated in the reconstruction. Maximal RMS values are found in the Indian Ocean, as well as the Indonesian sea, around New Zealand and in the Southern Atlantic. The comparison shows that, the RMS is reduced in most tide gauge locations, especially around Japan and in the West Pacific. Also, the GPS corrections reduce the overestimation of the said variability patterns, leading to a visible reduction of error in the areas of maximum RMS.

The comparison with the results obtained by Church et al. [7] and the unsmoothed time series (Figure 68) show that the smoothing algorithm developed here is capable of recovering the original trend.

However, it must be kept in mind that ocean basins unconstrained by tide gauges will remain subject

Period	GPS smoothed (mm/yr)	GIA smoothed (mm/yr)	Church et al. [7] (mm/yr)	GPS unsmoothed (mm/yr)	GIA unsmoothed (mm/yr)
1970-2001	1.75	1.28	1.92	1.85	0.52
1974-1993	1.75	1.12	1.32	0.27	-0.89
1994-2001	2.87	3.22	3.12	8.68	8.04

Table 10: Influence of the smoothing applied to different estimation periods.

to spurious variability. The trends are determined for the validation period (1994-2001), the whole reconstruction period (1970-2001) and a 20-year period where high reliability can be assumed as less gauges are missing.

The smoothing results in more realistic trends for all three periods. For the 1974-1993 period, the results lie only slightly outside the error estimate of ±0.3 mm/yr given by Church et al. [7].

For the 1994-2001 period, the GPS correction reduces the trend by -0.35 mm/yr, which is comparable to the -0.28 mm/yr reduction estimated by the Douglas /Wöppelmann method [41]. A similar reduction cannot be observed for the other two periods.

Overall, the quality of the estimates is largely improved by the smoothing.

Using the technique developed here, it is now finally possible to rectify the errors caused by gaps in the tide gauge time series, and the inclusion or exclusion of tide gauges, to the largest possible extent. Of course, the further a reconstruction goes back in time, the less tide gauge information will be available, so that the reliability of the reconstructed maps will inevitably decrease. This is especially true for regions with few tide gauges and such that are subject to phenomena with high variability. Still, unphysical jumps in the reconstruction, which in the past have led to incorrect estimates of the global trend, can now be avoided. This is extremely important in the context of a possible acceleration of sea level rise, which was detected by Church et al. ([7], [6]) but has since been questioned by other authors (e.g. [39]). Results from this paper strongly suggest that the apparent accelaration may indeed be, at least in part, an artifact of the OI(C) algorithm.

6.6.1 Summary

The sensitivity analysis gives the following results:

- For reasons of stability, it is advisable to remove the seasonal cycle from the tide gauge data. Removing all information but the nonlinear trend gives an even better result. The trend deviations for this kind of filtering lie beyond the accuracy limit in the simulated bootstrap.
- Correlation and trend differences between tide gauge and TOPEX grid point affect the reconstruction strongly, even in a simulation where only one time series of observational tide gauge data is

used. The errors caused amount to ±0.5 mm/yr. This strongly disagrees with the assumption in [7] that correlation is unimportant when using the OI algorithm, but is in agreement with the findings of Christiansen [5].

- The position of the tide gauge, especially its position with respect to the maxima and minima of the EOFs obtained from the altimetry data, plays a major role in the reconstruction. For once, tide gauges at positions with low variability serve as stabilizers, as they help determine which variability pattern should be activated. On the other hand, the inclusion or exclusion of tide gauges at positions with strong variability during the course of the reconstruction leads to major jumps in the reconstruction.

- Land movement corrections applied to the tide gauge data may lead to spurious activation of variability patterns, since large areas of the global ocean are not covered by tide gauges. Even in areas where the density of gauges is very high, nonlocal effects will stretch over the unconstrained open ocean.

- Spurious activation of variability patterns is the main weakness of the OI algorithm. The primary cause for this is a time-changing tide gauge array. Gaps in the time series can and should be filled using conventional methods. Still, it is also not advisable to add or delete any tide gauges from the initial set, as this will invariably lead to major jumps in the reconstruction. Given the scarcity of tide gauges with long records, this would limit the number of eligible tide gauge records even further, especially when keeping in mind that badly correlated data also has a detrimental effect on the reconstruction. Also, the non-local effects gain more influence as greater areas of the global ocean remain unconstrained. These negative effects can be significantly reduced, but not eliminated, by using the smoothing algorithm developed here.

7 Discussion and Outlook

A reconstruction of sea level anomalies using satellite altimetry data and GPS-corrected tide gauge data has been presented in this study. The initial aim of this work was to reconstruct monthly SLA maps for the use in data-assimilated ocean models. For this reason, an attempt was made to retain the seasonal signal. Due to the scarcity of tide gauges with co-located GPS stations, the effects of using few tide gauges in an OI(C) reconstruction were also examined. The results can be summarized as follows:

Geographical distribution of tide gauges There is strong evidence that, contrary to earlier studies, the location of the tide gauges *with respect to the lower-order EOFs* is a major influence when few tide gauges are available for a reconstruction. This effect is independent of the number of EOFs used in the reconstruction and does not stem from solving an underdetermined problem. Even though the impact on a long-term trend may be negligible, the integrity of SLA fields obtained from such a reconstruction cannot be relied on. This caveat concerns sea level data as well as, e.g., temperature or sea level pressure

data obtained with the OI(C) algorithm. It is advised to use such reconstruction data with proper care and highly augmented error approximations, especially when data from the 19th century is concerned (e.g., in [6]). Subtracting the seasonal cycle from the data or retaining only the nonlinear trend will does not eliminate the problem, although the stability of the trend is improved.

Correlation, variance and heteroscedasticity In combination with the above-mentioned effect, it is strongly advised to use only tide gauges that are well correlated with the open ocean, and which show similar variance patterns. This study has shown that using of a large amount of in-situ data cannot cancel out the detrimental effects of using "bad" data. This indicates that the caveats stated by Douglas [12] and others must be observed, even tightened, also when using the OI(C) algorithm. Badly correlated tide gauges can lead to massive erroneous under- or overestimation of variability patterns. This is especially the case when tide gauges located at a "neutral" position, i.e. a position where there is usually little variability, show strong anomalies.

Length of the validation period Concerns issued by Christiansen [5] as to the length of the validation period have not been examined any further this study. Tests have shown that, in the reconstruction of the validation period, the insertion of the artificial "EOF-0" has only a minor effect on the result, since a homogeneous sea level rise from a short validation period will be "hidden" in other lower-order EOFs, rather than split up into a single pattern. From this, it is clear that, when reconstructing a period other than the validation period, the algorithm's "choice" of appropriate EOFs is no longer unambiguous. This means that, for any month, the algorithm may chose to explain this constellation using EOFs that are not "responsible" for it. This is especially true for reconstructions using unfiltered tide gauge data, which generally shows much larger variability than the deseasonalized data.

Effects of a time-varying tide gauge array / Smoothing algorithm The fact that the inclusion or exclusion of a single tide gauge may change the result significantly challenges the whole concept of a time-varying tide gauge array. This problem can be minimized by thoroughly testing how the various constellations of tide gauges perform in reconstructing the validation period. Gaps in the tide gauge time series should be avoided at any cost, e.g. by employing gap-filling methods like those of Kondrashov and Ghil ([23]) or [39]. Still, it is important to remember that also the inclusion of tide gauges will lead to major jumps in the reconstruction. This effect should be avoided by using the smoothing algorithm described in this paper.

Effects of a time-varying tide gauge array: GPS and GIA corrections When employing GPS or GIA corrections, the use of a time-varying tide gauge array may lead to jumps in the reconstruction result. For example, if a time series that has been "dampened" by the application of a strong (or long-term) subsidence correction, the reconstruction result will "jump up" when the time series ends and is, hence, no longer included in the set. This effect is naturally more pronounced for long time series. An example for this effect in this study is Auckland, where the time series ends in 1999. Obviously, the same

effect occurs when a time series is gappy, however, in this case, the error cancels out in the long-term trend. Church et al. ([6]) handle this problem by increasing the error estimates in their solution. When using GPS corrections, the effect is usually more pronounced, since they tend to be much larger than the respective GIA corrections. As a result, for the comparison of GIA and GPS corrections, it may be more efficient to limit oneself to a reconstruction from tide gauges alone (e.g., in [41]). Also, GPS corrections lead to increased spurious activation of variability patterns. The integrity of monthly GIA- or GPS-corrected SLA maps reconstructed with the OI(C) algorithm cannot at this point be guaranteed. With smoothing applied, the integrity of the reconstruction is improved significantly. Still, unconstrained areas will tend to be reconstructed poorly.

The results presented in this study yield several implications for future sea level reconstructions. One major problem arises from the fact the OI(C) and related algorithms show strong stochasticity when only few tide gauges are used. Results using only very few records should, therefore, be treated with caution. Although the long-term linear trend from such reconstructions is robust, a simple weighted mean of relevant tide gauges may give a more reliable estimate.

As far as the application of GPS corrections is concerned, the concept of a varying tide gauge array, where single tide gauges (and their respective corrections) are included or excluded during the course of the reconstruction, can lead to spurious jumps in the trend. Another problem results from the fact that, of the comparably few stations for which GPS corrections are available, not all show good correlation and homoscedasticity values.

For future reconstructions, it is strongly recommended to use a stationary array of tide gauges, or use the smoothing algorithm described in this paper. Gauges showing low correlation with the altimetry data at adjacent grid points, or such showing strong heteroscedasticity, should be excluded from the configuration, since these may spoil a reconstruction even when a moderate number (± 30) of stations is used.

Another possibility would be to perform an OI(C) reconstruction using all eligible tide gauges, whether GPS corrections are available for them or not; then determine a trend correction using a weighted mean for the GPS-corrected gauges; and finally apply this trend correction to the OI(C) reconstructed trends. This would, however, result in a loss of information about the regional effects of land movement corrections.

However, summing up, it can be said that the findings in this study provide important information for the selection of tide gauges in sea level reconstructions. The eligibility criteria proposed by Douglas [11] have been confirmed for the use in the OI(C) and related algorithms, and it is highly probable that they will remain valid for future reconstruction algorithms as well.

GPS corrections at tide gauges have been shown in this work to yield valuable information on land movement processes, especially if these are not related to GIA (in the case that GIA is the cause for land movement, GPS and GIA models give equally good results). At a majority of stations, the processes governing land movement could be reliably identified in the time series, and the correction could be applied in an individual assessment of the tide gauge station. Also, it has been shown that, even if a GPS station has only been active for several years, processes that have been going on at a tide gauge for decades could be consistently explained by the GPS trends. At most stations, the trends could easily be

interpolated into the past. A further extension of the GPS network at tide gauges is, therefore, beneficial for future as well as for historical sea level change assessments.

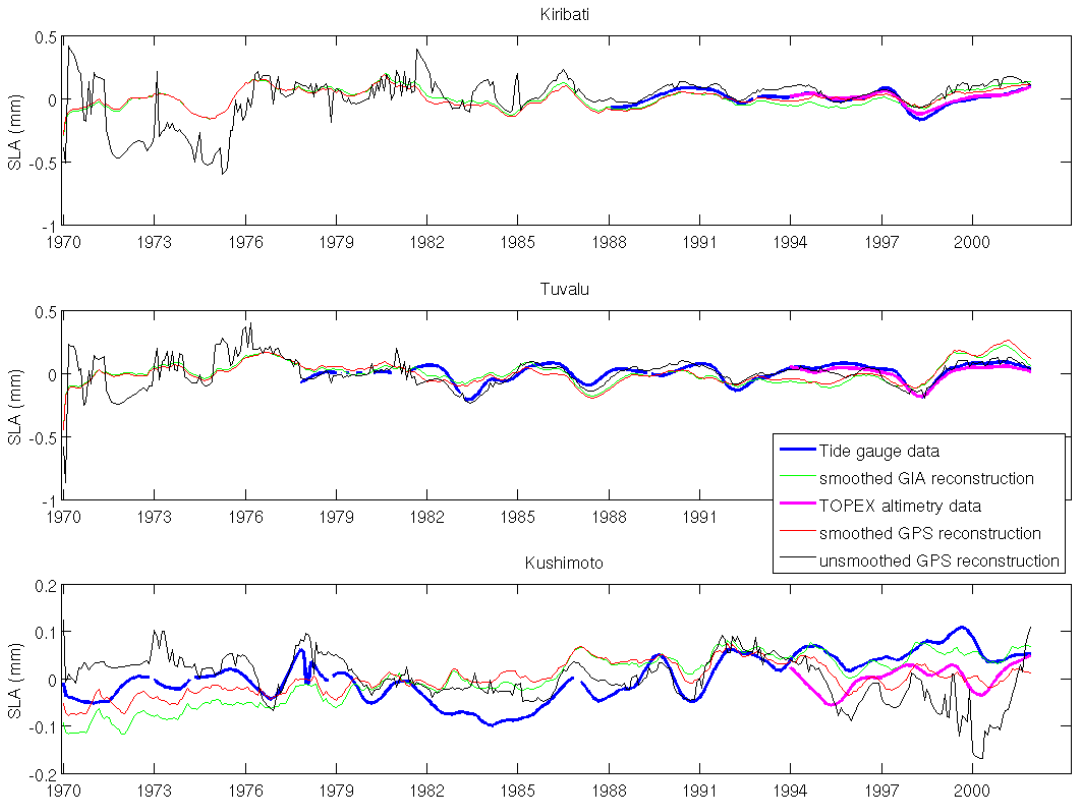

Figure 62: Effect of the smoothing at three different tide gauges: Kiribati, Tuvalu, and Kushimoto. Shown are the tide gauge data, the TOPEX altimetry data at the respective grid point, the smoothed GIA- and GPS-corrected reconstructions and the unsmoothed GPS-corrected reconstruction. The unsmoothed reconstruction results in large, spurious and clearly unphysical sea level jumps in the unconstrained period (i.e. the period before tide gauge data is available. The smoothing reduces this effect. For Kushimoto, data is available from the beginning of the reconstruction. Still, the smoothing reduces unphysical jumps related to changes in the tide gauge array.)

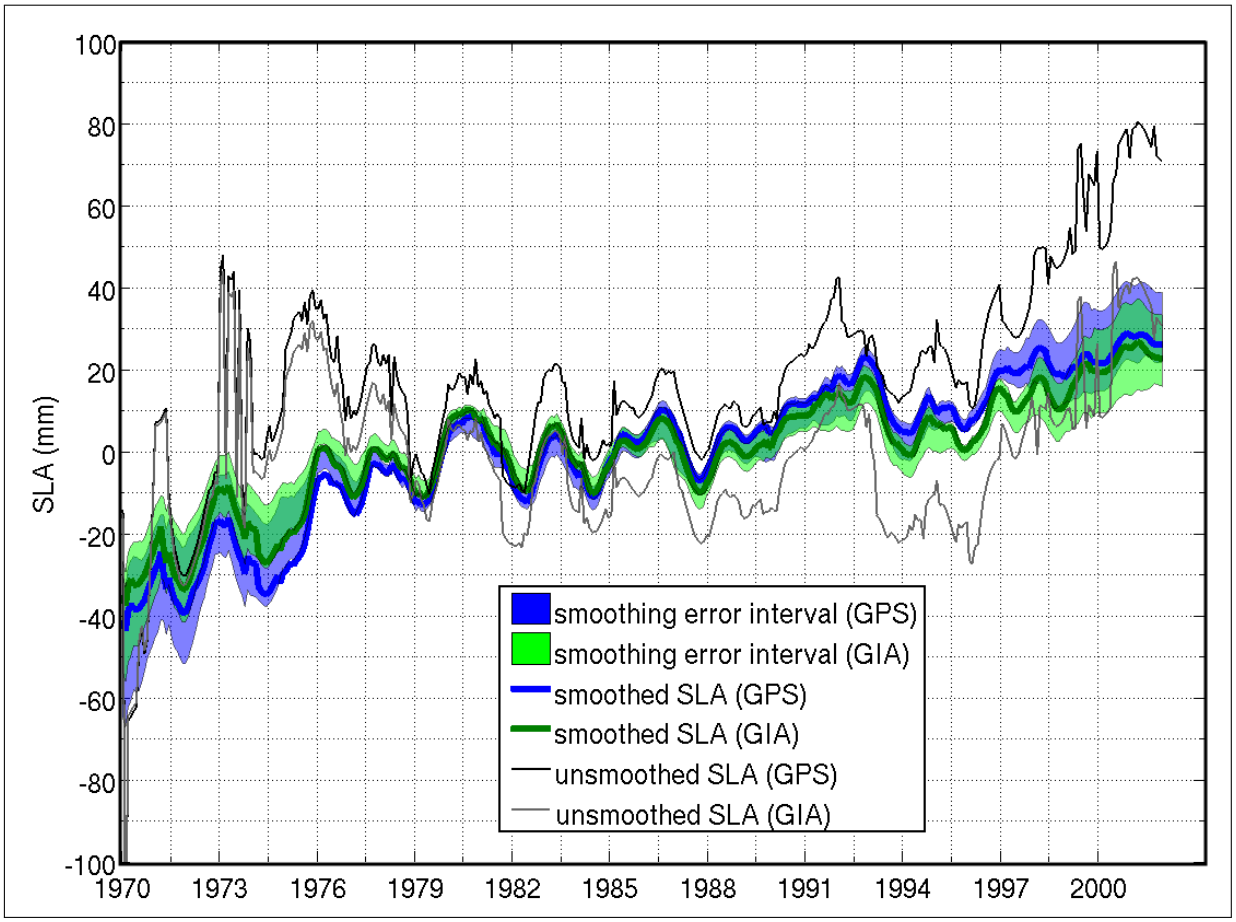

Figure 63: The plot shows the reconstruction results with a smoothing threshold of 3.6 times the standard deviation for GPS- (blue) and GIA-corrected (green) tide gauges. The error intervals show the respective results for smoothing thresholds of 2.0 to 4.0 times the standard deviation. The thin black (GPS) and grey (GIA) lines show the original (unsmoothed) reconstructions for comparison. The beneficial effect of the smoothing is especially apparent in the beginning of the reconstruction period, where a large part of tide gauges are missing; and at the times when tide gauges are added or deleted from the set.

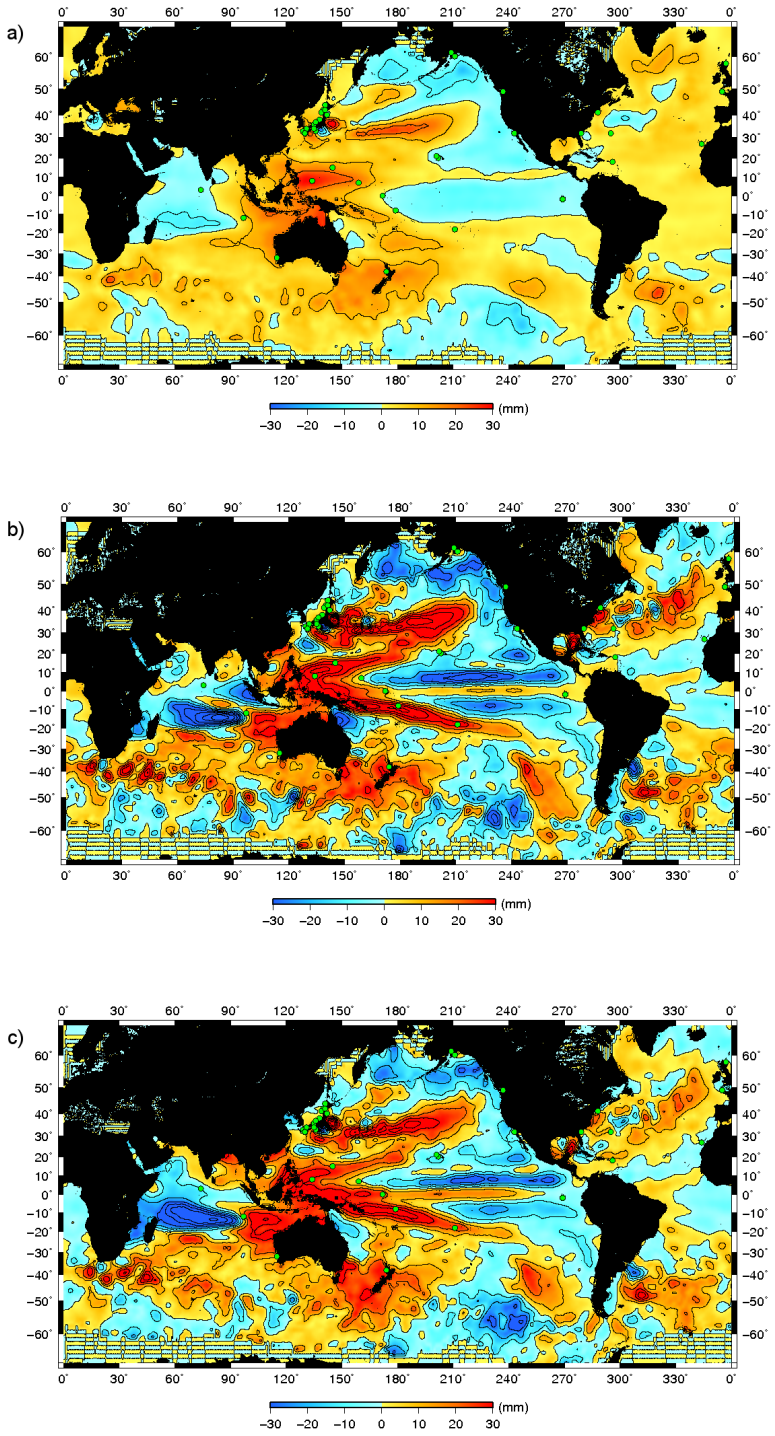

Figure 64: The regional SLA trends from a) TOPEX altimetry data, b) the GPS-corrected, smoothed reconstruction and c) the GIA-corrected, smoothed reconstruction. While the spatial patterns agree well, the amplitude of the reconstructed trends is much higher than in the original data. Qualitatively, the reconstruction of the patterns also compares well with the Church et al. [7] reconstruction, which used more tide gauges.

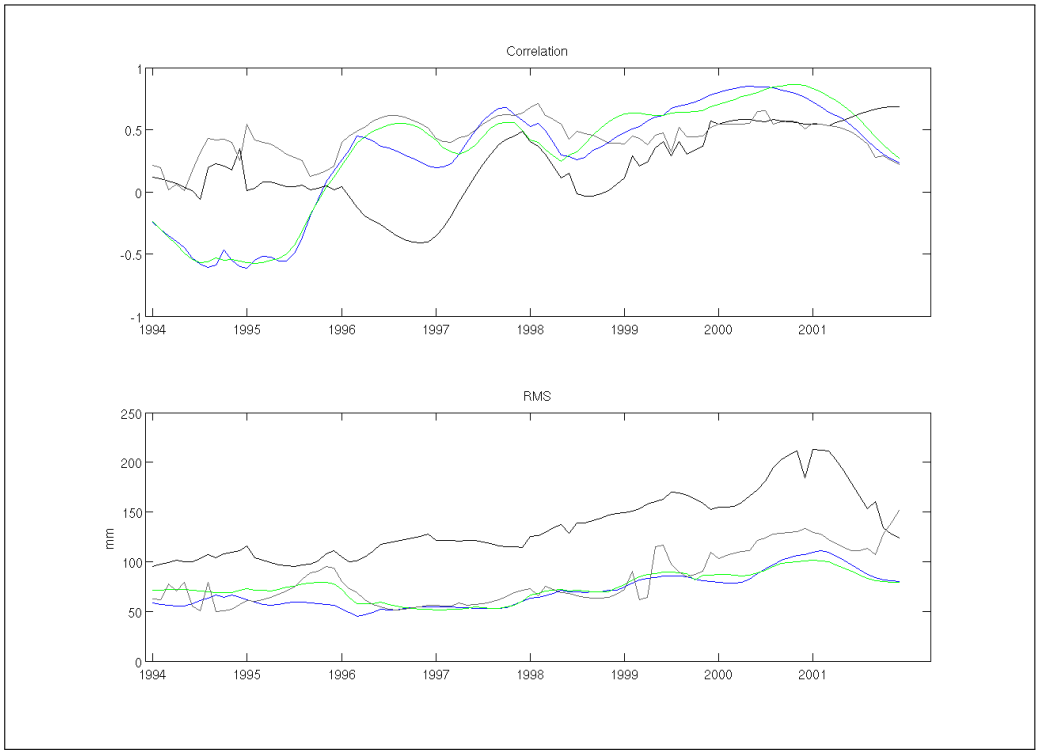

Figure 65: (a) The correlation of the GPS- (blue) and the GIA-corrected (green) smoothed reconstructions. The unsmoothed versions are shown in black (GPS) and grey (GIA). (b) RMS differences to the original TOPEX altimetry fields. Colors as in (a).

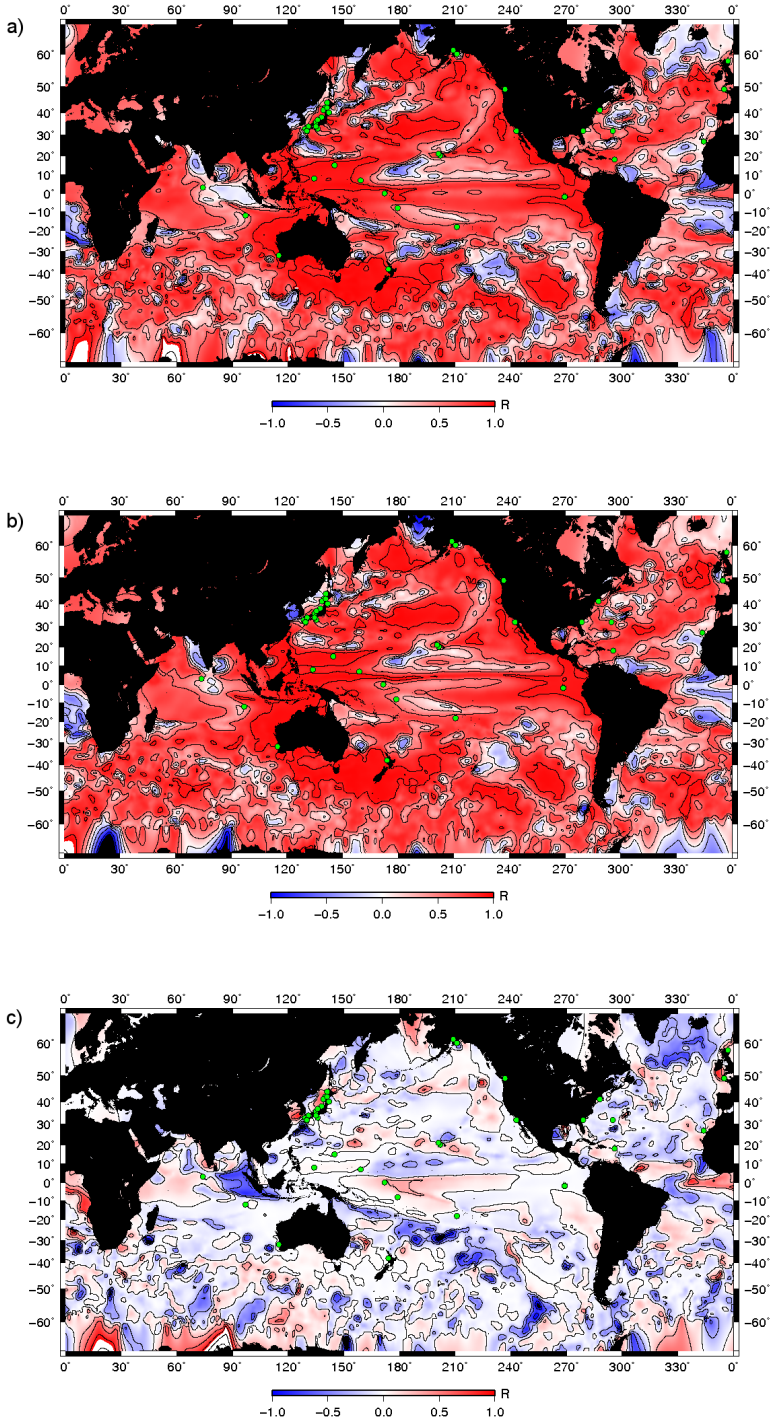

Figure 66: Difference of the regional correlation map of the GPS- minus the GIA-corrected, smoothed reconstruction for 1994-2001 with the original TOPEX altimetry fields. Red areas in c) indicate regions where the GPS-corrected version performs better than the GIA version. This is the case for almost all tide gauge locations.

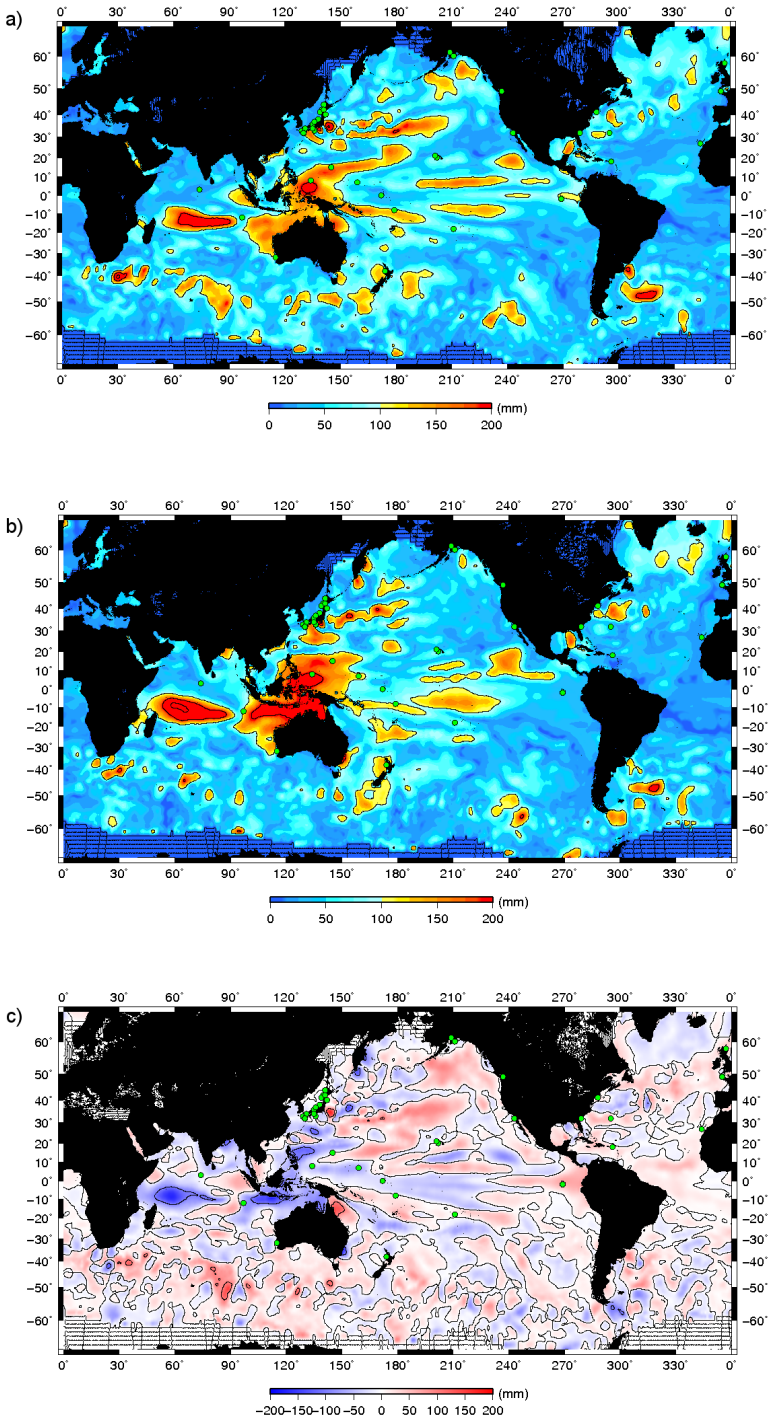

Figure 67: Difference of the regional RMS map of the GPS- minus the GIA-corrected, smoothed reconstruction for 1994-2001 with the original TOPEX altimetry fields. Blue areas in c) indicate regions where the GPS-corrected version performs better than the GIA version. This is the case for almost all tide gauge locations.

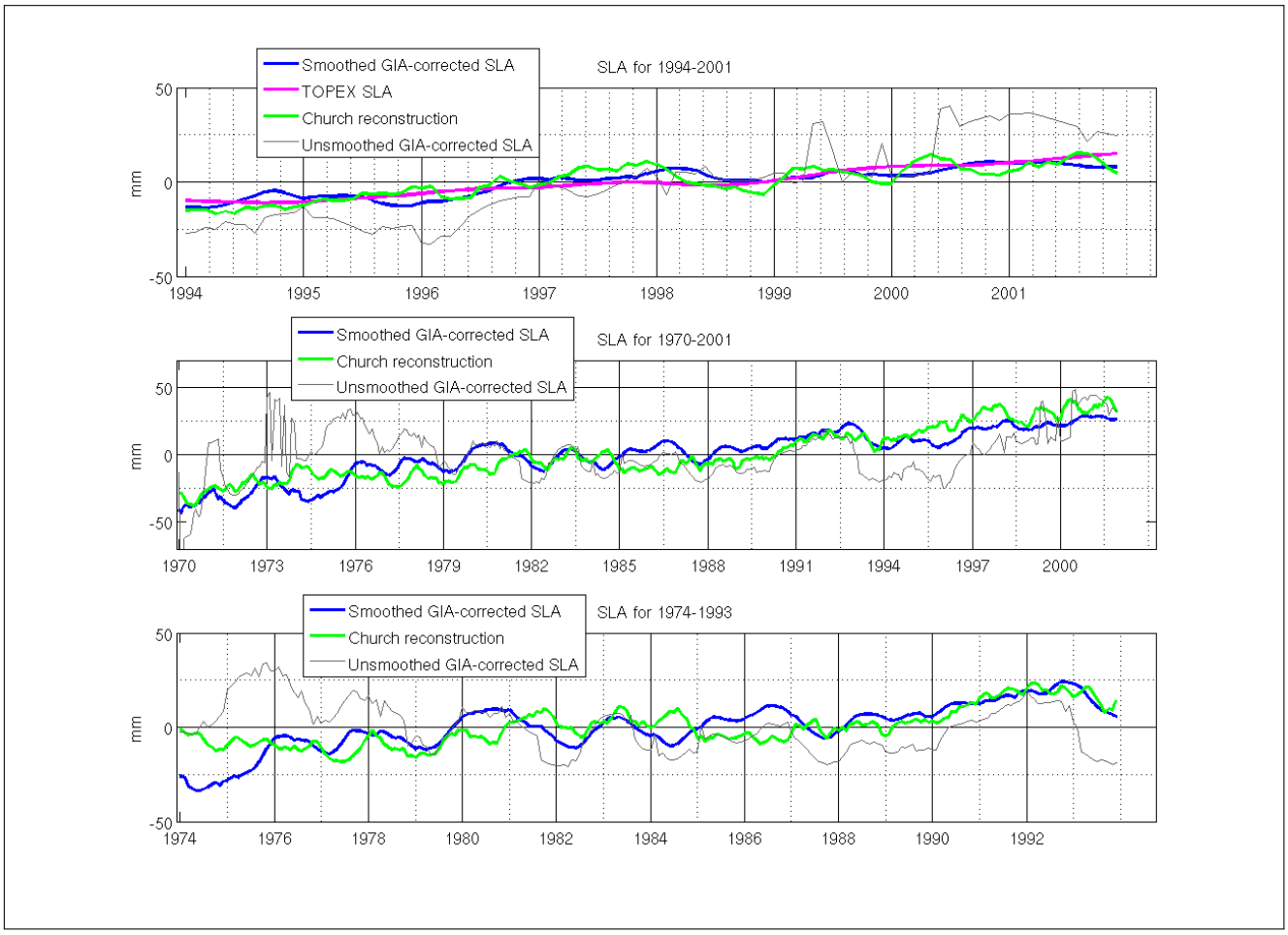

Figure 68: Comparison of the smoothed, GIA-corrected reconstruction (blue) with the Church reconstruction (green), the TOPEX altimetry date (pink), and the unsmoothed, GIA-corrected version (grey).

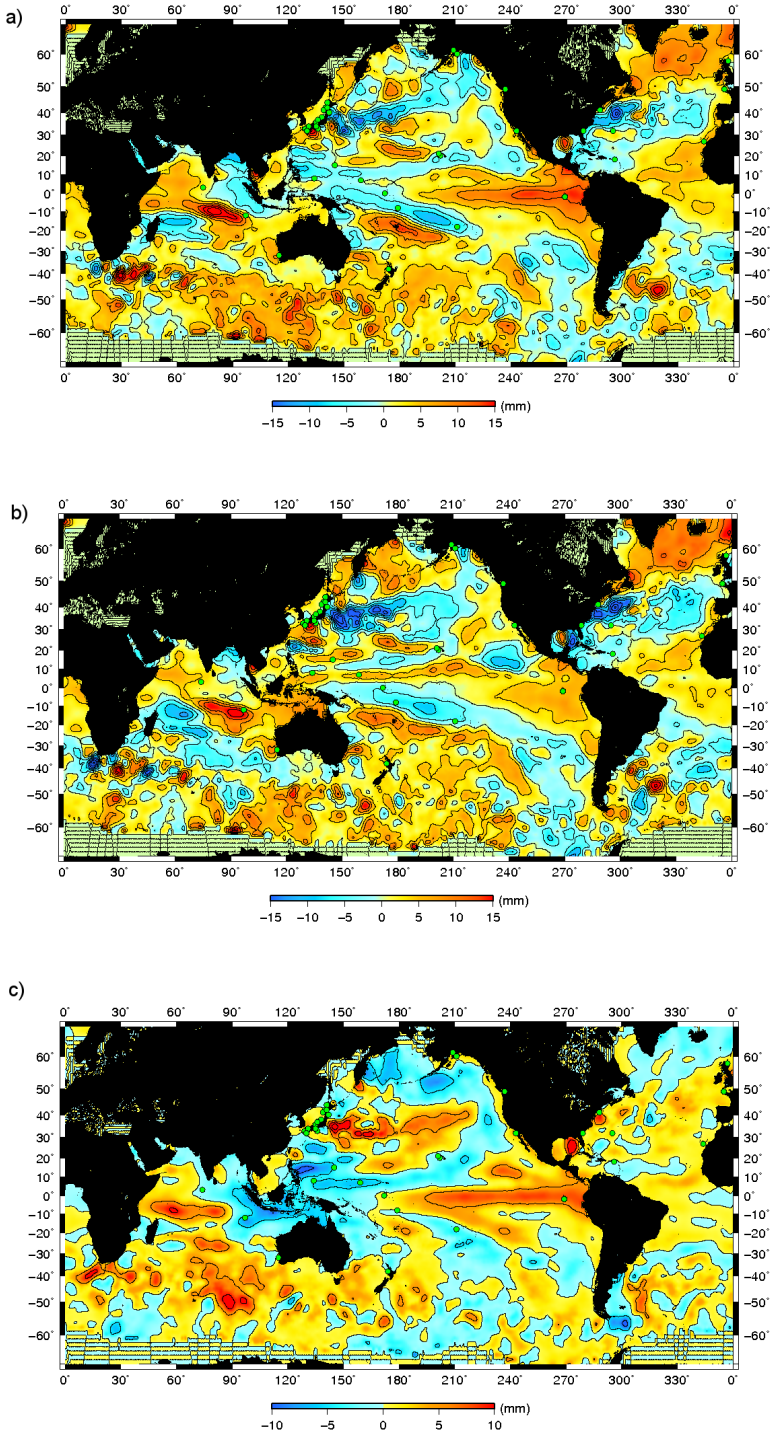

Figure 69: Trend estimates from the 1974-1993 reconstructions: (a) smoothed GPS-corrected version and (b) smoothed GIA-corrected version. c) shows the differences (GPS-GIA) between the two reconstructions. Again, it should be kept in mind that trends from unconstrained areas are less reliable than such with a high density of tide gauges. This is especially the case for the large negative trends in the Northern Pacific and on the North American East Coast, which cannot be validated. These spurious trends are decreased in the GPS-corrected version. On the other hand, the GPS-corrected version shows a stronger trend in the Eastern Pacific, which, due to its form, can be identified as spurious activity of the EOF-1. A comparison with the regional correlation values (Figure 66) shows that, at Galapagos, the correlation of the GPS-corrected reconstruction is lower than that of the GIA-corrected version. In comparison with Church et al.[7] (1950-2000), the trends show stronger intensity. This may in part be caused by the shorter reconstruction period, but is also related to the lower number of tide gauges used (compare Figure 64).

References

[1] J. M. Beckers and M. Rixen. EOF calculations and data filling from incomplete oceanographic data sets. J. Atmosph. And Ocean Techn., 20:1839–1856, 2003.

[2] M. Berge-Nguyen, A. Cazenave, A. Lombard, W. Llovel, J. Viarre, and J.F. Cretaux. Reconstruction of past decades sea level using thermosteric sea level, tide gauge, satellite altimetry and ocean reanalysis data. Global and Planetary Change, 62(Issues 1-2):1–13, 2008.

[3] G. Blewitt and D. Lavallée. Effect of annual signals on geodetic velocity. J Geophys Res, 107(B7):2145, 2002.

[4] D. P. Chambers, C. A. Mehlhaff, T. J. Urban, D. Fujii, and R. S. Nerem. Low-frequency variations in global mean sea level: 1950-2000. J. Geophys. Res., 107(C4):3026–3035, 2002.

[5] B. Christiansen, T. Schmith, and P. Thejll. A surrogate ensemble study of sea level reconstructions. J. Climate, 2009. submitted.

[6] J. Church and N. J. White. A 20th century acceleration in global sea-level rise. Geophys. Res. Lett., 33:L01602, 2006.

[7] J. Church, N. J. White, R. Coleman, K. Lambeck, and J. X. Mitrovica. Estimates of the regional distribution of sea-level rise over the 1950 to 2000 period. J. Climate, 17(13):2609–2625, 2004.

[8] R. B. Cleveland, W. S. Cleveland, J. E. McRae, and I. Terpenning. STL: A seasonal-trend decomposition procedure based on Loess. Journal of Official Statistics, Sweden, 6(1):3–73, 1990.

[9] Rhode Island Coastal Resources Management Council. Rhode Island Coastal Resources Management Program Redbook, volume Section 145. Rhode Island Coastal Resources Management Council, 2008.

[10] G. H. Davis. Land subsidence and sea level rise on the Atlantic coastal plain of the United States. Environmental Geology, 10(2):67–80, 1987.

[11] B. C. Douglas. Global sea level rise. J. Geophys. Res., 96(C4):69816992, 1991.

[12] B. C. Douglas. Sea level change in the era of the recording tide gauge. In Sea level rise: history and consequences., pages 37–64. International Geophysics Series, 75 2001.

[13] K. O. Emery and D. G. Aubrey. Sea levels, land levels, and tide gauges. Springer, 1991.

[14] J. T. Freymueller, P. J. Haeussler, R. L. Wesson, and G. Ekstroem. Active deformation processes in alaska, based on 15 years of GPS measurements. In R. Wesson J.T. Freymueller, P.J. Haeussler and G. Ekstrom, editors, Active Tectonics and Seismic Potential of Alaska, pages 1–42. AGU Geophysical Monograph 179, 2008.

[15] M. Ge, G. Gendt, G. Dick, F. P. Zhang, and C. Reigber. Impact of GPS satellite antenna offsets on scale changes in global network solutions. Geophy. Res. Lett., 32:L06310, 2005.

[16] Y. Isoda, F. Kitamura, and T. Murakami. Interannual variations of the yearly mean sea level around the Japanese islands. Bulletin of Fisheries Sciences, 55(2):85–95, 2004.

[17] A. Kaplan, M. A. Cane, and Y. Kushnir. Reduced space approach to the optimal analysis interpolation of historical marine observations: Accomplishments, difficulties, and prospects. In Advances in the Applications of Marine Climatology: The Dynamic Part of the WMO Guide to the Applications of Marine Climatology, pages 199–216. World Meteorological Organization, Geneva, Switzerland, WMO/TD-1081 2003.

[18] A. Kaplan, M. A. Cane, Y. Kushnir, A. C. Clement, M. B. Blumenthal, and B. Rajagopalan. Analyses of global sea surface temperatures 1856-1991. J. Geophys. Res., 103(18):18,567–18,589, 1998.

[19] A. Kaplan, Y. Kushnir, and M. A. Cane. Reduced space optimal interpolation of historical marine sea level pressure: 1854-1992. J. Climate, 13:2987–3002, 2000.

[20] A. Kaplan, Y. Kushnir, M. A. Cane, and M. B. Blumenthal. Reduced space optimal analysis for historical datasets: 136 years of Atlantic sea surface temperatures. J. Geophys. Res., 102(27835-27860), 1997.

[21] K. Karhunen. Zur Spektraltheorie stochastischer Prozesse. Ann. Acad. Sci. Fennicae, 37, 1946.

[22] M. Kendall. A new measure of rank correlation. Biometrika, 30:81–89, 1938.

[23] D. Kondrashov and M. Ghil. Spatio-temporal filling of missing points in geophysical data sets. Nonlin. Processes Geophys., 13:151–159, 2006.

[24] H. Lassen and W. Siefert. Zur Windstauentwicklung in der südöstlichen Nordsee. Die Küste, 53, 1992.

[25] H. Levene. Robust tests for equality of variances. In I. Olkin et al., editor, Contributions to Probability and Statistics: Essays in Honor of Harold Hotelling. Stanford University Press, 1960.

[26] W. R. Peltier. Global glacial isostasy and the surface of the ice-age Earth: the ICE-5G (VM2) model and GRACE. Annu Rev Earth Planet Sci, 32:111–149, 2004.

[27] R. W. Preisendorfer. Principal component analysis in meteorology and oceanography. Developments in Atmospheric Science, 17:425 ff., 1988.

[28] N. H. Saji, B. N. Goswami, P. N. Vinayachandan, and T. Yamagata. A dipole mode in the tropical Indian Ocean. Nature, 401(6751):360–363, 1999.

[29] T. Schneider. Analysis of incomplete climate data: Estimation of mean values and covariance matrices and imputation of missing values. J. Climate, 14:853–871, 2001.

[30] T. Schöne. Linking GPS to tide gauges and tide gauge benchmarks. In World Climate Research Program Workshop on Understanding Sea-level Rise and Variability, 6-9 June 2006, UNESCO/IOC, Paris, France, 2006.

[31] T. Schöne, D. Thaller, and N. Schön. IGS tide gauge benchmark monitoring pilot project (TIGA) - scientific benefits. J.Geodesy, 83(3-4):249–261, 2009.

[32] T. M. Smith, R. W. Reynolds, R. E. Livezey, and D. Stokes. Reconstruction of historical sea surface temperatures using empirical orthogonal functions. J. Climate, 9:1403–1420, 1996.

[33] R. Snay, M. Cline, W. Dillinger, R. Foote, S. Hilla, W. Kass, J. Ray, J. Rohde, G. Sella, and T. Soler. Using global positioning system-derived crustal velocities to estimate rates of absolute sea level change from North American tide gauge records. J. Geophys. Res, 112(B04409):1–11, 2007.

[34] F. N. Teferle, R.M. Bingley, S.D.P. Williams, T.F. Baker, and A.H. Dodson. Using continuous GPS and absolute gravity to separate vertical land movements and changes in sea-level at tide-gauges in the uk. Phil. Trans. R. Soc. A, 364(1841):917–930, 2006.

[35] P. Tregoning, P. J. Morgan, and R. Coleman. The effect of receiver firmware upgrades on GPS vertical timeseries. Cahiers du Centre Europeen de Geodynamique et de Seismologie, 23:37–46, 2004.

[36] P. Tregoning and T. van Dam. Atmospheric pressure loading corrections applied to GPS data at the observation level. Geophy. Res. Lett., 32:L22310, 2005.

[37] H. von Storch. Statistical Analysis in Climate Research. Cambridge UP, 2002.

[38] E. R. Wahl and C. M. Ammann. Robustness of the Mann, Bradley, Hughes reconstruction of northern hemisphere surface temperatures: Examination of criticisms based on the nature and processing of proxy climate evidence. Climatic Change, 85(1-2):33–69, 2007.

[39] M. Wenzel. Reconstruction of regional mean sea level anomalies from tide gauges using neural networks. J. Geophys. Res., 115(C0813):doi:10.1029/2009JC005630, 2010.

[40] P. L. Woodworth and R. Player. The permanent service for mean sea level: an update to the 21st century. J. Coastal. Res., 19:287–295, 2003.

[41] G. Wöppelmann, B. Martin Miguez, , M.-N. Bouin, and Z. Altamimi. Geocentric sea-level trend estimates from GPS analyses at relevant tide gauges world-wide. Glob Planet Change, 57:396–406, 2007.

[42] F. Zhang, G. Gendt, and M. Ge. GPS data processing at GFZ for monitoring the vertical motion of global tide gauge benchmarks. technical report for projects TIGA and SEAL. GeoForschungsZentrum Potsdam, Scientific Technical Report, STR07/02, 2007.

8 Acknowledgements

First and foremost, I would like to thank Dr. Tilo Schöne for his supervising, help and general scientific as well as moral support during my PhD years. Thanks for your enthusiasm, your good teaching, good company, and good ideas. Thank you also for keeping me on my toes by sending emails at nights, weekends, and, of course, over Christmas all these years.

Very special thanks go to Dr. Daniela Thaller at Uni Bern for providing the GPS data used in this Thesis. Daniela, I cannot thank you enough for sacrificing your weekends to process the combination.

Special thanks go to Prof. Maik Thomas for agreeing to be my supervisor and to PD Dr. Gregor Leckebusch for agreeing to review this Thesis. To the two of you, as well as Prof. Uwe Ulbrich, and Prof. Peter Nevir - thank you very much for giving me an extra 8 weeks to finish this on a new contract. I would also like to thank Prof. Ulrike Langematz and Prof. Jürgen Fischer for agreeing to be on my PhD comittee.

Thanks go to Dr. Saskia Esselborn and Prof. Markus Rothacher for supervising the first half of this project, to Prof. Jens Schröter for his oceanographic expertise, as well as to the BMBF for sponsoring my PhD position through the GEOTECHNOLOGIEN project SEAVAR (03F0434A). Special thanks go to the GFZ Potsdam for granting me an extra 3 months of contract as compensation for my maternity leave.

Thanks go out to Norman Teferle, Martin Stendel and Jeff Freymüller for helpful advice. Special thanks go to Sveta Jevrejeva at POL for her help with the Japanese tide gauges, and for pointing out Bo's paper to me in Paris.

Thanks to Julia Illigner and Andrea Homberg for keeping me great company through all our smoking and non-smoking breaks, to Nanett Hemmerling and to all my colleagues at the Tsunami group, it has been a pleasure working and lunching with you (except for the food at the GFZ canteen, of course).

This Thesis is dedicated to my family. I would like to thank my mother for sparking in me the love of books; my father, for the interest in science; and both of you for your unending love and support.

Deep, heart-felt thanks go out to my wonderful kids, Beckett and Lucy; and to my husband Danny, who put up with me during all the hard times. You know I love you more than words can say.

Nana Schön, Berlin, 12. Januar 2010.